CCMS-87-15
VPI-E-87-20

VIRGINIA TECH

CENTER FOR COMPOSITE MATERIALS AND STRUCTURES

INTERFACIAL STRENGTH DEVELOPMENT IN THERMOPLASTIC RESINS AND FIBER-REINFORCED THERMOPLASTIC COMPOSITES

Jeremy C. Howes
Alfred C. Loos

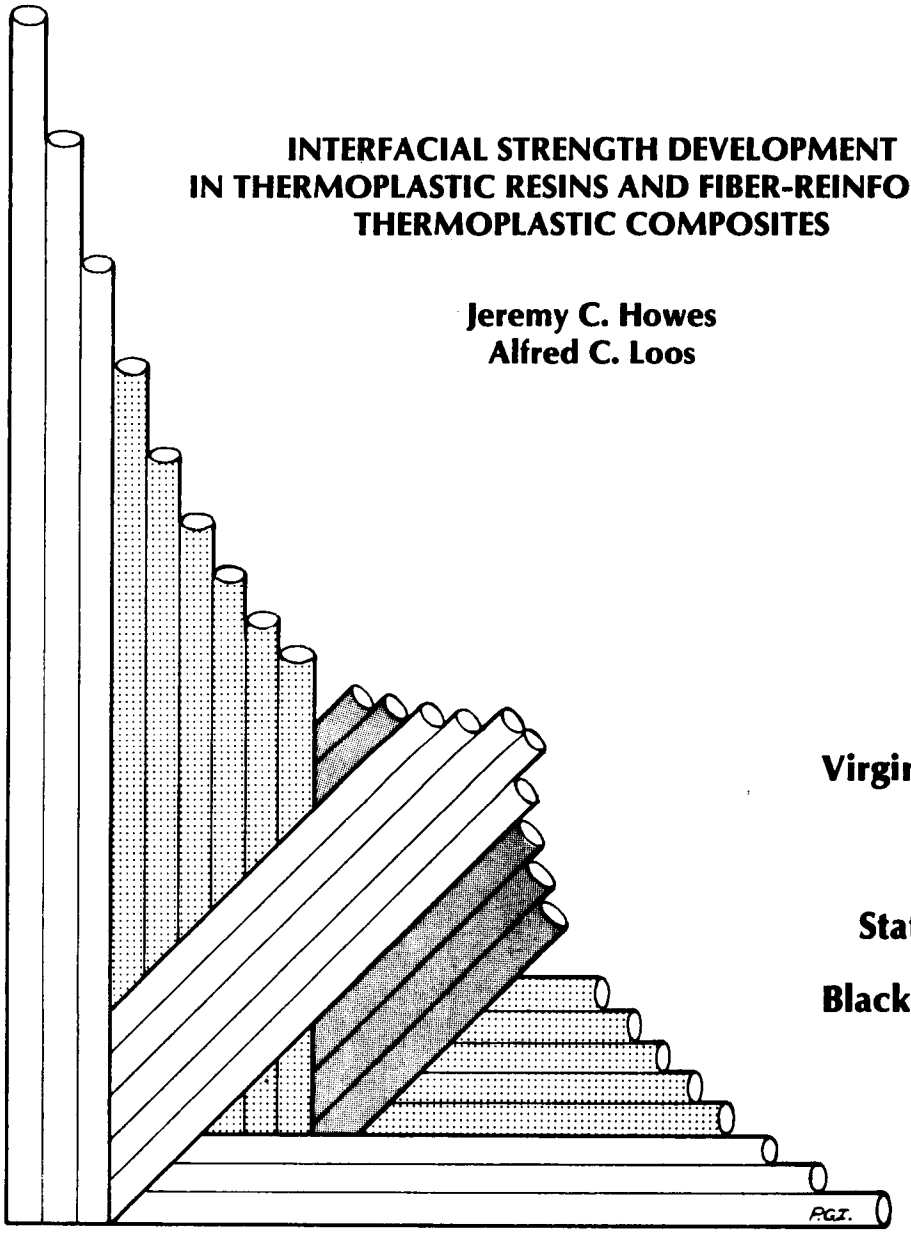

Virginia Polytechnic Institute and State University

Blacksburg, Virginia 24061

College of Engineering
Virginia Polytechnic Institute and State University
Blacksburg, Virginia 24061

September 1987

CCMS-87-15
VPI-E-87-20

Interfacial Strength Development in Thermoplastic Resins and Fiber-Reinforced Thermoplastic Composites

Jeremy C. Howes[1]
Alfred C. Loos[2]

Department of Engineering Science & Mechanics

Interim Report 67
The NASA-Virginia Tech Composites Program
NASA Grant NAG-1-343

Prepared for:

Polymeric and Applied Mechanics Branches
National Aeronautics and Space Administration
Langley Research Center
Hampton, Virginia 23665

---

[1] Graduate Student, Department of Engineering Science & Mechanics

[2] Professor, Department of Engineering Science & Mechanics

Interfacial Strength Development in Thermoplastic Resins and Fiber-Reinforced Thermoplastic Composites

by

Jeremy C. Howes

Committee Chairman: Alfred C. Loos
Engineering Science and Mechanics

(ABSTRACT)

The objective of this study was to develop tests that could be used to characterize autohesive strength development in amorphous thermoplastic resins and fiber-reinforced thermoplastic prepregs. All tests were performed using polysulfone P1700 thermoplastic resin and AS4/P1700 graphite-polysulfone prepreg.

Two test methods were examined to measure autohesion in neat resin samples. These included an interfacial tension test based on the ASTM tensile adhesion test (ASTM D897) and a fracture toughness test using a compact tension (CT) specimen (based on the ASTM toughness test for metals ASTM E399-83). The interfacial tensile test proved to be very difficult to perform and with an unacceptable amount of data scatter. The data obtained using the compact tension test were repeatable and could be correlated with temperature and contact time.

Autohesive strength development in fiber-reinforced prepreg samples was measured using a double cantilever beam (DCB) interlaminar fracture toughness test. The fracture mechanisms were determined to be different in the healed DCB specimen than the virgin specimen due to resin flow at the crack plane during the healing tests.

The CT test was found suitable for use in determining the autohesive properties and self-diffusion coefficient of neat resin. The DCB test, although not suitable for autohesive testing, indicated that repair of thermoplastic matrix composites is possible; however, the repair will not be as tough as the virgin material.

Acknowledgements

This work was supported by the NASA-Virginia Tech Composites Program through NASA Grant NAG-1-343.

Table of Contents

List of Illustrations

List of Tables

1.0 Introduction

The use of advanced fiber-reinforced composites has increased significantly in recent years. The high specific strengths and stiffnesses of these materials make them ideal for aerospace applications. However, typical fiber-reinforced organic matrix composites using thermosetting resins, such as epoxies, have low damage tolerance and low service temperatures when compared to the more traditional aerospace materials, such as aluminum.

To overcome the shortcomings in thermosetting resins, there is great interest in the use of thermoplastic resins as matrix materials for fiber-reinforced composites. Thermoplastic resins are generally high toughness materials and subsequently can improve the damage tolerance of composites. However, the mechanisms by which thermoplastic matrix composites form are very different than the mechanisms by which thermosetting matrix composites cure. Major differences between the processing characteristics of thermoplastic and thermosetting resins are shown in Table 1.1. The extreme tow height non-uniformity and the lack of flow in thermoplastic prepregs make them more difficult to process than thermosetting prepregs. Unlike thermosetting resins, which rely on low viscosity flow and wetting ability of the resin to coalesce the ply interfaces, thermoplastic matrix composites must be physically deformed to cause coalescence.

The mechanisms explaining the consolidation and interfacial deformation in thermoplastic composites have been established as viscoelastic deformation and

Table 1.1 Comparison of Thermoset and Thermoplastic Matrix Composites

	Thermoset	Thermoplastic
Prepreg	Uniform	Nonuniform
Minimum Viscosity (Poise)	10	10^4
Flow	High	Low
Solidification	Chemical (Irreversible)	Physical (Reversible)
Processing Temperature	250 - 350°F	600 - 700°F

autohesive bonding. These mechanisms are not well quantified and present processing models developed for thermosetting resin composites cannot be directly applied to thermoplastic matrix composites. Processing cycles for thermoplastic composites are currently derived empirically by trial and error . These methods do not lead to processing cycles which result in fully consolidated composite structures with strong interfacial bonds. In order to improve the processing theory for continuous fiber-reinforced thermoplastic matrix composites, the processing parameters temperature, pressure, and time must be related to the overall state of consolidation in the composite.

Common methods of processing thermoplastic composites from prepreg materials include matched die press molding or autoclave molding. Thermoplastic prepregs are often produced by first dissolving the polymer in a solvent. The minimum attainable viscosity of a neat thermoplastic resin during processing is very high ($\geq 10^4$ Poise). A solvent is used to lower the viscosity ($\approx$10 Poise) to ensure good fiber wetting and even matrix distribution which leads to a good fiber matrix bond. The solvent must be removed from the prepreg prior to processing to eliminate the possibility of voids forming due to solvent outgassing. The solvent is normally removed by drying in a forced air or vacuum oven.

The prepreg must be processed in order to produce the composite. The prepreg is cut to the dimensions of the structure and fiber directions oriented (laid up) to obtain the desired mechanical properties of the finished product. Thermoplastic prepregs have little or no tack and often the prepregs are spot welded to prevent slippage during processing. The lay-up is then placed in the die press or autoclave and processed at an elevated temperature and pressure for a known period of time, called the processing cycle. During

the processing, the resin undergoes rheological and physical changes dependent on both the applied pressure and temperature. This causes the prepreg plies to coalesce and consolidate into the finished laminated structure. The magnitudes of the temperature, pressure, and time greatly affect the quality of the finished composite.

In order to develop a processing model, the physical processes that occur during production of thermoplastic composites must be fully understood both quantitatively and qualitatively. The mechanism controlling the interfacial bond formation (consolidation) has been recognized as autohesion or self-diffusion. There are numerous theories describing autohesion in neat resin, and tests to determine autohesive strength are available. Autohesion in fiber-reinforced thermoplastic prepregs is not well understood due to the complications of the fiber matrix interface. Thus, the objective of the present study is to develop simple test methods that can be used to characterize interfacial strength development in advanced amorphous thermoplastic matrix resins and fiber-reinforced amorphous thermoplastic prepregs, and to model the results for incorporation into future processing theories.

2.0 Literature Review

In previous studies and by independent observation of the composite during processing, it has been established that individual prepreg plies consolidate by interfacial bonding [1]. The resulting bond strength is a function of the processing parameters temperature, pressure, and time to which the interface is subjected. The mechanism governing the formation of interfacial bonds has been established as autohesion [2].

2.1 Autohesion

Thermoplastic high polymers adhere to themselves through a mechanism known as autohesion or self-diffusion. It is the consensus that interfacial strength is a function of the number of molecules that penetrate across the interface. The following is a brief description of the autohesive phenomenon as it is presented in the literature [2-16].

Autohesive strength is controlled by two mechanisms: 1) Intimate contact between the interfacial surfaces and 2) Diffusion of the macromolecules across the interface [4,7,9,12]. Figure 2.1 shows the phenomenon of autohesion. At time zero, the two surfaces are pressed together. Providing the temperature is high enough (normally above the glass transition temperature, T_g), the surfaces will deform viscoelastically, come into contact and wet (Figure 2.1a). The polymer chains will begin to diffuse across the interface due to random thermal motions. After some time has passed, the chains will have partially diffused across the interface and entangled with

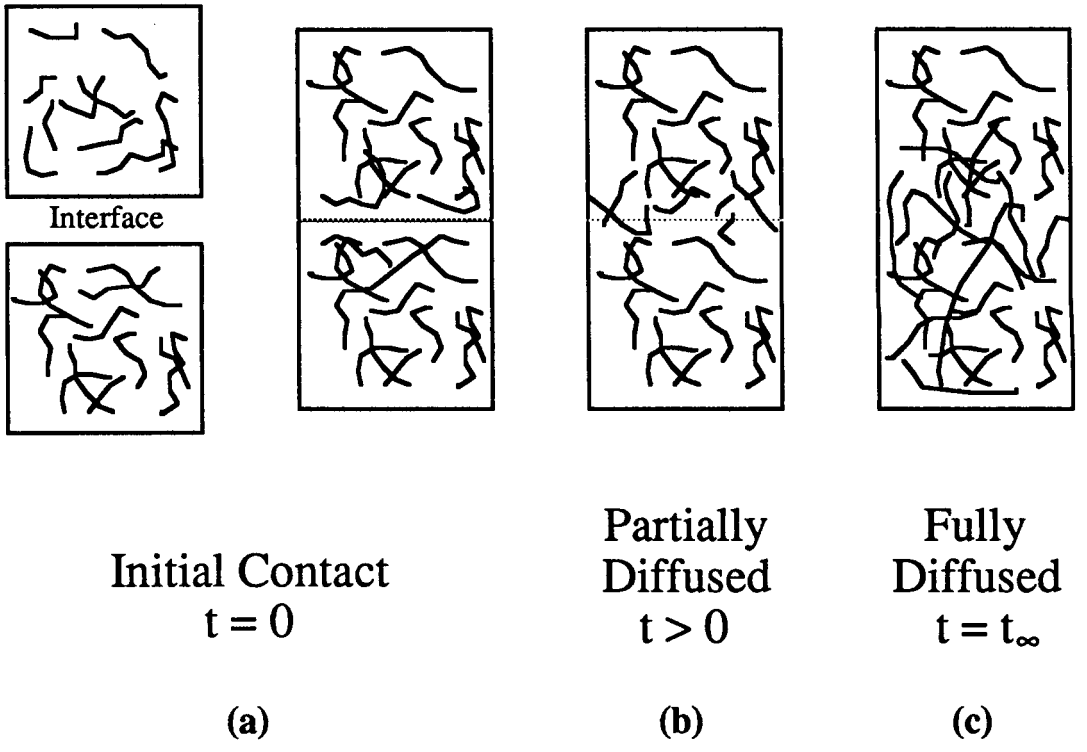

Figure 2.1. Schematic representation of the autohesive phenomenon.

molecular chains on the other side of the interface, thus giving the interface some strength (Figure 2.1b). Following a long enough period of time, the polymer chains will have penetrated and entangled into the adjacent interface enough so that the interface is no longer distinguishable from the bulk polymer. The interface is considered completely healed (Figure 2.1c). Either wetting or diffusion can account for significant proportions of the interfacial strength. Diffusion is conditional upon the surfaces being in intimate contact, as the molecules cannot move across open space [8]. Theories to describe polymer diffusion and deformation are based on DeGennes' Reptation theory of molecular motion.

2.1.1 DeGennes' Reptation Theory

DeGennes [3] derived a model of molecular dynamics assuming that very high molecular weight polymers (characteristic in thermoplastic resins) behave as long linear chains of many links, each of which is free to rotate (Figure 2.2). Furthermore, these molecules are constrained by other molecules in the polymer melt so they can be modeled as being confined to a tube. Any movement of the molecule must be within this tube. Local movements of the chain in its tube cause it to slip out of the end of its original tube. Simultaneously to moving from the original tube, the chain is forming a new tube that represents the new constraints on its motion (Figure 2.3). Eventually after a long enough period of time has transpired, the chain will have no memory of the original tube and will be entirely within a new tube. This time is called the reptation time for the molecule. DeGennes [3] states that if one considers time intervals that are comparable to the reptation time, one can ignore the details of the movement of the chain in its tube take a macroscopic view of chain movement.

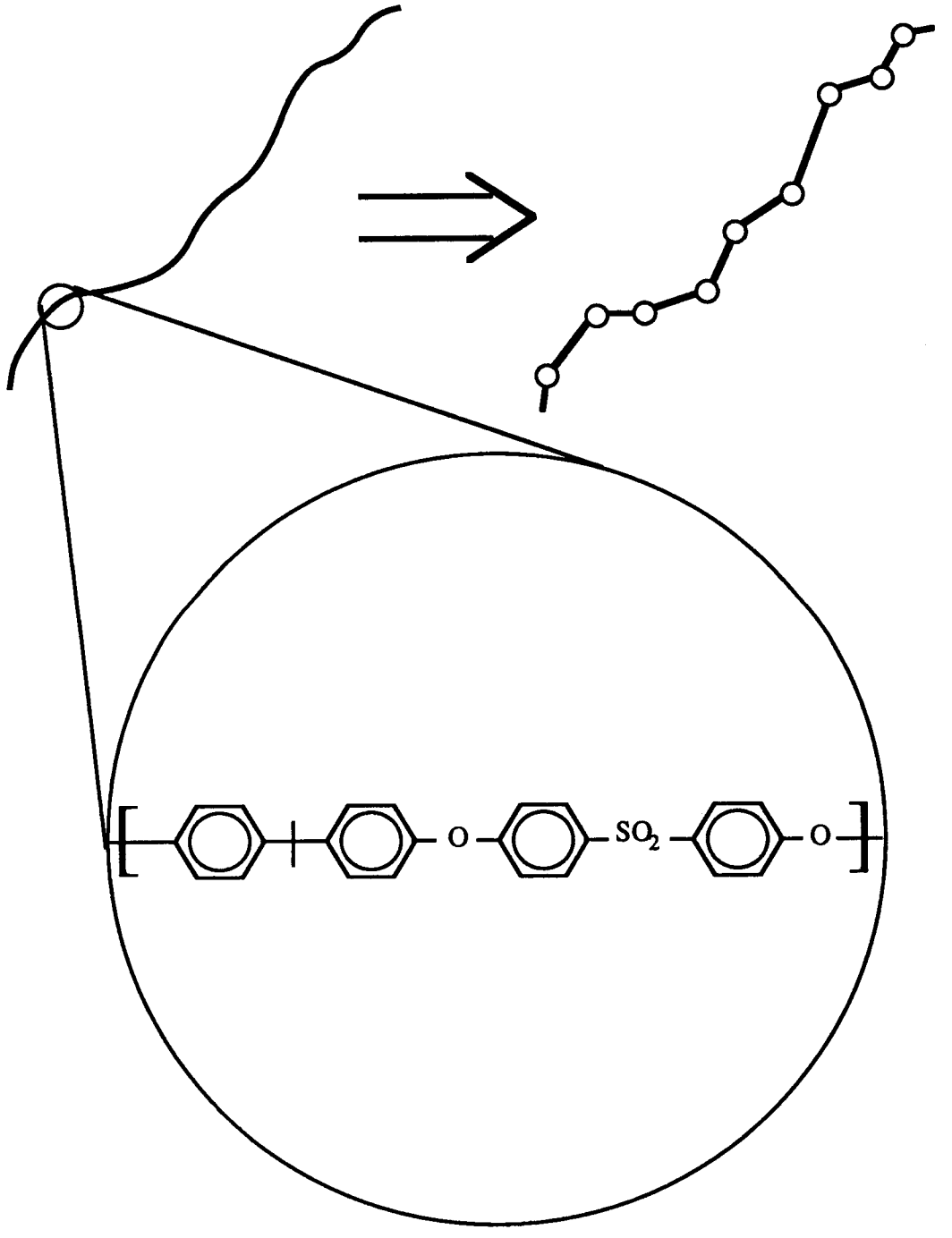

Figure 2.2. Representation of Polysulfone macromolecule by stiff chain segments attached by freely rotating joints. The structure of Polysulfone is shown in the magnified area.

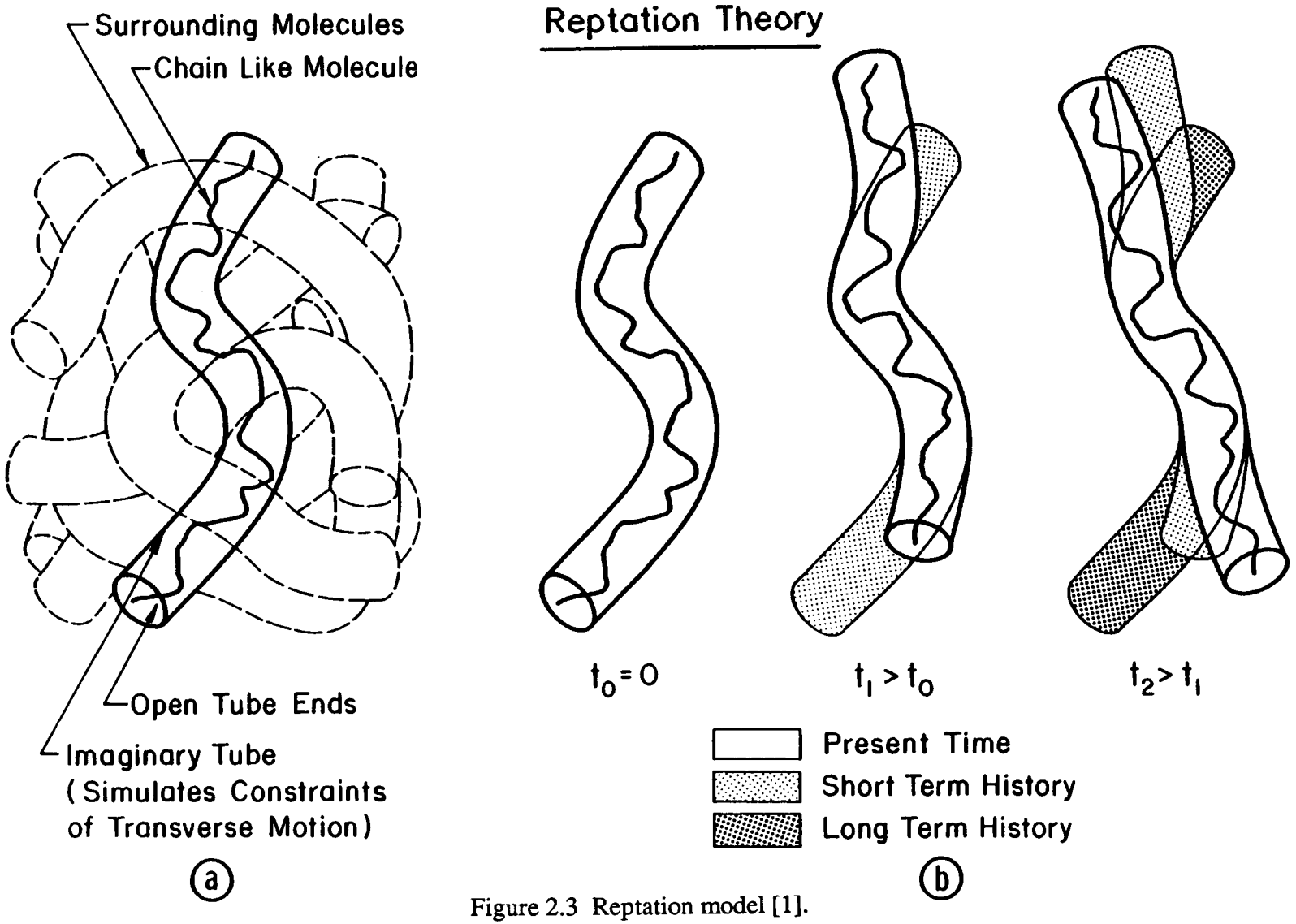

Figure 2.3 Reptation model [1].

Using this physical model, DeGennes derived relationships between the chain length, chain mobility, time, and length of chain diffused. Using Einstein's [3] diffusivity relation, DeGennes developed an expression for the mean square distance that the center of mass of the chain moves during time t

$$x^2 = 2D_{rep}\, t \qquad (2.1)$$

where x^2 represents the mean square distance that the center of mass of the chain moves, D_{rep} is the self-diffusion coefficient, and t is time. DeGennes subsequently shows that the root mean displacement of the center of mass of the chain becomes

$$x(t) \sim [S(t)]^{1/2} \sim t^{1/4} \qquad (2.2)$$

where S(t) is the length the chain has moved along its constraining tube.

The above relationships are the basis for models of crack healing and welding in high polymers developed by Wool, Wool and O'Connor, Jud et al., and Prager and Tirrell's [4,5,8,9,10]. The mechanistic and experimental approaches taken by each of these researchers are different; however, the conclusions and experimental results are similar.

2.1.2 Wool's Theories of Polymer Healing

Wool [4, 5, 8] and Wool and O'Connor [6, 7] reported in a series of papers theories explaining the interfacial strength development and crack healing in thermoplastic polymers. They redefine intimate contact of the surfaces as three separate temperature dependent mechanisms; surface rearrangement, surface approach, and wetting.

Diffusion is time, temperature and pressure dependent. In the case of instantaneous wetting, Wool defines total interfacial strength, σ as consisting of a wetting strength, σ_w and a diffusion dependent strength, σ_d . Using the Reptation model where $x \propto t^{1/4}$ (equation 2.2) and a fracture model to describe the formation of load bearing molecular entanglements in which $\sigma \propto x$, the time dependency of the diffusion strength can be determined as

$$\sigma_d = C(T)\, t^{1/4} \tag{2.3}$$

where C(T) is a temperature dependent constant. The total strength is given as

$$\sigma = \sigma_w + \sigma_d = \sigma_w + C(T)\, t^{1/4} \tag{2.4}$$

where the temperature dependence of C(T) can be modeled using different theories. Wool and O'Connor [6] suggest either an Arrhenius or Williams, Landel, and Ferry temperature dependence.

Because it is a function of surface energy changes, wetting strength (σ_W) is constant with respect to time for a given surface area. However, when two surfaces are brought into contact under external pressure, some areas will be in intimate contact immediately while others will come into intimate contact only after viscoelastic deformation of the surface has occurred. So, even though the wetting strength per unit area is a constant, the actual strength gain from intimate contact may be time dependent. Intimate contact must be established before diffusion can occur. Therefore, the effect of the intimate contact function will be to alter the time dependence of the relations derived above. If diffusion is not initiated immediately there will be another time dependent function due to diffusion initiation [6]. Due to the nonuniformity of the thermoplastic prepregs, it is reasonable to expect that complete intimate contact of the entire interfacial area will not be established immediately during composite processing. Therefore, to describe the processing of prepregs it will be necessary to account for a wetting function.

Wool also developed relationships to describe the autohesive strength for two different failure mechanisms, chain pull-out and chain fracture [8]. A chain pull-out failure is similar to the diffusion process of the polymer chains in reverse. Upon the application of an outside tensile load, the chains will disentangle from their constraints due to both the thermal motion and the energy supplied by the external load. The external load will cause the thermal motions to be driven in such a way that the polymer chains work away from the interface and precipitate failure. The chain pull-out mechanism of failure is favored at high temperatures (above T_g of the thermoplastic) and slow strain rates which allow the chains sufficient time to disentangle from the molecular entanglements.

Chain fracture failure occurs when the applied tensile load is great enough to cause the covalent bonds in the polymer backbone to fail before the polymer chain can disentangle from its constraints. Chain fracture failure is favored at low temperatures and high strain rates. If the polymer is tested well below the T_g, it is reasonable to assume that chain fracture is the major failure mechanism regardless of the strain rate because the free volume of the polymer is so low that the polymer chains have little overall motion. Whichever form of failure occurs, the time dependence of the relationships derived by Wool for the failure strength are the same; however the molecular weight dependence and the strain rate dependence vary with fracture mode[8].

Using the linear elastic fracture mechanics approximation, $G = \sigma^2/2E$, where G is fracture energy, E is the tensile modulus, and σ the tensile stress, Wool [6] also obtained the following relationships between fracture energy and contact time. Assuming instantaneous wetting and a negligible wetting strength, the critical strain energy release rate, G_{IC} is proportional to the square root of time .

$$G_{IC} \propto t^{1/2} \tag{2.5}$$

The stress intensity factor K_{1C} is related to the critical strain energy release rate by the relationship $K_{IC} \propto G_{IC}^{1/2}$ [18]. From this a relationship between the stress intensity factor K_{IC} and contact time can be written as

$$K_{IC} \propto t^{1/4} \tag{2.6}$$

Wool develops relationships between fracture energy and other parameters, a summary of which is given in reference [4].

2.1.3 Prager and Tirrell's Theories of Polymer Healing

Using DeGennes theory of polymer dynamics and a probability model that predicts the number of polymer chain bridges per unit area across the interface, Prager and Tirrell [9] derived two relationships that relate contact time to interfacial strength. The first,

$$\sigma \propto t^{1/2} M^{-3/2} \tag{2.7}$$

where M is molecular weight, applies to surfaces that have been held against a gas or inert surface long enough for the number of chain ends to reach equilibrium. In this situation the concentration of chain ends at the interface is less than in newly fractured surfaces because some of the chain ends will have reptated back into the bulk of the material. The second,

$$\sigma \propto t^{1/4} M^{-1/4} \tag{2.8}$$

applies to newly fractured surfaces and surfaces with many chain ends. The second of these relationships agrees with Wool's theories and with experimental data. Prager and Tirrell report no experimental results [9].

2.1.4 Jud, Kausch and Williams' Theory of Polymer Healing

Jud, Kausch and Williams [10] assume that the bond strength due to wetting is negligible and conclude that "to achieve practical strength," diffusion of the molecules across the interface is necessary. They assume that the strength of the interface is directly proportional to the number of links formed across the interface. The number of links per unit surface area is proportional to the average depth of penetration, Δx, of molecules which can be related to contact time through the Einstein diffusivity relationship

$$\langle \Delta x^2(t) \rangle = 2 D t \tag{2.9}$$

where D is the self-diffusion coefficient.

Using these assumptions they derived the following relationship for the strain energy release rate G_C.

$$\frac{G_c(t)}{G_{C0}} = \frac{n(t)\, A_0}{n_0\, A_0} = \left[\frac{t}{\tau_0}\right]^{1/2} \tag{2.10}$$

where G_{C0} represents the strain energy release rate of the undamaged material, n(t) represent the number of links across the interface after time t , n_0 represents the number of links across the interface in the undamaged or completely healed polymer, A_0 is the contact area, t is time, and τ_0 is the time to achieve complete healing of the interface. The stress intensity factor, K_I can be written as

$$\frac{K_I}{K_{I0}} = \left[\frac{G_C}{G_{C0}}\right]^{1/2} = \left[\frac{t}{\tau_0}\right]^{1/4} \qquad (2.11)$$

Jud et al. [10] performed crack healing tests on compact tension specimens made of poly (methyl methacrylate), PMMA and verified the relationship between K_{IC} and time given in equation (2.11). An Arrhenius temperature dependence was fit to the data which gave a measured activation energy of 274 kJ mol^{-1}. Absolute values of the self-diffusion coefficient for PMMA were also calculated in this study.

2.1.5 Bothe and Rehage's Model of Autohesion

Bothe and Rehage [12] derived a relationship between contact time and interfacial tensile strength. Using Einstein's equation for diffusion and a molecular description of the interface which assumes that strength is proportional to the number of molecular segments diffusing across the interface in time t, they derived the following relationship between adhesive strength and the square root of contact time

$$\sigma_H = k\left[\frac{\rho}{M}\right]^{2/3} D^{1/2}\, t^{1/2} + \sigma_A \qquad (2.12)$$

where σ_H is the adhesive or autohesive strength, k is a proportionality constant, ρ is the density, M is the molecular weight, D is the self-diffusion coefficient, t is time, and σ_A is

an initial adhesion independent of time.

Bothe and Rehage introduce the concept of saturation pressure. Saturation pressure is defined as the pressure above which, at constant time and temperature, no further increase in pressure produces an increase in bond strength. They report experimental results that support equation (2.12) and also the existence of two different failure mechanisms, chain fracture and chain pull-out [12].

2.1.6 Autohesion in Elastomers

A number of other researchers, many of them in the rubber industry, have studied the formation of bonds in polymers and elastomers [13-16]. None of the papers reviewed derived time and temperature dependent mechanisms or models to predict formation of autohesive bonds; however, they do present interesting data and qualitative explanations for the observed results.

Bauer [13] studied tack in rubbers and determined that diffusion and intimate contact are the important mechanisms behind good bonds. Bauer assumes that the molecules diffuse due to relaxation of local stress concentrations and that the diffused molecules are held in the network by secondary bonds which can slip upon application of stress. He also assumes that diffusion is instantaneous and differences in strength between samples are due to differences in actual contact area (i.e., that the strength of the bond is constant).

Rhee and Andries [14] also studied autohesion in rubbers and elastomers. They state that

bond strength is caused by a diffusion-adsorption (molecular attractions between the surface molecules) process. They tested a number of rubbers for the effect of different parameters including aging, molecular weight, processing oil, and particle size of additives.

Hamed [15] studied rubbers for the effects of surface roughness, green strength, different molecular weights and blends, testing rate, contact load, and time. Hamed concludes that interdiffusion, while important, does not control tack in the samples tested.

Boenig, Willer and Shottafer [16] studied urethan elastomers for the effects of contact time, bonding pressure, time left to oxidize in ambient air, and solvents. They state that chain diffusion is the controlling mechanism behind bond formation and that the temperature dependence can be modeled using an Arrhenius equation.

2.2 Test Methods

In order to measure the autohesion and self-diffusion of high polymers, a number of test methods have been used. They can be crudely broken down into two approaches: 1) Direct measurement of the movement of molecules through the use of tagged molecules (normally radioactive) and a detector to measure the penetration or movement of these molecules with respect to time; 2) Indirect measurement by mechanical tests that measure properties dependent on the diffusion of the molecules. This study is concerned only with the latter testing method.

In mechanical tests the two polymer surfaces are normally pressed together at a given temperature for a specified length of time. The fracture stress or fracture energy of the interface is then measured using the appropriate test.

Tack measurements, used by Skewis [11], Bauer [13], and by Rhee and Andries [14], measure the interfacial tensile strength of two surfaces that have been pressed together under pressure for a known time. All of the tack tests were performed at room temperature which was well above the T_g of the elastomers being studied.

Fracture toughness tests were performed by Wool and O'Connor [6,7] and Jud et al. [10]. Wool and O'Connor studied the rehealing of elastomers with double cantilever beam toughness tests, and rehealing of PMMA and polystyrene with Izod impact tests. The polymers were healed above the T_g of the polymer in question. Jud et al. used a compact tension fracture toughness test to measure autohesion in rehealed PMMA specimens. The specimens were rehealed in a hot press at temperatures above the T_g of PMMA (approximately 100°C).

Hamed [15] investigated tack formation by using a T-peel test of polymer spread over a flexible base. A T-peel test measures the energy required per unit area to separate the two surfaces. The polymer was dissolved in a solvent and spread on a flexible base. Two strips of the polymer/base material were pressed together for a measured time and then the strips were separated in a tensile testing machine.

Interfacial tests were performed by Wool and O'Connor [7], Boenig et al. [16], Dara and

Loos [1], and Bothe and Rehage [12]. Wool and O'Connor used notched tensile bars of HTPB that were fractured and healed to evaluate fracture stress, fracture strain, and fracture energy as a function of healing time. Boenig et al. used the ASTM D412-51T, type C tensile test to measure tack in urethran elastomers [16]. Dara and Loos used a parallel plate plastometer fitted with a tensile/compressive load cell to measure autohesion in P1700 polysulfone resin The specimens were bonded at elevated temperature and mechanically tested at the bond temperature in a nitrogen purged atmosphere. Bothe and Rehage used a through the thickness tensile test at room temperature to test autohesion in polybutadiene (BR), crosslinked acrylonitrile-butadiene copolymer (NBR), ethylenepropylene copolymer (EPM) and polychlorobutadiene (CR). They studied the effects of contact pressure, contact time, polymer structure, and strain rate.

A close examination of the literature reveals that only a few studies have addressed autohesion of thermoplastic resins suitable for use as matrix materials for advanced composites. Furthermore, autohesion in fiber-reinforced thermoplastic composites has received almost no attention.

3.0 Experimental Procedure

In most of the tests described in the last chapter the specimens were healed and mechanically tested at temperatures well above the glass transition temperature of the polymer. Based on the theories presented in Section 2.1, it is reasonable to assume that the interface will continue to heal during mechanical testing.

Jud et al. [10] healed PMMA samples above the glass transition temperature and cooled the specimens to ambient temperature before testing. This approach eliminates healing during mechanical testing but introduces thermal effects such as non-isothermal healing during heat up.

In order to reduce the effects mentioned above, a testing program was designed that allowed better control over the healing parameters. The first test, an interfacial tension test, was designed to allow the polymer to reach a setpoint temperature before the two surfaces were brought into contact. After healing, the polymer specimens were cooled to room temperature (well below the T_g) for mechanical testing. The second test, a compact tension test, followed the experimental procedure used by Jud et al [10]; however, transient thermal effects were accounted for in the data analysis.

3.1 Materials

The polymer system used in this study was polysulfone thermoplastic resin. It was chosen due to availability and low cost. Other investigations have characterized both the rheological and some of the autohesive properties of this polymer thus allowing comparisons to be made between previous studies [1, 17, 18, 19, 20] and the present study.

The neat resin, UDEL® P1700 polysulfone manufactured by Union Carbide Corporation, was obtained in a sheet 1.575 mm (0.062 in.) thick and in an annealed sheet 6.35 mm (0.25 in.) thick from Westlake Plastics Company. The prepreg consisted of UDEL® P1700 (bead form) polysulfone polymer impregnated on Hercules AS-4 graphite fibers. The U.S. Polymeric Division of Hitco prepregged the AS-4 fiber with the P1700 Resin using the solvent cyclohexanone to achieve fiber wetting.

3.2 Testing Facilities and Equipment

Mechanical testing was performed at NASA Langley Research Center using an Instron mechanical testing machine equipped with a 1000 lb. resistance type load cell that could be calibrated to measure 0-100 lb. full scale (Figure 3.1). Load versus time was plotted on a chart recorder with the chart speed dependent upon the test being run.

Healing of the interfacial specimens and the compact tension (CT) specimens was

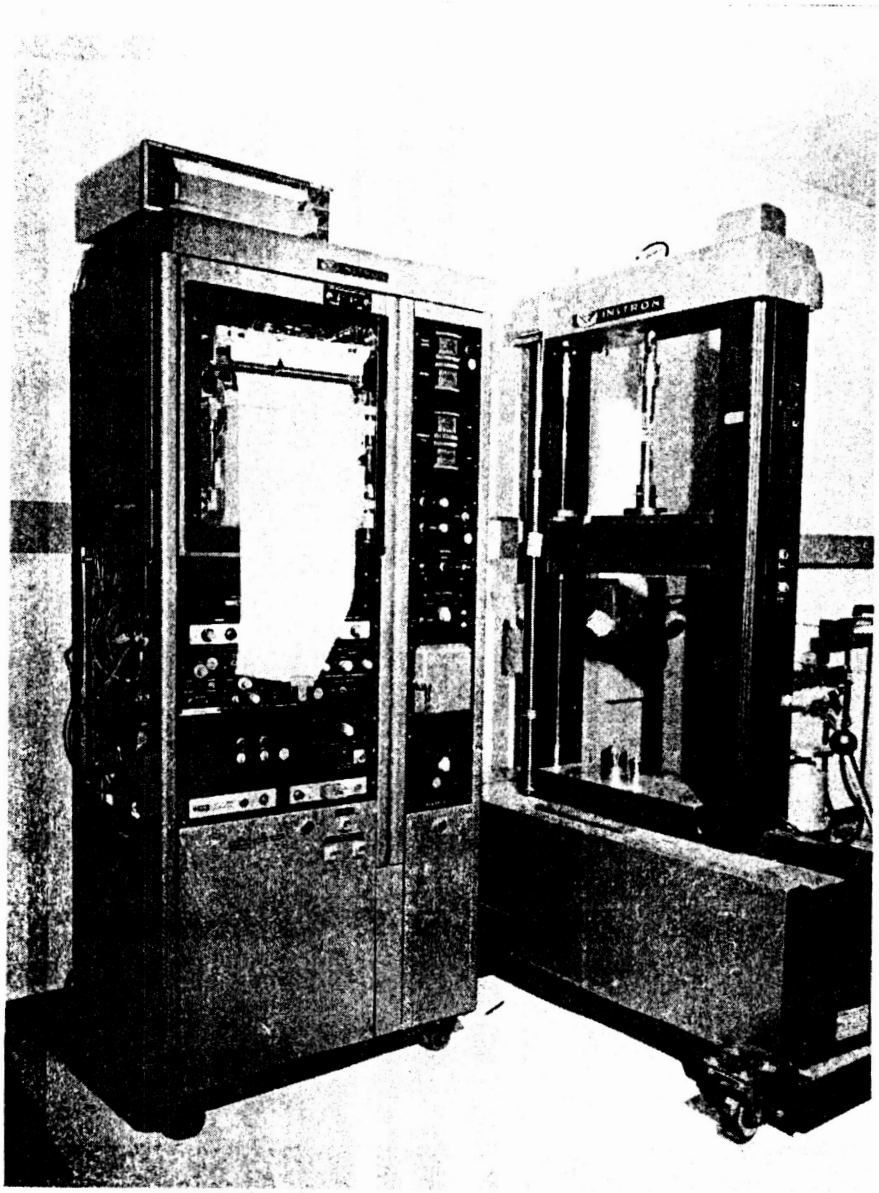

Figure 3.1 Instron mechanical testing machine used in this study.

performed in a forced air oven manufactured by Blue M, Incorporated (Figure 3.2). The oven had a closed-loop temperature control system that was monitored by a digital readout. The double cantilever beam (DCB) specimens were rehealed in a Wabash hot press with closed-loop heating and cooling systems on both the upper and lower platens (Figure 3.3).

3.3 Interfacial Tension Test

3.3.1 Sample Preparation

The 1.575 mm (0.062 in.) thick sheet was supplied in a nonannealed 2.58 m x 1.29 m (8 ft. x 4 ft.) sheet. The sheet was annealed in an oxygen purged nitrogen oven for 20 to 48 hours at 200°C and then for 2 hours at 220 to 225°C. The nitrogen oven was used to minimize oxidation of the polymer surface during annealing. A separate infrared (IR) surface analysis was performed on polysulfone samples that were processed in a forced air oven at 200°C for 24 hours followed by 220°C for 3 hours. No surface oxidation was detected by the IR analysis. Based on the information obtained from infrared analysis, all rehealing of the polysulfone was done in forced air ovens; however, annealing was still performed in a nitrogen atmosphere due to the long exposure periods at elevated temperature.

The interfacial tension test required 28.58 mm (1.125 in.) diameter disks of the polysulfone. These were punched from the annealed sheet using an Osborne arch punch.

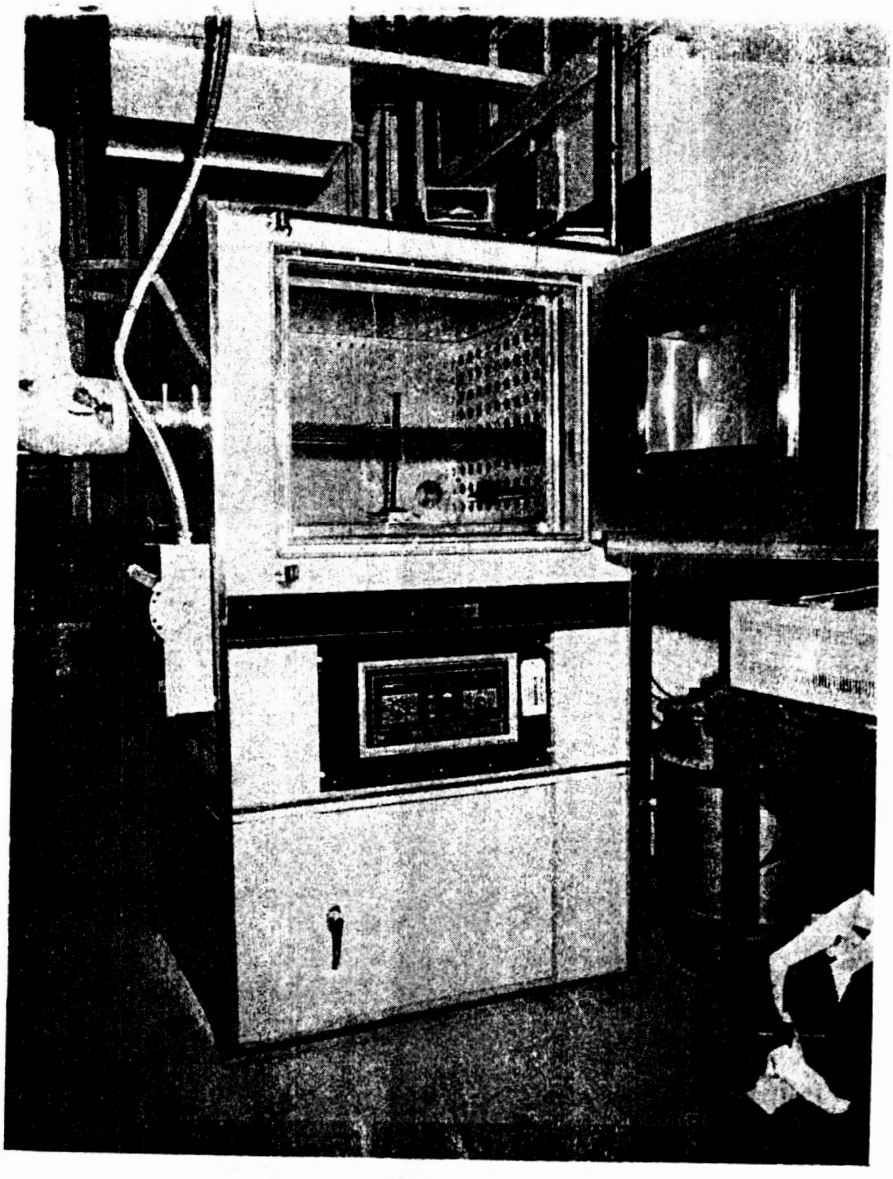

Figure 3.2 Blue M oven used for the neat resin healings.

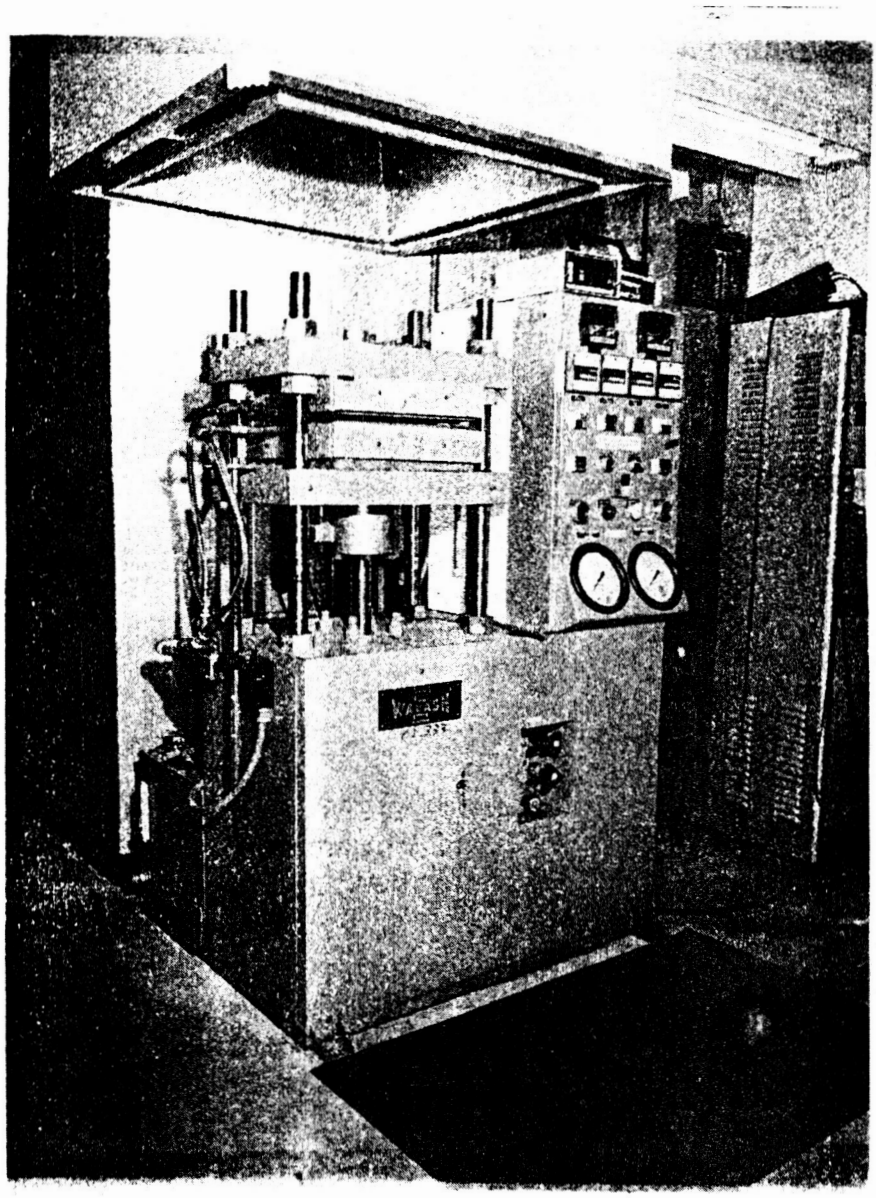

Figure 3.3 Wabash press used to heal the DCB specimens.

ORIGINAL PAGE IS
OF POOR QUALITY

A 50.8 mm (2 in.) diameter disk was punched from a 0.0254 mm (1 mil) thick sheet of Kapton. A central hole 12.7 mm (0.5 in.) in diameter and three 3.175 mm (0.125 in.) holes spaced 120° apart and 15.875 mm (0.625 in.) from the center were punched in the Kapton disk as shown in Figure 3.4. The purpose of the Kapton was twofold. First, it reduced the cross sectional area of the polysulfone so that during testing, failure would be ensured at the bonded interface rather than at the polymer to metal adherend bond. Second, when the disks were punched, stresses and strains were introduced along the edge of the annealed disk. The Kapton prevented the edges from touching and ensured that only stress free areas of the disk healed.

3.3.2 Testing Procedure

Prior to use, each polysulfone disk was inspected under crossed polarizers and a low power optical microscope (x20). If surface irregularities, stress concentrations, or gel particles were apparent, then that specimen was discarded.

Two polysulfone disks were placed in the bonding fixture separated by the Kapton film, as shown in Figure 3.5. The bonding fixture consisted of a base plate with three 3.175 mm (0.125 in.) diameter alignment pins located around the circumference of a 28.575 mm (1.125 in.) circle at regularly spaced intervals and a weight that fit over the alignment pins free to slide up and down (Figure 3.6). The weight was used to apply contact pressure to the specimen and was attached to a rod protruding from the top of the oven. The assembly was placed in a forced air oven preheated to the desired bonding

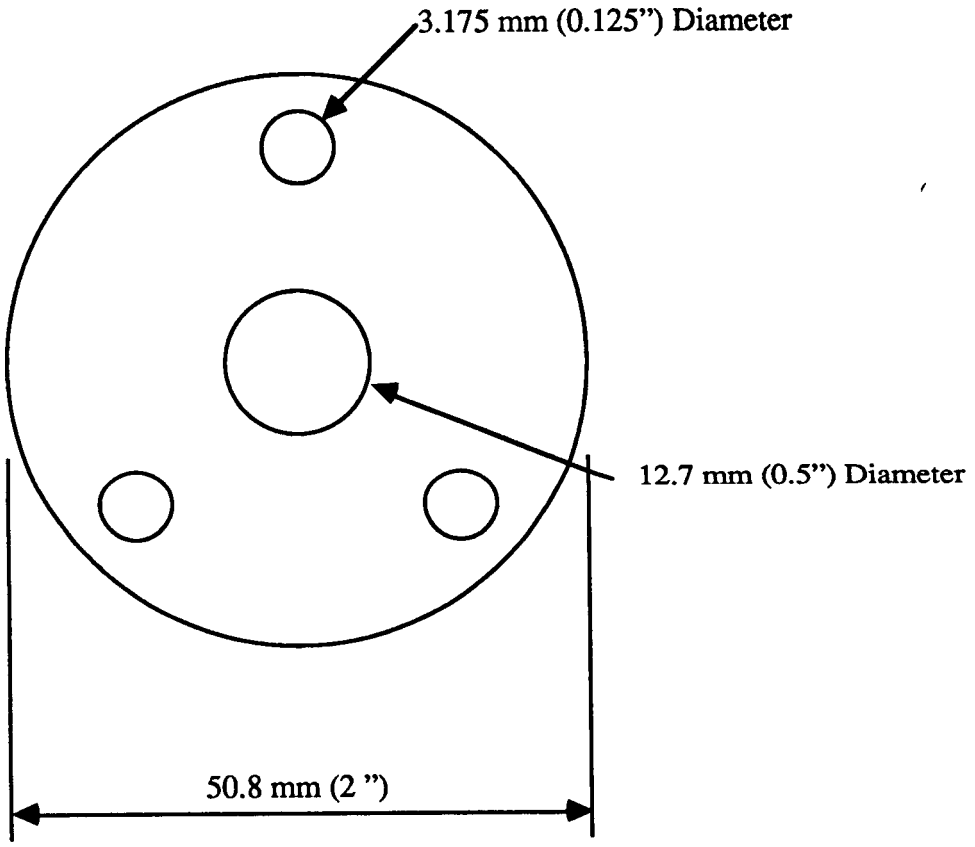

The alignment pins fit through the smaller holes (3.175 mm) and the test section is the larger 12.7 mm hole.

Figure 3.4 Dimensions of Kapton disk.

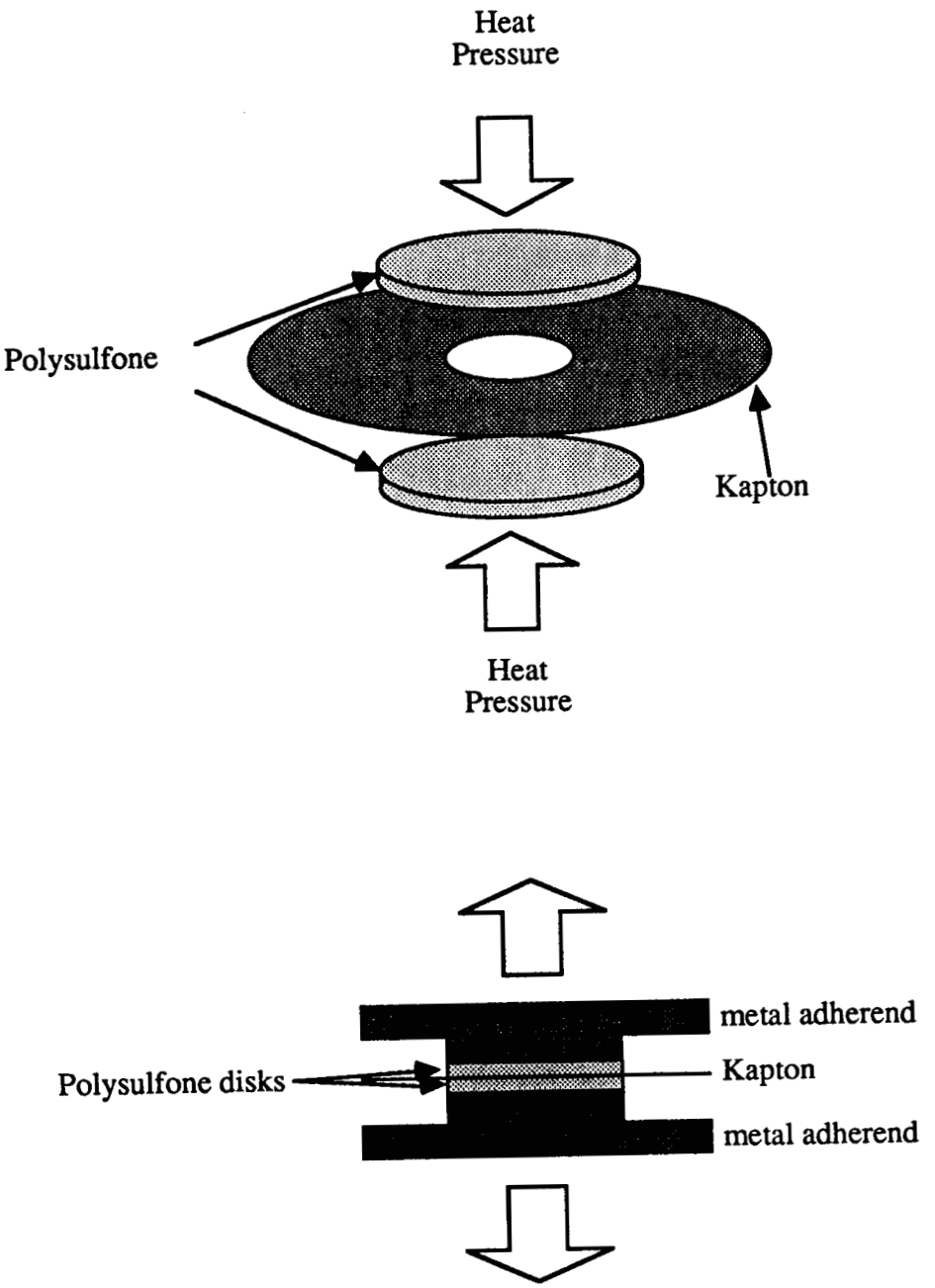

Figure 3.5 Schematic of interfacial test assembly.

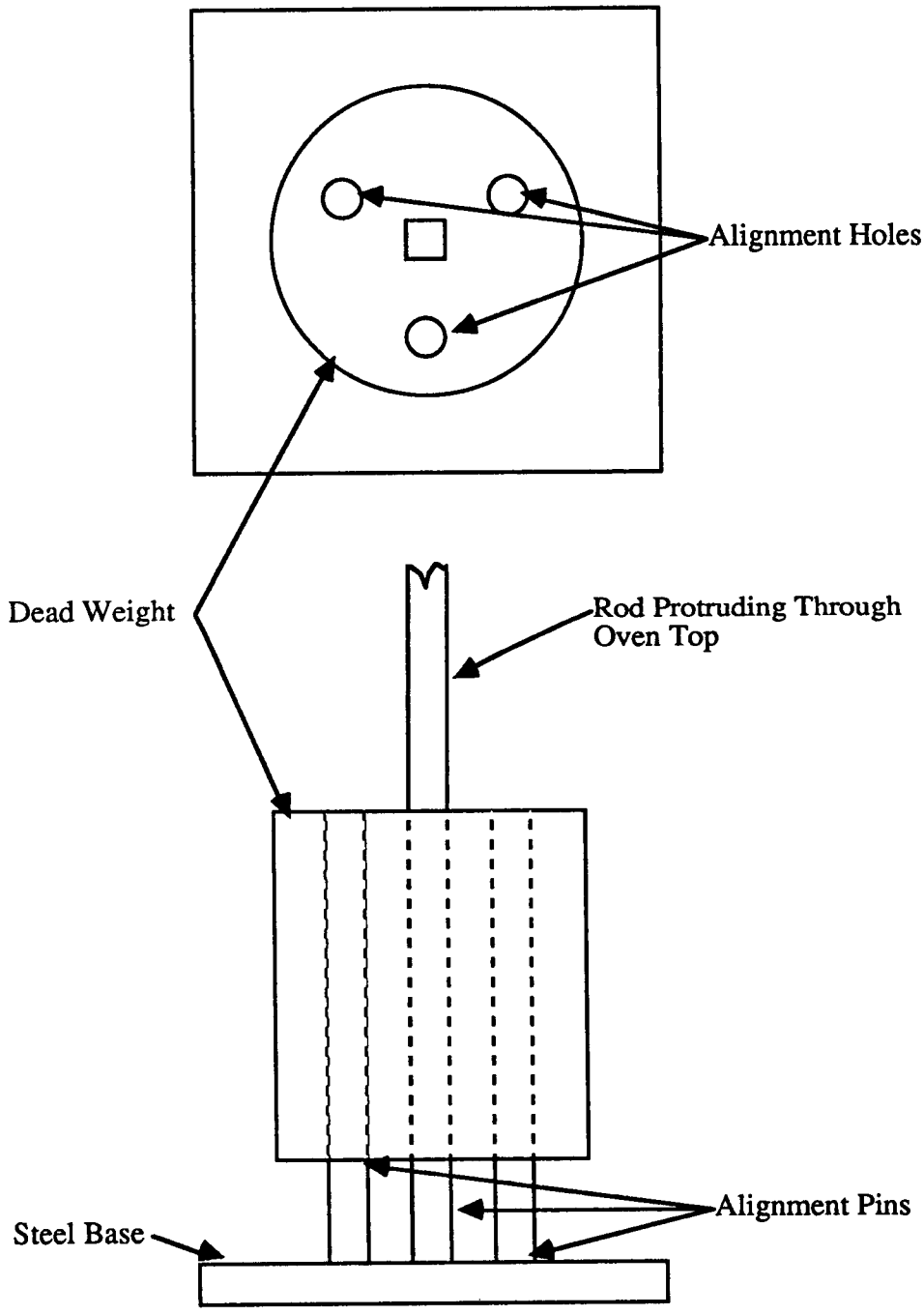

Figure 3.6 Schematic of interfacial test bonding fixture.

temperature and allowed to reach the oven temperature. Temperature of the specimen was monitored by a thermocouple attached to the base of the fixture.

Upon reaching the setpoint temperature, external pressure was applied to the specimen by a dead weight. A 6.45 kg (14.2 lb.) weight was applied for 15 seconds followed by 1.87 kg (4.1 lb.) weight for the remaining bonding time. The high initial pressure ensured initial contact of the entire interface, but resulted in excessive flow and specimen deformation if left on for extended periods of time. Based on Wool's theories, once the polymer is in intimate contact, additional pressure is not necessary for bonding [4, 8]. The low pressure was applied only to ensure that the samples remained in contact without excessive flow during the longest tests. Therefore, high pressure was applied only for a short time to ensure initial contact and the low pressure was maintained to ensure continuous contact throughout bonding.

The disks were bonded for a given time and temperature. After processing, the healed specimens were removed from the bonding fixture and allowed to cool to ambient temperature. If the disks were not bonded following processing, they were recorded as a no bond specimen and discarded.

Following the procedure in the ASTM Test for Tensile Properties of Adhesive Bonds (D897-78), the healed disks were bonded to sandblasted and degreased metallic parallel plate fixtures using a room temperature cure epoxy adhesive (Figure 3.5). The epoxy was allowed to dry for at least one hour and then the specimen thickness was measured with a micrometer. If the thickness of the specimen varied by more than ±0.3 mm around its

circumference, then it was discarded. This range was set because specimens with thickness variations greater than ±0.3 mm consistently had low autohesive strengths. The test specimen was inserted between self-aligning grips attached to the fixed and moveable members of an Instron mechanical testing machine. All mechanical measurements were made in tension at room temperature with constant crosshead speeds of 0.05, 0.25, and 0.5 mm/min (0.002, 0.01, and 0.02 in/min).

3.3.3 Data Reduction

Autohesive strength as a function of bonding time and temperature was calculated from the maximum recorded load divided by the cross sectional area of the center hole in the Kapton disk. The results from identical tests were averaged and the standard deviation of the data calculated.

3.4 Compact Tension Toughness Test

3.4.1 Sample Preparation

The CT specimen geometry is shown in Figure 3.7. Prior to testing the samples had to be sized. In CT tests the main concern is to ensure the sample is thick enough to guarantee plane strain conditions across most of the crack front. The specimens were sized using the requirement in the ASTM Test for Plane-Strain Fracture Toughness of Metallic Materials (E399-81), that the sample thickness, b, be greater than $2.5\ (K_c / \sigma_{ys})^2$. Using

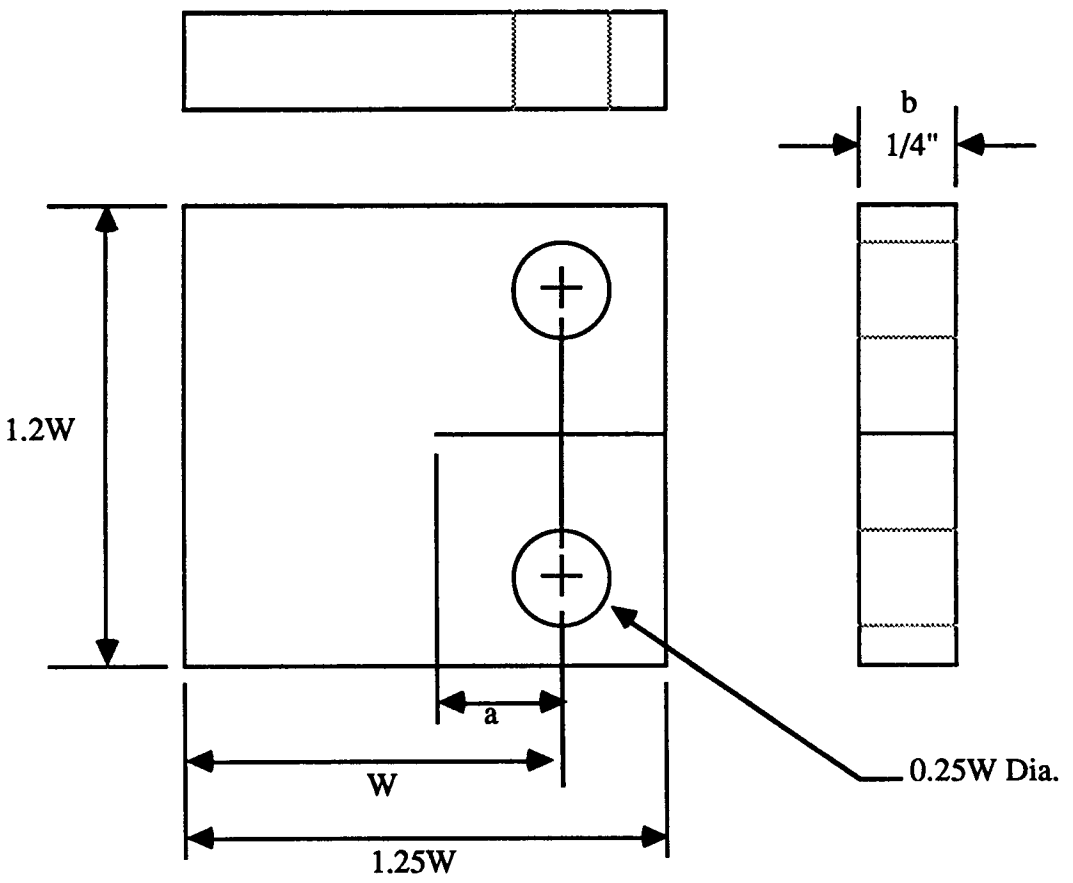

Figure 3.7 Schematic of compact tension specimen.

the highest toughness reported for polysulfone of 3.4 MPa-$m^{1/2}$ [17] and the yield strength of 70.3 MPa (10,200 psi.) reported by Union Carbide, a minimum thickness of 5.8 mm (0.230 in.) was calculated. The width and height of the specimen were determined by selecting the dimension of W in Figure 3.7 to be 25.4 mm (1 in.). This ensured that the crack length, a, was large compared with the size of the plastic zone. The requirements on the dimensions of a, from the ASTM standards, are a > b which is satisfied by taking W of 25.4 mm and ensuring the initial crack length, a is greater than b. Hinkley [17] used smaller CT specimens (W of 12.7 mm), also satisfying the ASTM conditions, of both polysulfone and other tough polymers with great success.

Specimens were cut from the 6.35 mm (0.25 in.) thick annealed sheet and machined to size. Sharp, naturally arrested cracks were introduced into the specimens by driving a new, chilled razor blade into the sawed notch. The samples were examined between crossed polarizers and those with stress concentrations near the crack tip were discarded.

3.4.2 Testing Procedure

The CT specimens were placed in the Instron machine (Figure 3.8) and fractured at a crosshead speed of 0.5 mm/min (0.02 in./min). Peak load and crack length were recorded for calculation of the critical stress intensity factors. If the maximum load was followed by stable crack growth, the crosshead was stopped. The new crack length was marked on the specimen, the specimen was unloaded and reloaded until the load peaked again. Using this procedure up to four measurements could be obtained from each specimen;

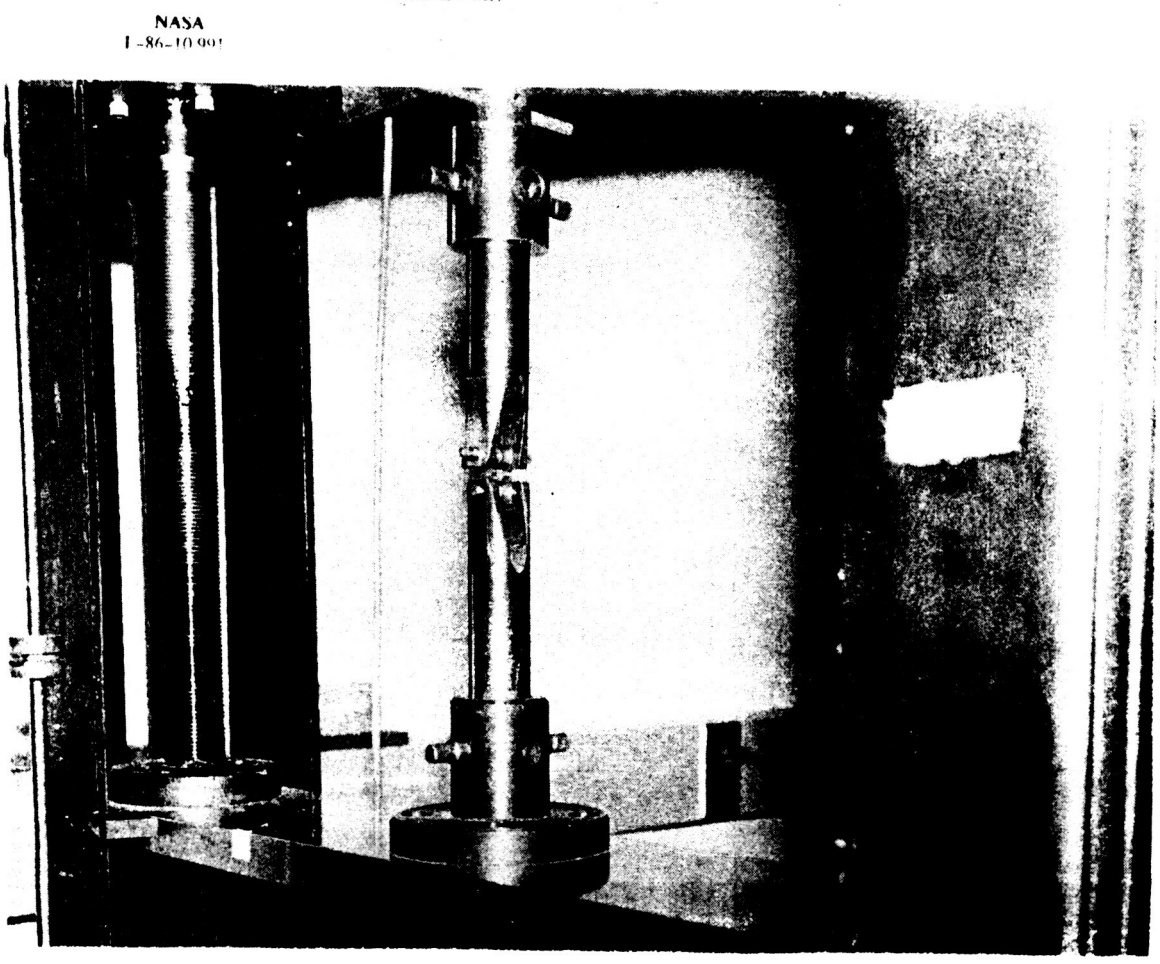

Figure 3.8 CT specimen in Instron testing machine.

however, some specimens had unstable crack growth and only one measurement could be recorded.

If the specimen was still in one piece following the fracture test it was used for a rehealing test. A sliver of 0.0127 mm (1/2 mil) thick Kapton was placed in the crack end and the specimen was wrapped in a sheet of 0.0254 mm (1 mil) thick Kapton. The Kapton sliver ensured that the same crack plane initially tested was broken upon retesting, and the Kapton wrap prevented the specimen from sticking to the rehealing fixture. To ensure dryness, the specimens were kept in a vacuum oven at 100°C for at least 24 hours prior to rehealing.

The CT specimens were rehealed by processing at elevated temperatures in a forced air oven for a specified length of time. The rehealing fixture was preheated to the test temperature. The Kapton wrapped CT specimen was placed in the preheated fixture and external pressure was applied to the specimen by a dead weight, as shown in Figures 3.9 and 3.10. After the desired rehealing time, the specimen was removed from the oven and allowed to cool in ambient air. The Kapton wrapping was removed and the rehealed specimen was visually inspected for holes, cracks or flaws near the crack tip. If the specimen was free of defects, it was retested according to the aforementioned procedures.

3.4.3 Data Reduction

Critical stress intensity factors were calculated using the following formulas

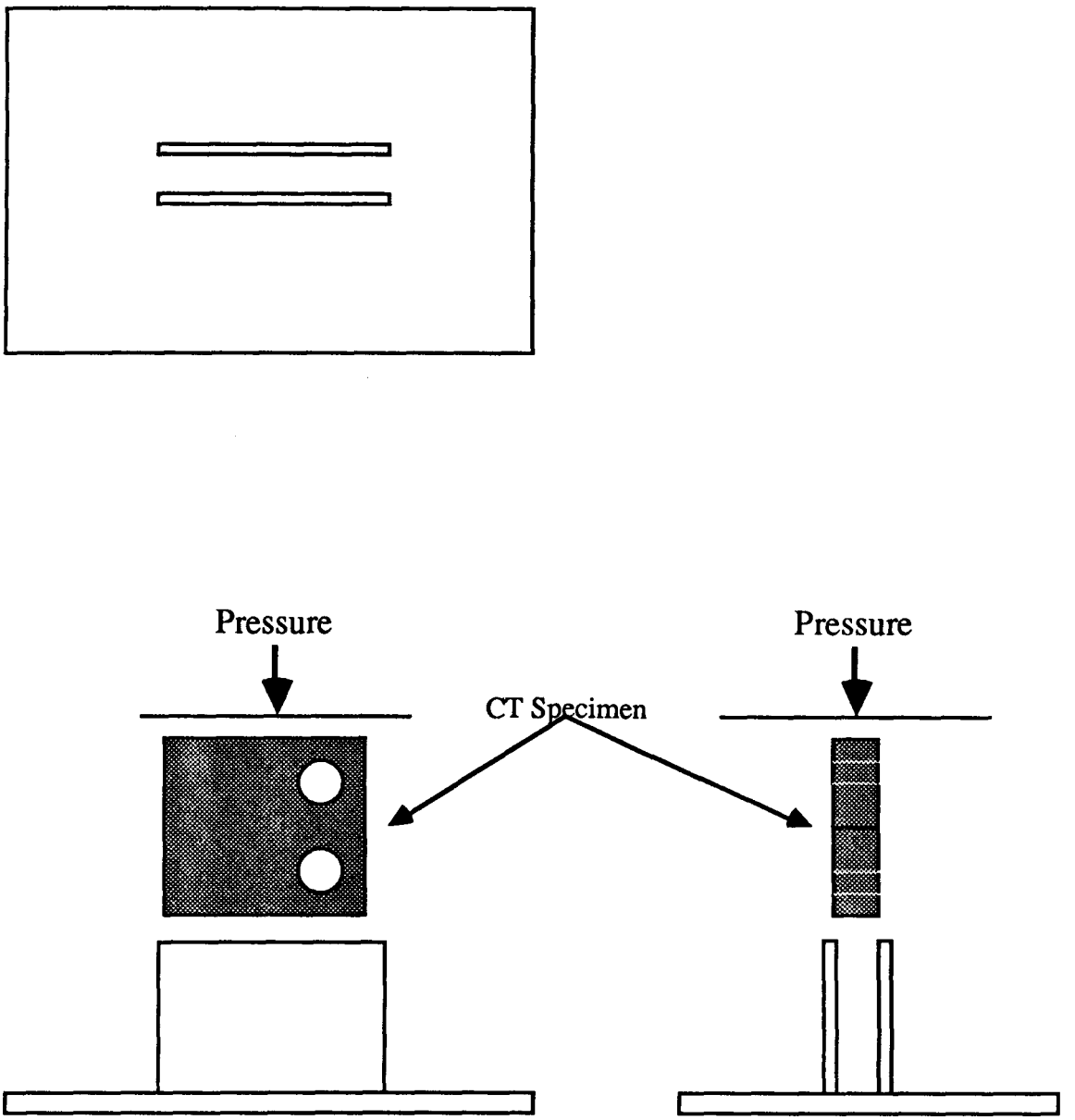

Figure 3.9 Schematic of CT specimen healing fixture.

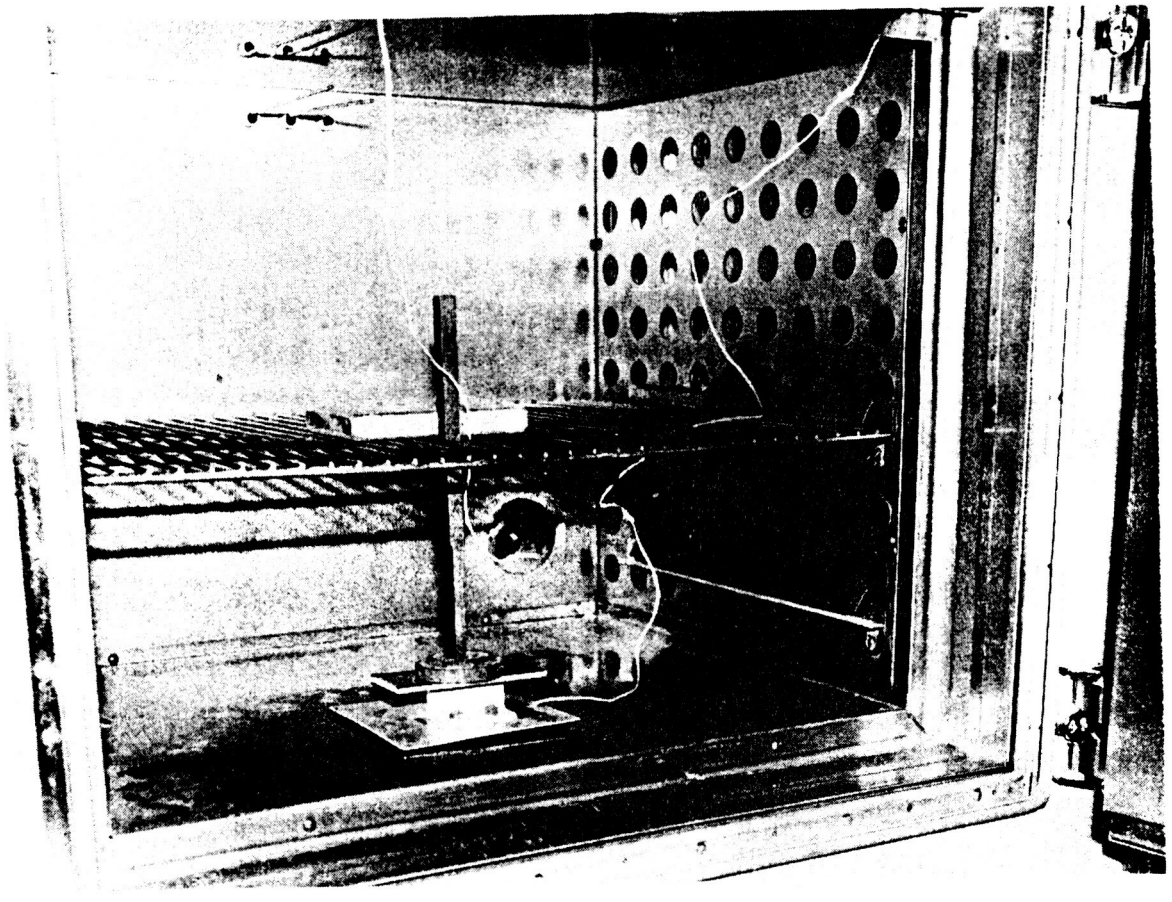

Figure 3.10 CT healing fixture and weight in Blue M oven.

$$K_c = \frac{P_c Y}{(b W^{1/2})} \tag{3.1}$$

where P_c is the peak load recorded by the chart recorder and Y is a geometrical factor for the compact tension specimen calculated as follows

$$Y = \frac{(2+X)(0.886 + 4.64X - 13.32X^2 + 14.72X^3 - 5.6X^4)}{(1-X)^{3/2}} \tag{3.2}$$

The parameter X is defined as

$$X = a/W \tag{3.3}$$

where a and W were previously defined in Figure 3.7 [17]. Values of X should fall between [17]

$$0.2 \leq a/W \leq 1.0.$$

The crack length used in the calculations was the average of the crack lengths measured on both sides of the specimen as the crack did not always grow perpendicular to the specimen sides. Critical strain energy release rates, G_{IC} can be calculated from the critical stress intensity factor by assuming that the material is linearly elastic and in a state of plane strain [21] as follows

$$G_{1C} = \frac{K_{1C}^2 (1.0 - \upsilon^2)}{E} \qquad (3.4)$$

where E is tensile modulus, K_{1C} is the critical stress intensity factor and υ is Poisson's ratio.

3.5 Double Cantilever Beam Composite Test

3.6.1 Sample Preparation

Unidirectional composite specimens were fabricated from AS4 / P1700 polysulfone prepreg tape using a processing cycle developed at NASA Langley Research Center. The specimens were 12 plies thick and were compression molded in a 76 mm (3 in) square steel mold. During lay-up, a 25 mm (1 in.) wide piece of 0.0127 mm (0.5 mil) thick Kapton was placed along one edge of the specimen at midplane for crack initiation.

The composite fabrication procedure is outlined as follows:

1. Cut prepreg that has been warmed to room temperature into 305 mm x 330 mm (12" x 13") sheets.
2. Dry prepreg in forced air oven for 16 hours at 100 °C then at 200 °C for 1 hour to remove any remaining solvent.
3. Cut into 76 x 76 mm (3" x 3") squares and stack 6 plies in mold. Place a 25 x 76 mm

(1" x 3") piece of Kapton film at one end of the mold. Then stack six more plies of prepreg over Kapton.

4. Free coat mold and place in preheated hot press.
5. Process at 370°C (700 °F) and 6900 kPa (1000 PSI) for 15 minutes.
6. Cool in ambient atmosphere and remove panel from mold.
7. C-scan panel for defects.

None of the panels C-scanned had any detectable defects other than the Kapton film.

DCB specimens were cut from the panels using a water cooled diamond edged saw. 4 to 5 specimens 12.7 mm (0.5 in.) wide were obtained from each panel. The sawed specimens were prepared for testing by bonding aluminum tabs to the precracked end of the DCB specimen for load introduction. The tabs were affixed with a room temperature cure epoxy and aligned by balancing the beam vertically on a non-stick surface of polyethylene, or Kapton. A schematic diagram of the test specimen is shown in Figure 3.11. The sides of the DCB specimen were painted with a water based white correction fluid to aid in measuring the crack length.

3.5.2 Testing Procedure

The DCB specimens were fractured at a crosshead speed of 0.5 mm/min (0.02 in./min) in the Instron mechanical testing machine (Figure 3.12). Peak load, crack length and a chart recording of load versus time were recorded for calculation of mode 1 critical strain energy release rates. In most of the specimens, the maximum load was followed by

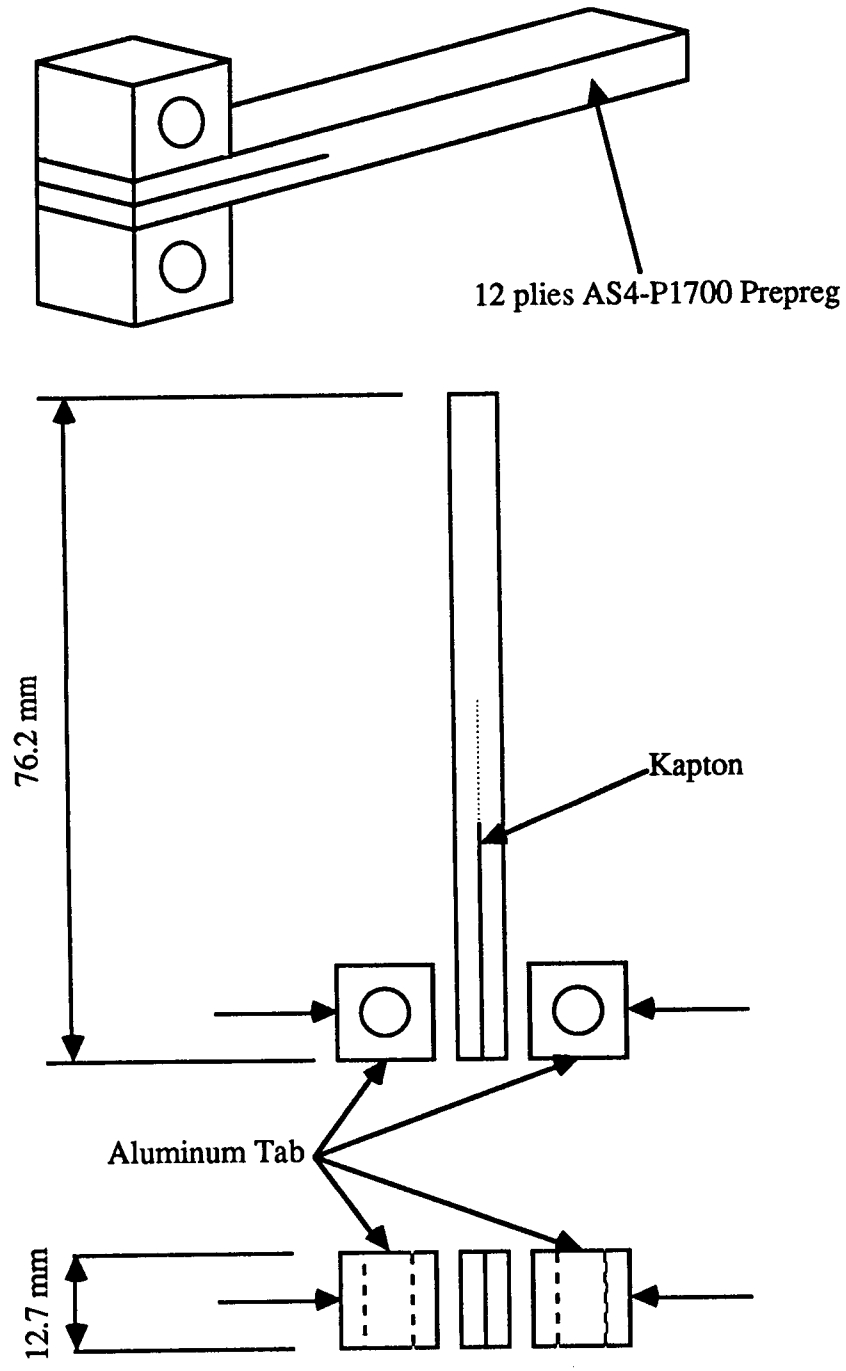

Figure 3.11 Schematic of DCB specimen.

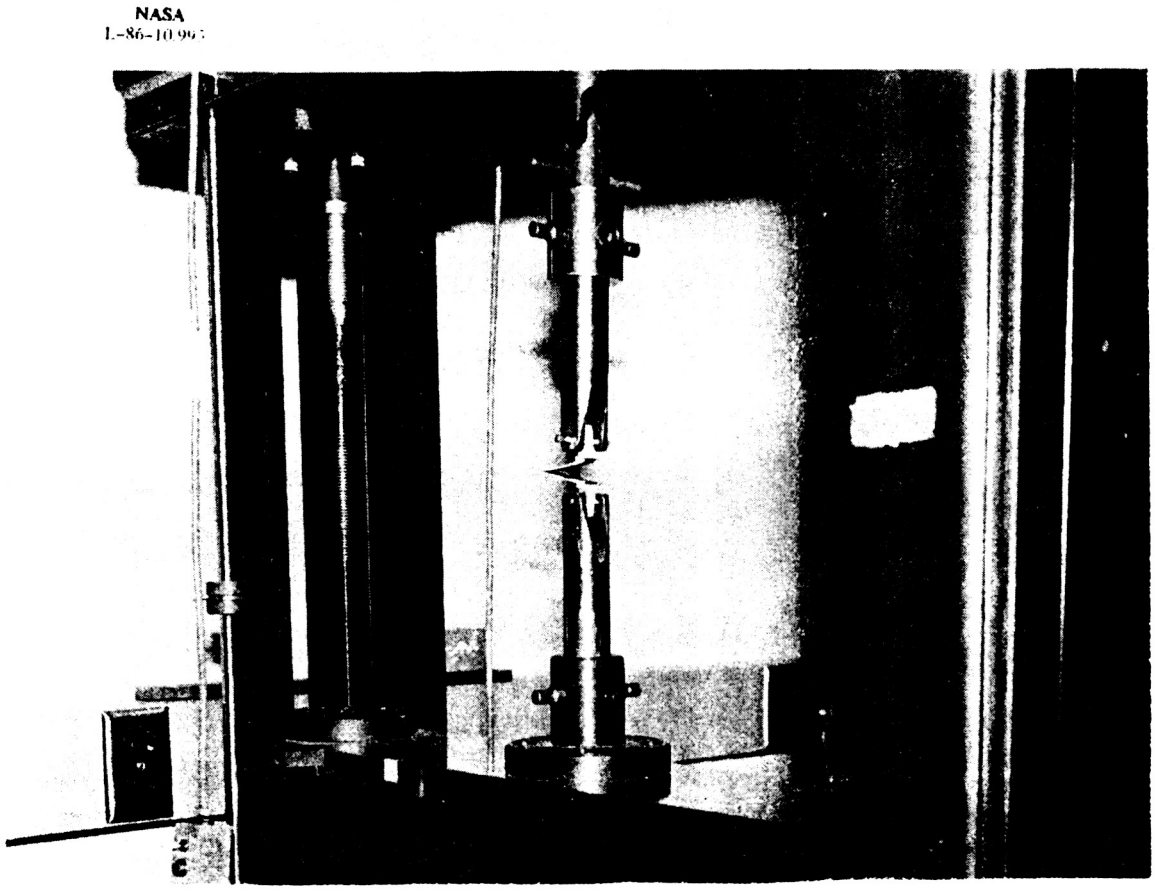

Figure 3.12 DCB specimen in Instron testing machine.

stable, slow crack growth. For these cases, the crosshead was stopped and one minute allowed for the crack to stop growing. The new crack length observed on both sides of the specimen was marked, the specimen was unloaded to at least one third of peak load, and the crosshead was started down again. This procedure was followed until the crack had grown to within 13 mm (0.5 in.) of the end of the sample and 8 to 10 measurements had been obtained. The crack was allowed to propagate approximately 6 mm (0.25 in.) for the first measurement and 7 to 13 mm (0.3 in. to 0.5 in.) for the later measurements where the beam properties were changing more slowly.

If the DCB specimen remained in one piece it was used for a rehealing test. The samples were placed in a special alignment fixture and rehealed for a predetermined time at a set temperature in the Wabash press.

Before rehealing, the specimen thickness was measured with a micrometer. If it was less than 7.62 mm (0.300 in.), Kapton shims were placed under the specimen to bring the total thickness to 7.62 mm (0.300 in.). The thickness was critical to ensure that all specimens were slightly above the rehealing fixture and pressure was applied to the specimen rather than the fixture. The rehealing fixture and hot press are shown in Figures 3.13 and 3.14, respectively.

The rehealing fixture and the Kapton shims were coated with a Teflon release substance to prevent sticking and preheated in the press to the desired temperature. The DCB specimen was placed in the rehealing fixture and the press was closed. The sample processing time was measured from when the pressure transducer on the press

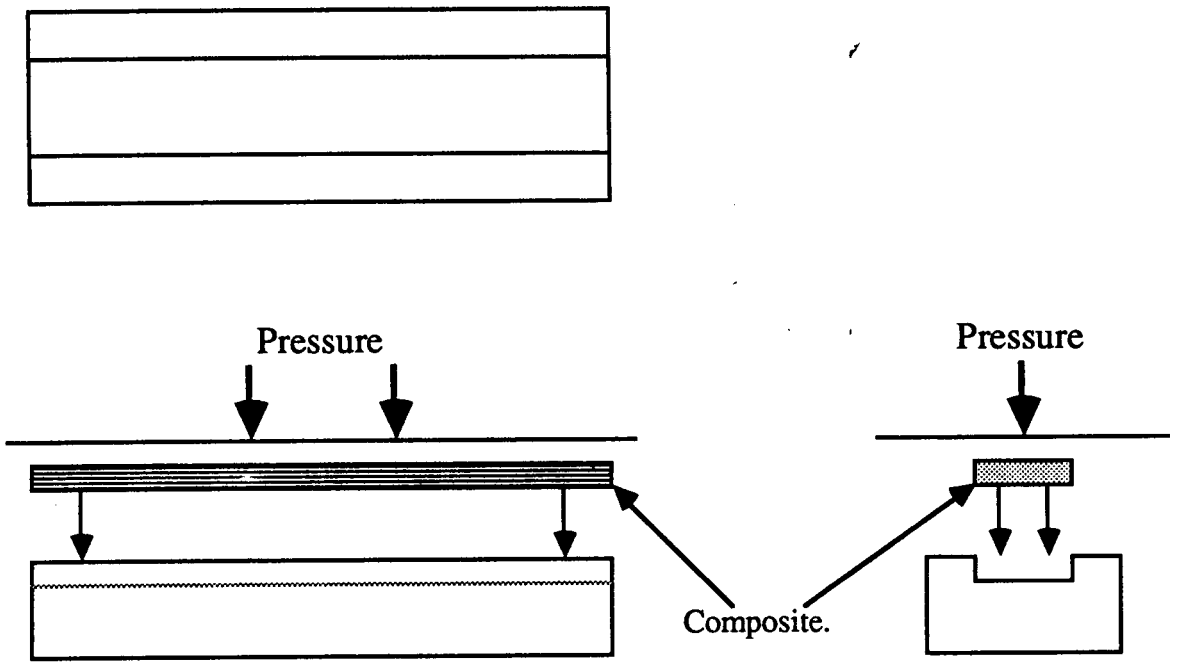

Figure 3.13 Composite DCB specimen rehealing fixture.

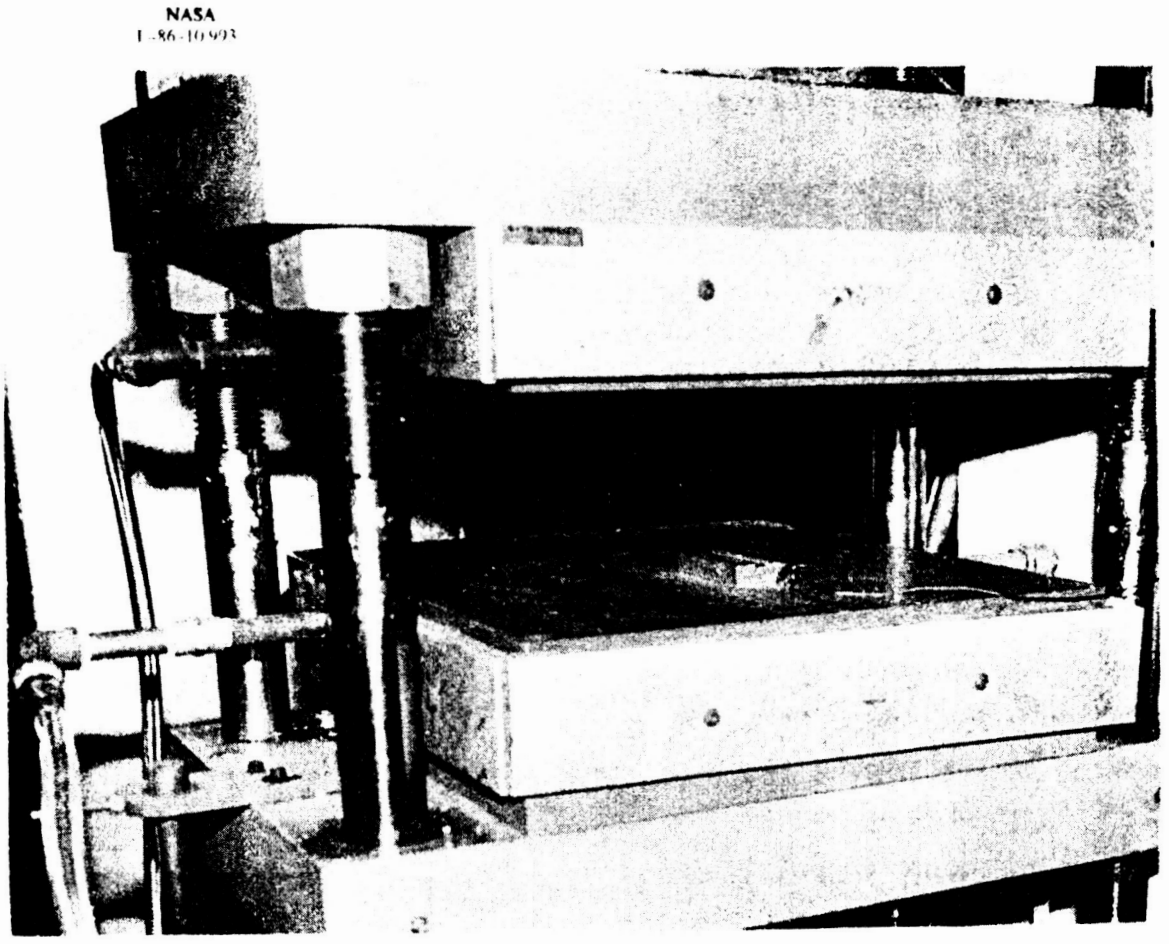

Figure 3.14 DCB specimen healing fixture in Wabash hot press.

registered a positive pressure. After the desired time had elapsed, the press was opened and the sample removed from the fixture and cooled under ambient conditions.

3.5.3 Data Reduction

To calculate the critical strain energy release rate, $G_{1C,}$ from the DCB tests the following data reduction procedure was used. From the chart recorder output (a typical output from the chart recorder is shown in Figure 3.15), the slope of the loading curve (load versus crosshead displacement) was determined by using a straight edge and the compliance of the beam was calculated from the measured slope (i.e., compliance = 1/slope). The linear assumption was good for all the specimens tested. The critical strain energy release rate was calculated from the following equation

$$G_{1c} = \frac{3 A_1 (A_2)^2}{2 b} \qquad (3.5)$$

where b is the sample width and A_1 and A_2 are geometrical factors determined from the compliance and peak load.

To determine A_1 and A_2, curves of both compliance versus (crack length)^3 and peak load versus (crack length)$^{-1}$ are plotted. Typical curves are shown in Figure 3.16. The slope of each of these curves was calculated using a least squares linear curve fit. A_1 corresponds to the best fit slope of the compliance versus (Crack length)^3 and A_2

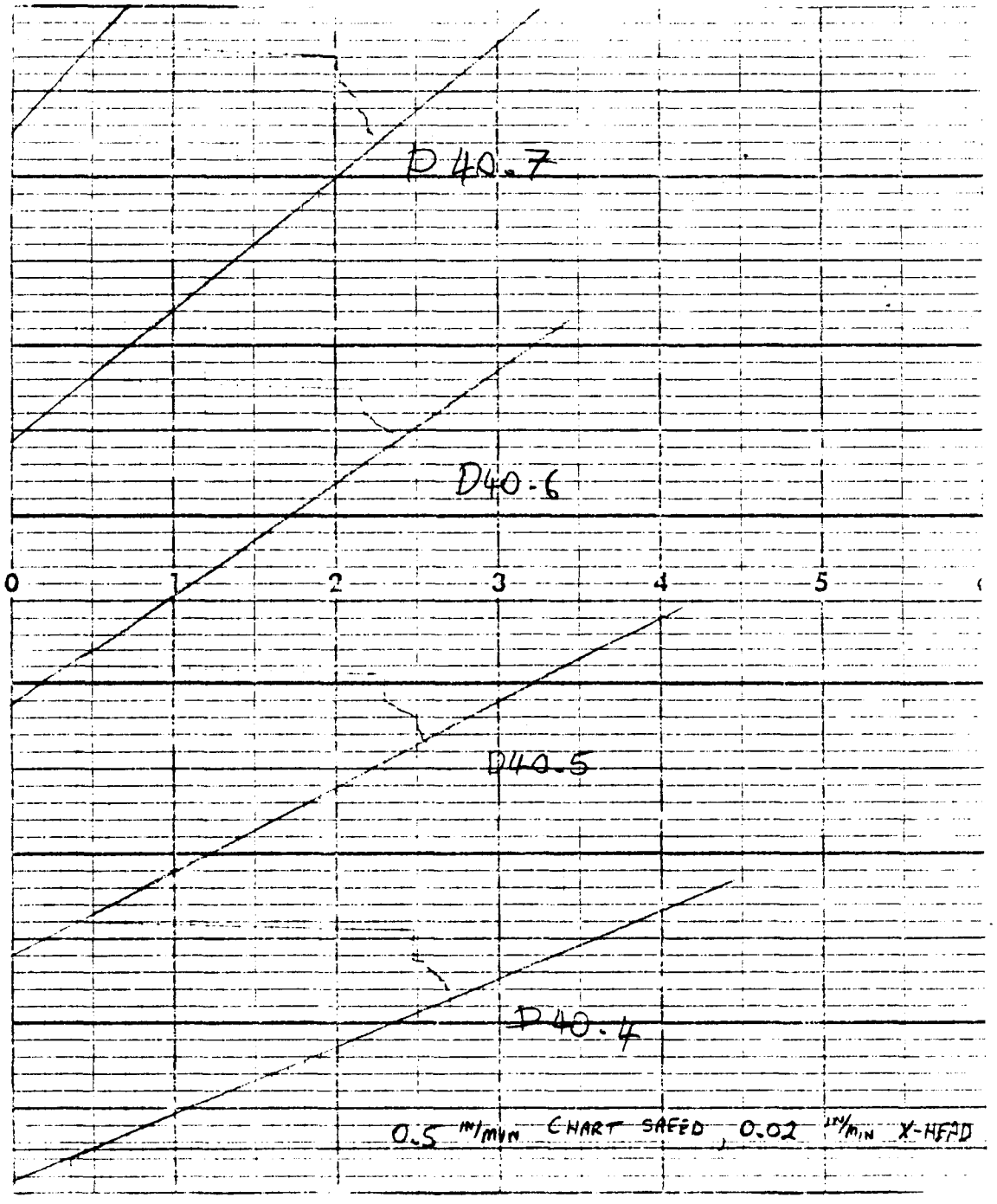

Figure 3.15 Typical chart recorder output from DCB test.

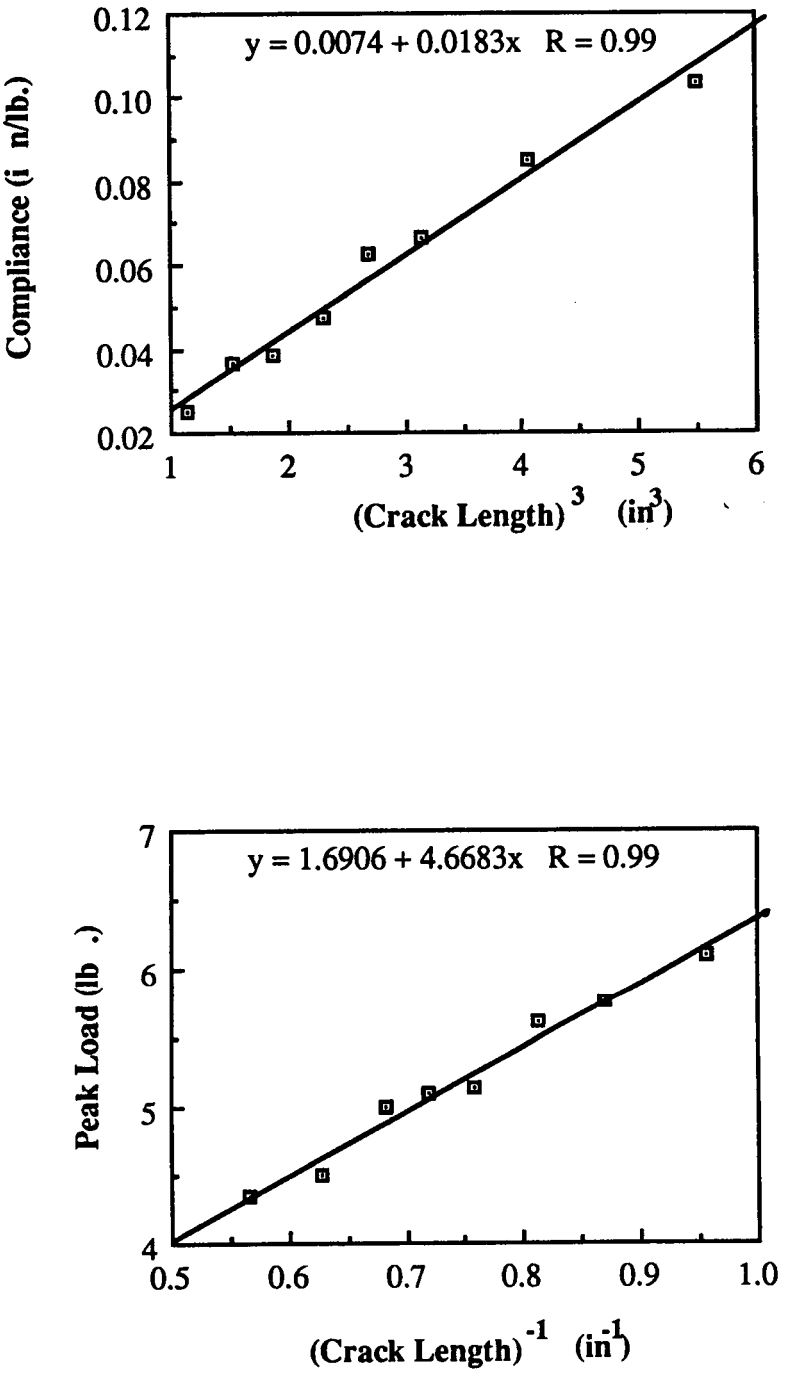

Figure 3.16 Typical curves used to obtain A_1 and A_2.

corresponds to the slope of the peak load versus (crack length)$^{-1}$ [27]. The critical strain energy release rate was calculated as a function of crack length using the following equation

$$G_{IC} = \frac{P_C^2}{2b}\left[3 A_1 a^2\right] \qquad (3.6)$$

where P_C is the peak load corresponding to a certain crack length, a.

3.6 Post Failure Analysis

To study the effects of rehealing on the fracture mechanisms, both CT and DCB specimen failure surfaces were examined in a scanning electron microscope (SEM). Micrographs of the failure surfaces were obtained after initial fracture and after the specimen was rehealed and refractured a number of times.

3.6.1 Sample preparation

The specimens were cut to allow them to be mounted in the SEM chamber. The CT specimens were trimmed of excess material that was not fractured (i.e. the sawed notch and hole area) and the DCB specimens were cut into three 25mm (1 in.) sections. The section of the DCB specimen containing the Kapton flaw was discarded and the two

remaining specimens were used in the SEM study.

The sized samples were mounted on aluminum posts using a combination of double sided adhesive tape and a colloidal graphite suspension in isopropanol. The graphite ensured good electrical contact between the sample and the mounting. The samples were sputter coated with gold-palladium to reduce charging effects which produce poor images.

3.6.2 Testing Procedure

The samples were examined in a Philips 505 SEM and photographs of the fracture surfaces were taken using a Polaroid camera attached to the SEM. The samples were examined and photographs taken at different magnifications depending on the sample. The CT specimens were examined at magnifications of 48.6 X, 163 X, and 287 X and the DCB specimens at magnifications of 163 X, 326 X, and 1,310 X.

4.0 Results

4.1 Interfacial Tension Tests

The interfacial tension test measured the growth of interfacial strength as a function of temperature and contact time. Three groups of tests were performed: the first measured the effect of bonding temperature on the interfacial strength; the second the effect of contact time; and the third the effect of strain rate.

The pressure applied to bond the interfacial test specimens was calculated from the pressure data reported by Dara and Loos [1] for the same polymer. They used an interfacial tensile test to determine the lowest pressure, called the saturation pressure, at which the interfacial strength became independent of pressure. The applied pressure was 375 kPa (55 psi) at the lowest temperature of 210°C and was used for all tests. Interested readers are referred to their work [1].

The results of the interfacial tension test were disappointing. The data obtained from the test matrix shown in Table 4.1 had very high scatter and were difficult to correlate with contact time and temperature. Results of the tests are shown in Figures 4.1 and 4.2 for data rehealed at 210°C and 220°C, respectively. The square symbols represent the mean of the measured data and the bars represent one standard deviation from the mean. The results are determined from between five and twelve measurements at each time and temperature condition. The straight line is the best fit to the data in accordance with the

Table 4.1 Interfacial Test Matrix

Temperature, °C	Contact Time, sec	Crosshead Speed, in/min
210	30	0.02
210	60	0.02
210	120	0.02
210	180	0.02
210	300	0.02
220	15	0.02
220	30	0.02
220	60	0.02
220	120	0.02
220	210	0.02
220	300	0.02
220	600	0.02
220	1200	0.02
220	600	0.002
220	600	0.01
220	600	0.02

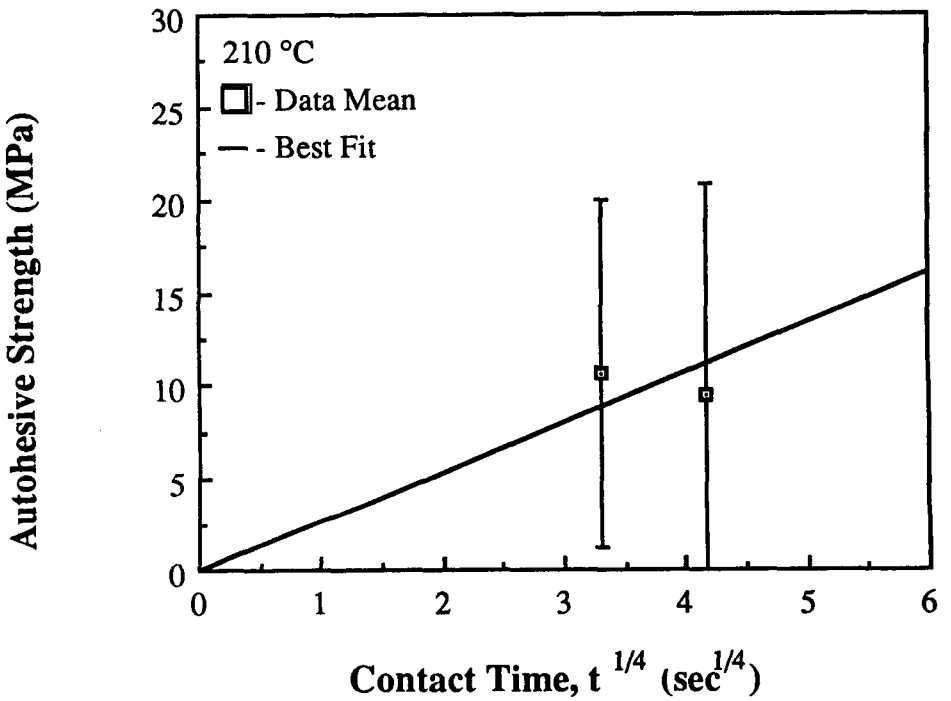

Figure 4.1 Autohesive strength versus fourth root of contact time for Udel® P1700 polysulfone specimens bonded at 210°C. The strength was measured using an interfacial tension test. Symbols represent the mean of the data. Error bars represent one standard deviation from the mean. Solid line is a best fit through the data and the origin.

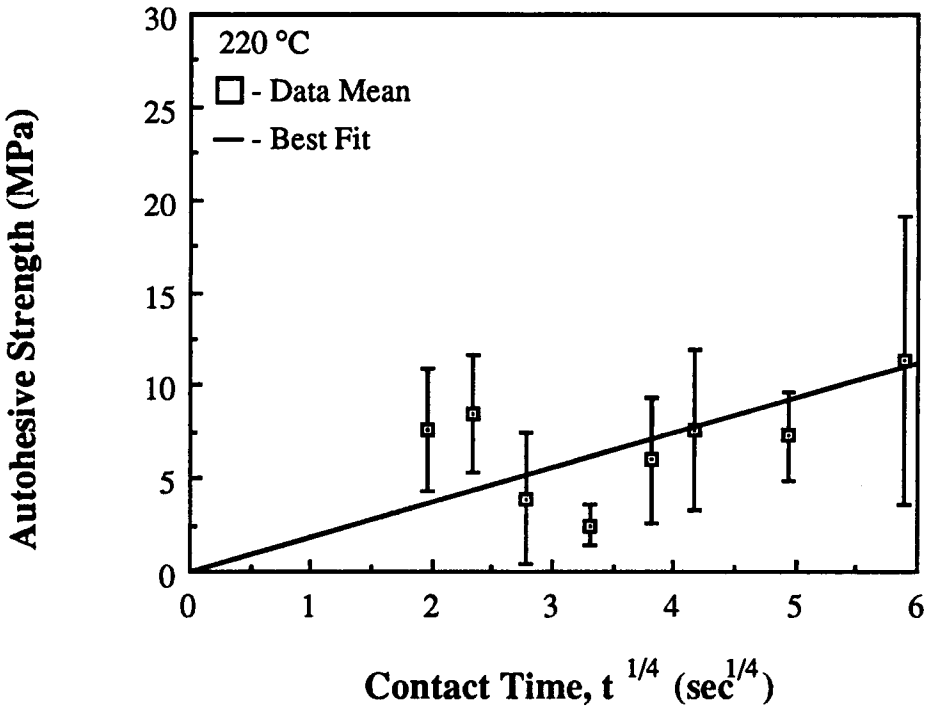

Figure 4.2 Autohesive strength versus fourth root of contact time for Udel® P1700 polysulfone specimens bonded at 220°C. The strength was measured using an interfacial tension test. Symbols represent the mean of the data. Error bars represent one standard deviation from the mean . Solid line is a best fit through the data and the origin.

rehealing theories of Wool outlined in Section 2.1.2 for instant wetting and neglecting stress due to wetting or surface attraction. Data at additional temperatures were not obtained due to the unacceptably high scatter at 210°C and 220°C.

Figure 4.3 shows the effect of crosshead speed or strain rate on the interfacial bond strength. All specimens were healed for 10 minutes at 220°C and tested at crosshead speeds of either 0.05, 0.25, and 0.50 mm/min (0.002, 0.01, 0.02 in/min). The data were not expected to show any significant strain rate effect since testing was performed at room temperature, far below the glass transition of the polysulfone. At ambient temperature, little macroscopic molecular motion exists (i.e. no reptation) and failure is by chain fracture. According to Wool, autohesive strength is independent of strain rate for chain fracture failure [4, 8]. The results plotted in Figure 4.3 show a slight upward trend in the measured interfacial strength with increasing crosshead rate. This may be due to some chain pull-out failures at very low strain rates; however, the observed trend is not proportional to the square root of strain rate as Wool asserts for chain pull-out fractures [4, 8].

The poor results of the interfacial tests can be explained by surface waviness, eccentricity of the load train during testing, and thermal effects. Each disk had some surface waviness prior to testing. Those with gross differences were discarded; however, it is unreasonable to assume that the disks used were perfectly flat. Surface waviness caused some areas of the disks to come into contact and wet before others, introducing a time dependent wetting function that varied from specimen to specimen. These effects were present even though the surfaces of the polysulfone disks were examined under a low power microscope in an attempt to identify and eliminate those with rough surfaces.

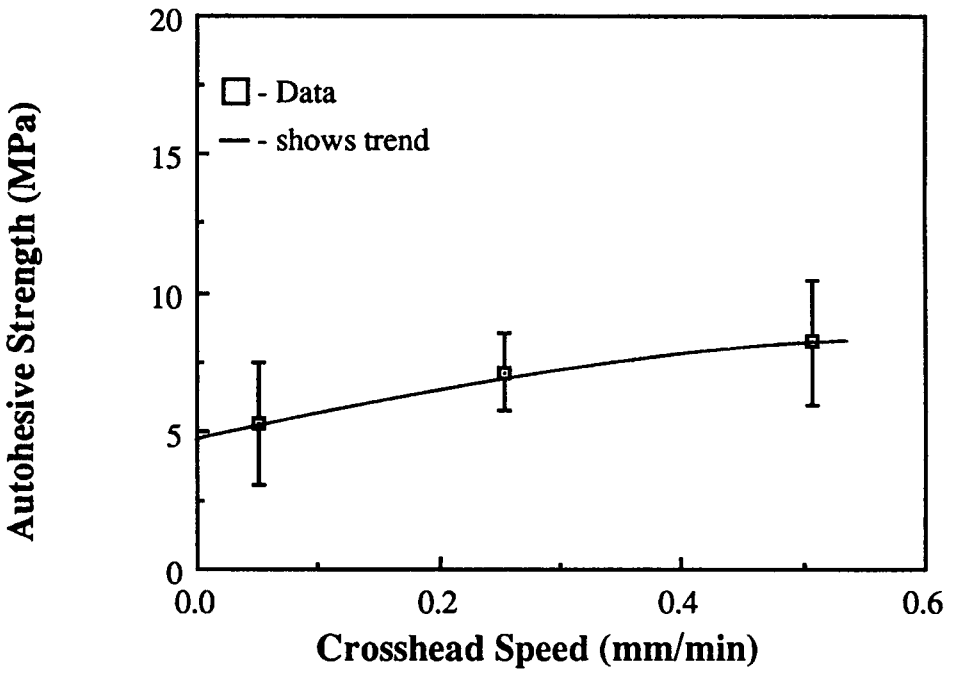

Figure 4.3 Autohesive strength versus crosshead speed for Udel® P1700 polysulfone specimens bonded at 220°C for 10 minutes. Symbols represent the mean of the data. Error bars represent one standard deviation from the mean. Solid line shows trend.

Some evidence of this phenomenon could be observed by looking through the test section with a light microscope following healing, and examining the interface. For two sets of disks bonded under identical time and temperature conditions, the interface was more visible in disks with wavy surfaces than in disks with smooth surfaces. This indicates that the saturation pressure used by Dara and Loos [1] was not high enough to ensure immediate wetting in this study.

The load eccentricity was introduced due to thickness variations in the polymer disks caused by flow and deformation during healing. After bonding the metal grips onto the polysulfone disks, the upper and lower plate fixtures were not perfectly parallel. The differences in the thickness from place to place in the assembly resulted in bending forces to be introduced along with tensile forces when the specimen was loaded. Every attempt was made to discard the assemblies with gross differences in thickness by measuring the thickness at four places around each assembly with a micrometer; however, some eccentricity was unavoidable.

Specimens were also subject to thermal loads. Rapid cooling of the healed specimen from the elevated bonding temperature to ambient temperature sometimes resulted in failure of the interfacial bonds, especially in specimens bonded for short times. It is possible that nonuniform and rapid cooling resulted in thermal stresses large enough to break or damage the fragile autohesive bonds.

The interfacial tensile test could also be analyzed using a fracture mechanics approach to calculate fracture strength. In the interfacial test, the thin Kapton disk between the two

polysulfone specimens introduces a crack. Also, at room temperature the polymer is glassy and brittle and so linear elastic fracture mechanics should apply. The fracture mechanics approach will show how the specimen geometry (i.e., diameter of center hole in Kapton disk and diameter of polysulfone specimens) influences the fracture toughness and the corresponding fracture strength. This information may help in sizing the Kapton hole diameter to reduce the influence of the flaw.

Others have used interfacial tests with good results. In these studies, the mechanical tests were usually performed at the healing temperature well above the T_g of the polymer [1, 8, 11, 12, 16]. This procedure reduces thermal effects and minimizes load eccentricity because the polymers are rubbery and the bulk of the specimen can deform until the specimens are parallel.

The poor results from the interfacial tension test were the incentive to adopt a different testing method that eliminated or minimized the problems associated with the interfacial test.

4.2 Compact Tension Tests

In an effort to eliminate the wetting and load eccentricity problems observed in the interfacial tests, a compact tension (CT) test was adopted. In the CT test, a crack was allowed to propagate only far enough to give a suitable amount of data without complete fracture of the specimen. Thus, the same surface that was broken was rehealed, eliminating the wetting and alignment problems that affected the interfacial tension test.

Since the specimen was in one piece during rehealing the dimensions remained the same, eliminating the load eccentricity found in the interfacial tests. It also had the advantage that one specimen could be used for a number of rehealings. The compact tension test matrix is shown in Table 4.2.

4.2.1 Pressure Tests

To ensure that data recorded at different temperatures are comparable, the rehealed specimens must have the same wetting functions regardless of temperature. One method of obtaining this is to apply enough pressure so that the surfaces come into intimate contact and wet immediately. This pressure is called saturation pressure and varies in accordance with temperature [12]. From the theory of autohesion, it was recognized that pressure should make little difference in the self-diffusion of the polymer; as it takes very large pressures to change the amount of free volume of the polymer[1, 2, 4]. However, intimate contact does depend on pressure. The upper and lower surfaces of the CT specimens are mirror images of each other and only a small amount of pressure is required to deform the surfaces and them into intimate contact.

In order to determine the saturation pressure for the CT tests, different pressures were applied to pre-cracked CT specimens at the beginning of rehealing. The effect of pressure on the measured refracture toughness is shown in Figures 4.4 and 4.5. The pressure was calculated by dividing the dead weight load applied during rehealing by the nominal area of the crack plane in the CT specimen [w times b from Figure 3.7, 161.3 mm^2 (0.25 in^2)].

Table 4.2 Compact Tension Test Matrix

Temperature, °C	Contact Time, Sec	Pressure (kPa)
196	900	46.4
196	3600	46.4
196	7200	46.4
196	12,600	46.4
196	18,000	46.4
200	600	46.4
200	750	46.4
200	900	46.4
200	1200	46.4
200	1500	46.4
200	900	60.4
200	900	74.5
200	900	88.5
200	900	102.5
200	900	116.7
200	900	130.7
205	300	46.4
205	420	46.4
205	600	46.4
205	900	46.4
213	300	46.4
213	360	46.4
213	480	46.4
213	600	46.4
213	900	46.4
213	360	60.4

Table 4.2 Continued

Temperature, °C	Contact Time, Sec	Pressure (kPa)
213	360	74.5
213	360	88.5
213	360	102.5
213	360	116.7
225	240	46.4
225	300	46.4
225	420	46.4
225	600	46.4
245	180	46.4
245	240	46.4
245	300	46.4
245	360	46.4

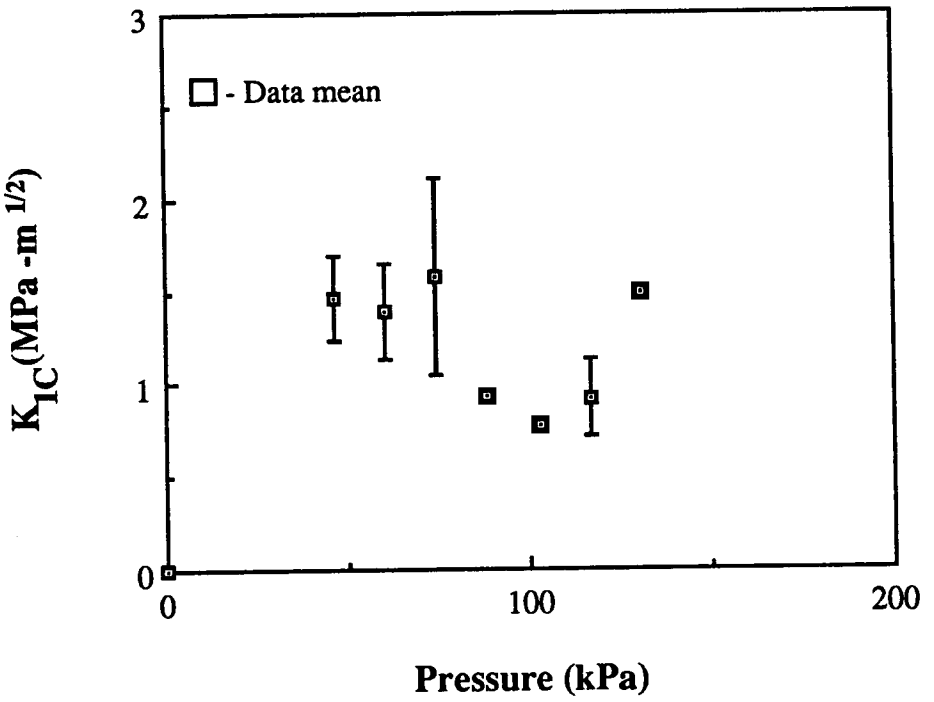

Figure 4.4 Fracture Toughness versus rehealing pressure for Udel® P1700 polysulfone CT specimens bonded at 200°C for 15 minutes. Symbols represent the mean of the data. Error bars represent one coefficient of variation from the mean.

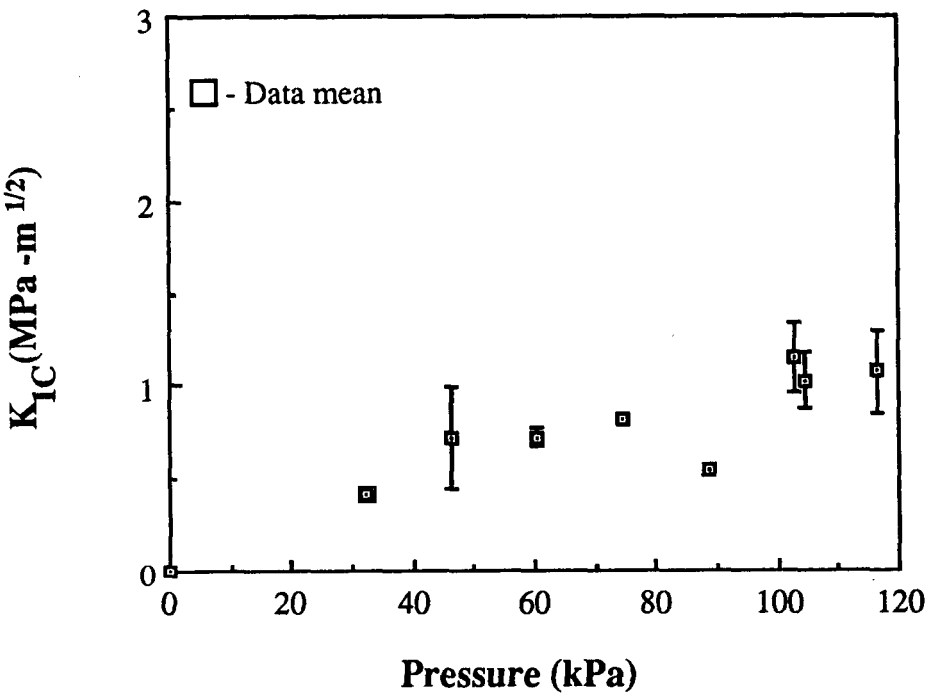

Figure 4.5 Fracture toughness versus rehealing pressure for Udel® P1700 polysulfone CT specimens bonded at 213°C for 6 minutes. Symbols represent the mean of the data. Error bars represent one coefficient of variation from the mean.

The square symbols represent the mean of the refracture toughness and the bars represent one coefficient of variation from the mean. The plots show the fracture toughness first increasing with increasing pressure (Figure 4.5), reaching a plateau and then decreasing at higher pressures (Figure 4.4). The increasing toughness with increasing pressure is the result of faster wetting in the specimens. The plateau indicates that the saturation pressure has been reached which implies immediate or extremely rapid interfacial wetting and complete interfacial contact. At elevated pressure, the specimen deformed extensively, resulting in a decrease in the measured refracture toughness as shown in Figure 4.4. The pressure used for all of the CT tests was the lowest pressure (46 kPa) in the plateau region at 200°C. This pressure was chosen because 200°C was the lowest temperature in the original test matrix. Saturation pressure decreases with increasing temperature due to the lower modulus of the polymer at higher temperatures. Thus, it can be assumed that intimate contact was achieved for all the temperature and contact time conditions in the test matrix.

4.2.2 Results of CT Tests

The CT tests measured the fracture toughness for the undamaged specimens and also the refracture toughness for subsequently rehealed specimens. The results from the undamaged specimens are plotted in Figure 4.6, which plots fracture toughness against the crack length. The values from the undamaged specimens do not vary with crack length, indicating that the geometrical factor used in the stress intensity factor calculations was accurate [17]. The measured fracture toughness varied between 1.8 and

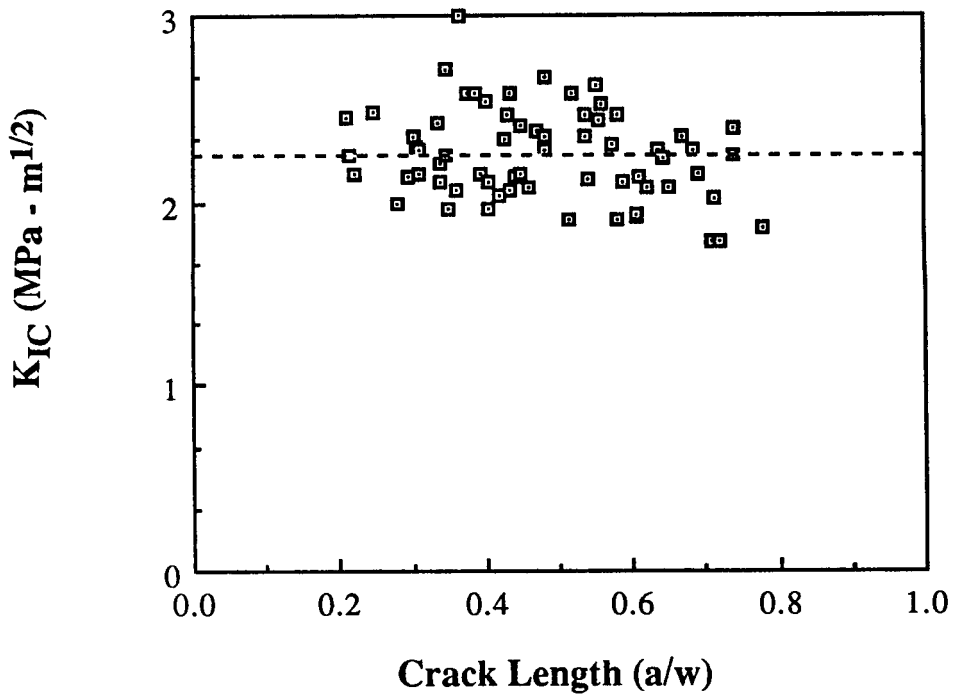

Figure 4.6 Fracture toughness versus crack length for Udel® P1700 polysulfone CT specimens. Symbols represent data and the dashed line represents the mean of the data.

3.0 MPa $m^{1/2}$ with the mean being 2.26 MPa $m^{1/2}$. Stress intensity factor values reported in the literature for polysulfone range between 2.4 and 3.4 MPa $m^{1/2}$. The lower value observed in this study may be due to the annealing process to which the polysulfone was subjected. However, 2.26 MPa $m^{1/2}$ is within the data scatter for the fracture toughness of polysulfone reported by Hinkley [17].

The results of the CT rehealing tests are shown in Figures 4.7-4.12 for specimens rehealed at 196, 200, 205, 213, 225, and 245°C, respectively. The square symbols represent the mean of at least 5 measurements at each time and temperature condition and the error bars represent one coefficient of variation from the mean. In both Figures 4.8 and 4.10, the CT specimens regain the original toughness of undamaged polysulfone, indicating complete healing of the interface. Furthermore, the rehealed fracture toughness data do not pass through the origin as reported in previous investigations [10] and there is a considerable time lag between the beginning of healing and the point where the fracture toughness increases.

The reason for the time lag lies in the experimental procedure used to reheal the specimens in the present investigation. Healing was performed in a forced air convection oven preheated to the desired temperature. Due to the finite surface heat transfer coefficient between the oven fluid and the specimen, the time required for the specimen to reach the healing temperature was a significant portion of the total healing time. Since healing begins at T_g, the specimens were rehealed non-isothermally. The non-isothermal rehealing will be addressed in a later section of this chapter.

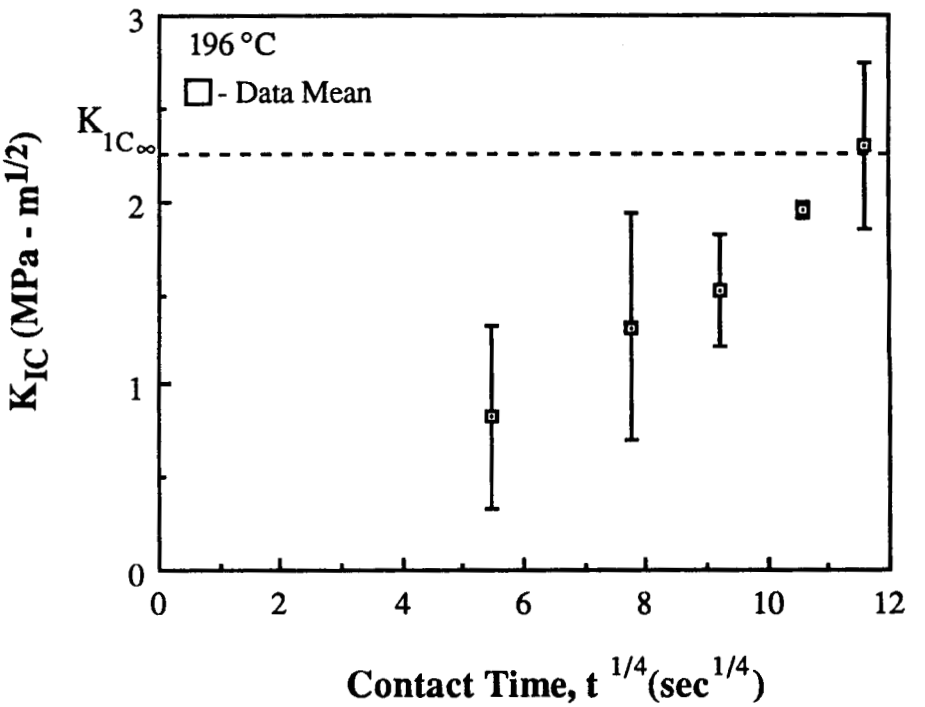

Figure 4.7 Fracture toughness versus fourth root of contact time for Udel® P1700 polysulfone CT specimens rehealed at 196°C. Symbols represent the mean of the data. Error bars represent one coefficient of variation from the mean. Dashed line represents the fracture toughness of undamaged material.

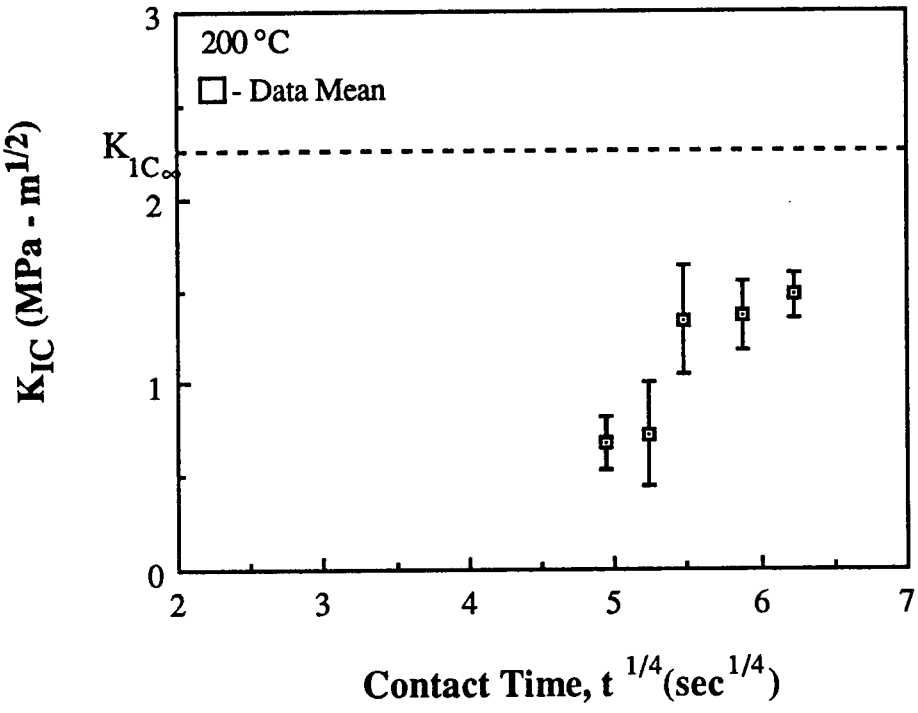

Figure 4.8 Fracture toughness versus fourth root of contact time for Udel® P1700 polysulfone CT specimens rehealed at 200°C. Symbols represent the mean of the data Error bars represent one coefficient of variation from the mean. Dashed line represents the fracture toughness of undamaged material.

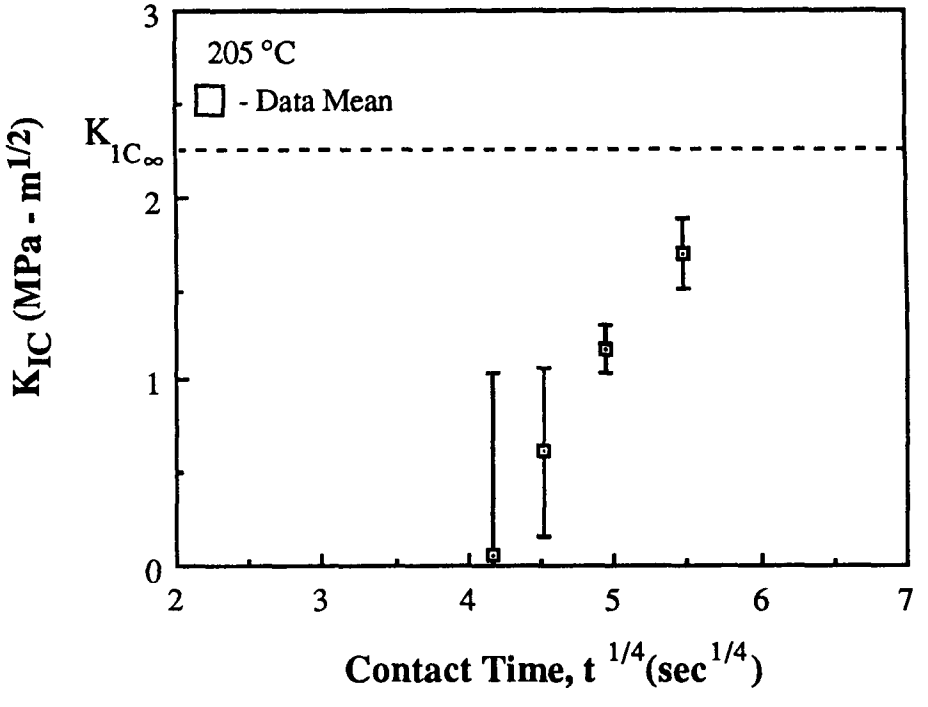

Figure 4.9 Fracture toughness versus fourth root of contact time for Udel® P1700 polysulfone CT specimens rehealed at 205°C. Symbols represent the mean of the data Error bars represent one coefficient of variation from the mean. Dashed line represents the fracture toughness of undamaged material.

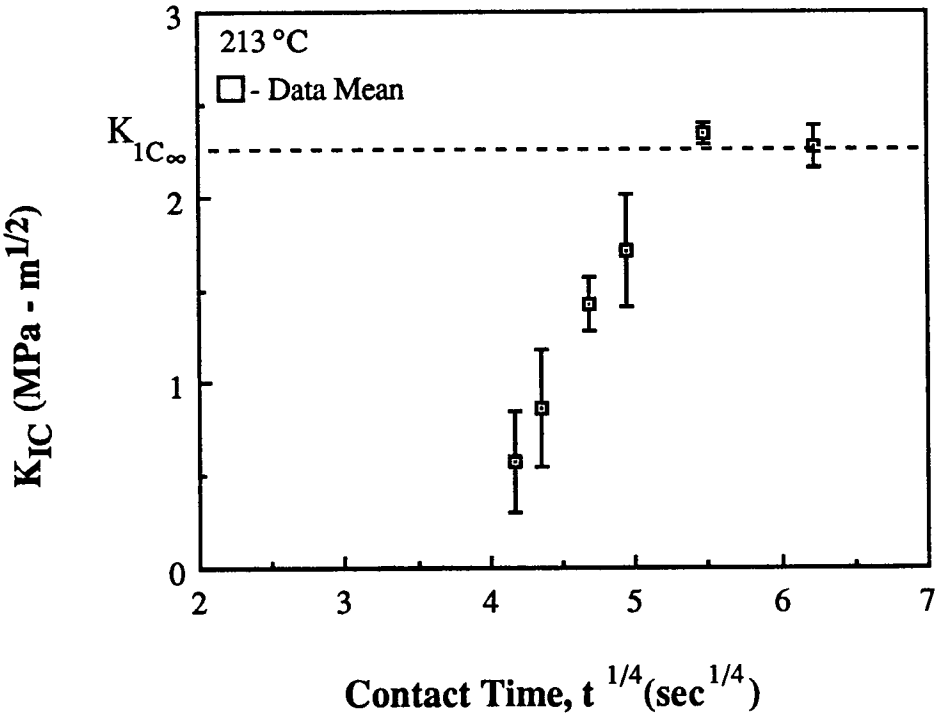

Figure 4.10 Fracture toughness versus fourth root of contact time for Udel® P1700 polysulfone CT specimens rehealed at 213°C. Symbols represent the mean of the data Error bars represent one coefficient of variation from the mean. Dashed line represents the fracture toughness of undamaged material.

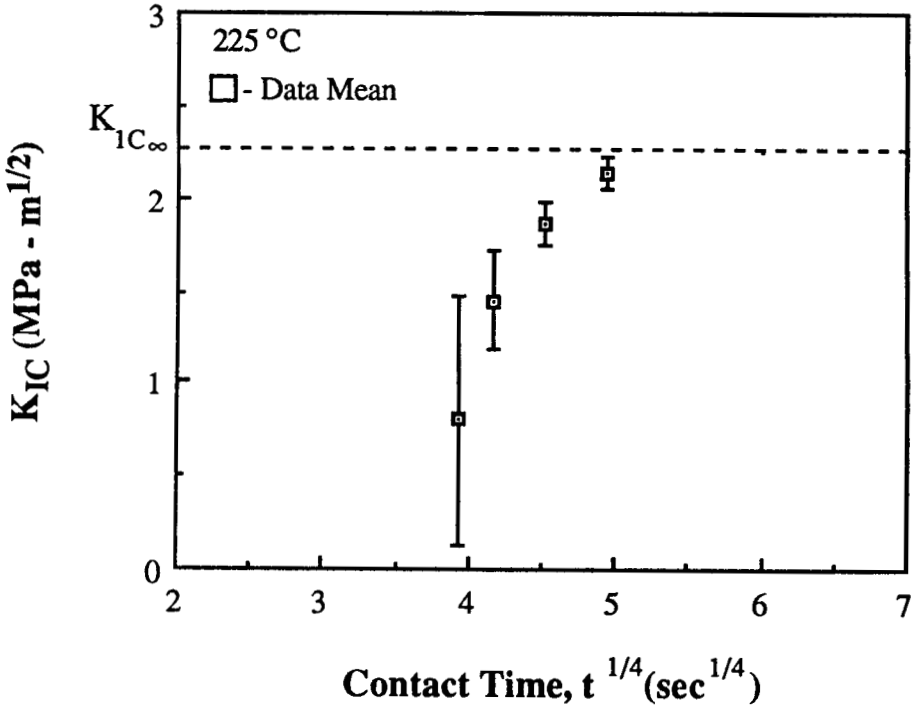

Figure 4.11 Fracture toughness versus fourth root of contact time for Udel® P1700 polysulfone CT specimens rehealed at 225°C. Symbols represent the mean of the data Error bars represent one coefficient of variation from the mean. Dashed line represents the fracture toughness of undamaged material.

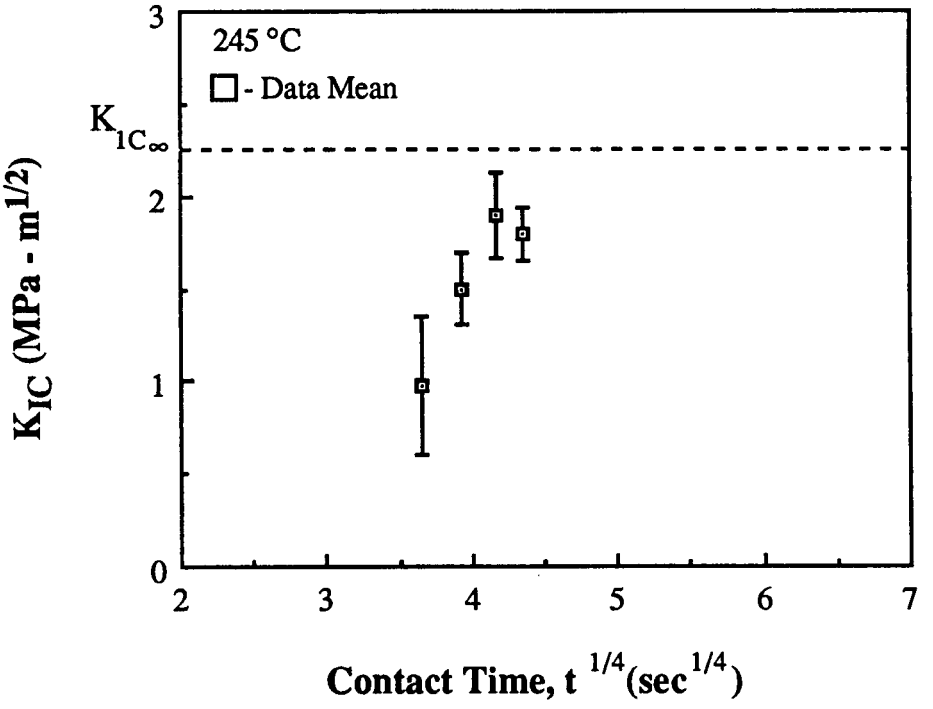

Figure 4.12 Fracture toughness versus fourth root of contact time for Udel® P1700 polysulfone CT specimens rehealed at 245°C. Symbols represent the mean of the data Error bars represent one coefficient of variation from the mean. Dashed line represents the fracture toughness of undamaged material.

4.3 Non-Dimensional Rehealing Function

In order to allow comparisons to be made between the neat resin CT tests and the composite rehealing data (see Section 4.8), the critical strain energy release rate was calculated for the neat resin CT tests. Assuming plane strain conditions, the critical strain energy release rate, G_{1C} was calculated from the fracture toughness data as follows [21]

$$G_{1C} = \frac{K_{1C}^2 (1-\upsilon^2)}{E} \tag{4.1}$$

where K_{1C} is the measured fracture toughness from the CT tests, υ is Poisson's ratio (0.40 for polysulfone [22]), and E is the tensile modulus (2.5 MPa for polysulfone [24]). The data was non-dimensionalized by dividing the calculated strain energy release rate by the critical strain energy release rate for the undamaged polysulfone specimens as follows

$$R = \frac{G_{1C}}{G_{1C_\infty}} \tag{4.2}$$

where R is defined as the rehealing function.

Shown in Figure 4.13 is a summary plot of the rehealing function, R, versus the square root of time. According to the rehealing model of Wool and O'Connor (see equation 2.5), if healing is isothermal and interfacial wetting is instantaneous and negligible, a plot of the rehealing function versus square root of time should be a straight line that passes

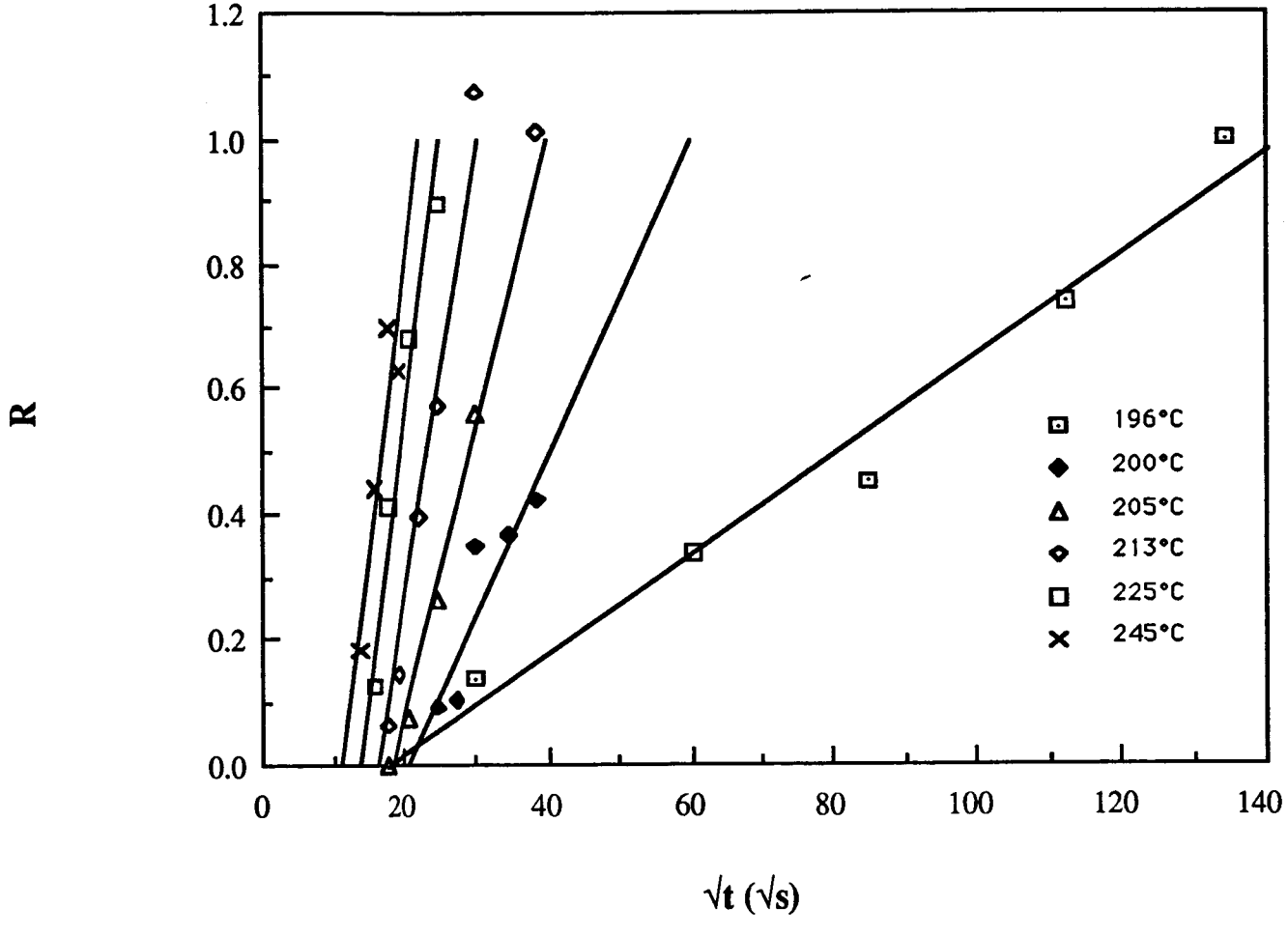

Figure 4.13 Rehealing function, R versus square root of contact time for Udel® P1700 polysulfone CT specimens bonded at different temperatures. Symbols represent the mean of the data. Solid lines linear regression curve fits to the data.

through the origin. The rehealing data obtained in the present investigation appear to follow the straight line relationship but do not pass through the origin. Furthermore, above 205°C the slope of the rehealing function is nearly constant. These differences are due to the non-isothermal healing effects as indicated in Section 4.2.2.

4.4 Heat Transfer Model

In order to measure temperature as a function of time during the rehealing tests, six thermocouples were embedded at various locations inside a CT specimen. One thermocouple was placed in each of the following locations: the top surface, bottom surface, front edge, and rear edge of the specimen. The other two thermocouples were embedded at the crack plane and the crack tip. The CT specimen was then placed in the oven and exposed to the same processing cycles that the rehealing CT specimens were subjected to. Each thermocouple was sampled at 30 second intervals by a Fluke scanning digital thermometer.

Two heat transfer solutions were compared with the measured data. These included a three dimensional quadrilateral solution with fixed specified boundary temperatures and a negligible internal resistance model with finite surface heat transfer coefficient. The negligible internal resistance (NIR) solution with a surface heat transfer coefficient of 32 w/(m^2-°C) gave an excellent correlation with the measured results.

In the NIR solution it is assumed that the body has a high enough thermal conductivity,

compared with the surface film coefficient and that the temperature of the body may be taken as uniform for any instant of time. An energy balance for the specimen over a small time interval gives

$$h A_s (T - T_f) = -\rho V C_p \frac{dT}{dt} \tag{4.3}$$

where h is surface heat transfer coefficient, A_s is exposed surface area, T is the specimen temperature, T_f is the fluid temperature, ρ is density, V is the volume of the body, C_p is the specific heat of the body, and t is time.

Rewriting equation (4.3) gives

$$\frac{d(T - T_f)}{T - T_f} = - \frac{h A_s}{\rho C_p V} dt \tag{4.4}$$

Integrating equation (4.4) with respect to time and with the initial condition $T = T_i$ at time $t = 0$, we obtain the expression [22]

$$\frac{T - T_f}{T_i - T_f} = \exp\left[\frac{- h A_s}{\rho C_p V} t\right] \tag{4.5}$$

For polysulfone CT specimens using a heat transfer coefficient, h of 32 w/m^2-°C, ρ of 1.24 Mg-m^{-3} [24], C_p of 1.13 kJ/kg-°C [25], V of 6.145 x 10^{-3} m^3, A_S of 2.276 x 10^{-3} m^2 we obtain the following

$$\theta = \frac{T - T_f}{T_i - T_f} = e^{\frac{-t}{98.707}} \qquad (4.6)$$

The heat transfer coefficient was obtained by using equation (4.5) to calculate temperature versus time for different values of the heat transfer coefficients until the calculated temperatures matched the thermocouple data. Figure 4.14 shows the correlation between equation (4.6) and the thermocouple data, for a heat transfer coefficient of 32 w/m^2-°C.

4.5 Temperature Dependence

To fully describe and model the autohesive phenomenon for thermoplastic resins, it was recognized that the temperature dependence must be determined. As discussed previously (see Section 4.2), the low convective heat transfer coefficient between the oven fluid and the CT specimen resulted in a finite amount of time to heat the specimen to the oven set point temperature. Thus, the CT specimens were healed non-isothermally. Furthermore, only data measured after the specimen reached the specified isothermal oven temperature can be used to determine the temperature dependence. To determine the time at which the temperature in the CT specimens became constant, the NIR heat transfer expression, equation (4.6), was solved for time, t as follows.

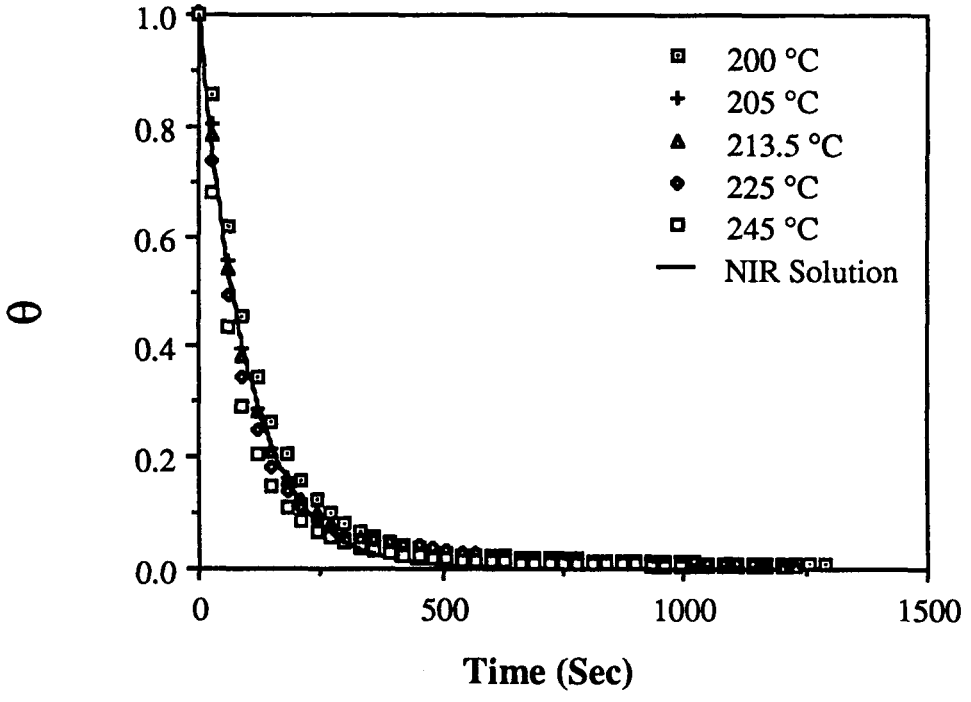

Figure 4.14 Non-dimensionalized temperature, θ versus time in oven for CT specimens. Symbols represent data gathered at different oven setpoint temperatures. The solid line represents the negligible internal resistance heat transfer solution using a surface heat transfer coefficient of 32 w/m^2 - °C.

$$t = -98.707 \ln\left[\frac{T - T_f}{T_i - T_f}\right] \tag{4.7}$$

The time to reach 0.5°C below oven setpoint temperature (T_f) was calculated for the CT specimens and verified by the thermocouple data. A temperature 0.5°C below the setpoint temperature was selected rather than the actual setpoint temperature because the NIR expression predicts infinite time to reach actual oven setpoint temperature. The half degree approximation agreed well with the thermocouple data in predicting the time required for the CT specimens to reach actual oven setpoint temperature. Rehealing data obtained after the specimen reached the oven setpoint temperature (T_f) was isothermal and can be used in the diffusion model developed by Wool and O'Connor (Chapter 2) to determine the temperature dependence. If wetting is instantaneous and the instantaneous wetting load at initial time is negligible then the rehealing function defined in equation (4.2) can be written as follows.

$$R = C(T)\, t^{1/2} \tag{4.8}$$

where C(T) is a temperature dependent constant (self-diffusion parameter) proportional to the polymer self-diffusion coefficient. In order to determine the self-diffusion parameter, C(T) the non-isothermal data points were removed from the plots of the rehealing function versus square root of contact time and a linear least squares curve was fit to the isothermal data at each temperature condition (Figure 4.15). Measurement of the slope of each curve gave the self-diffusion parameter C(T). Table 4.3 shows the time to obtain the

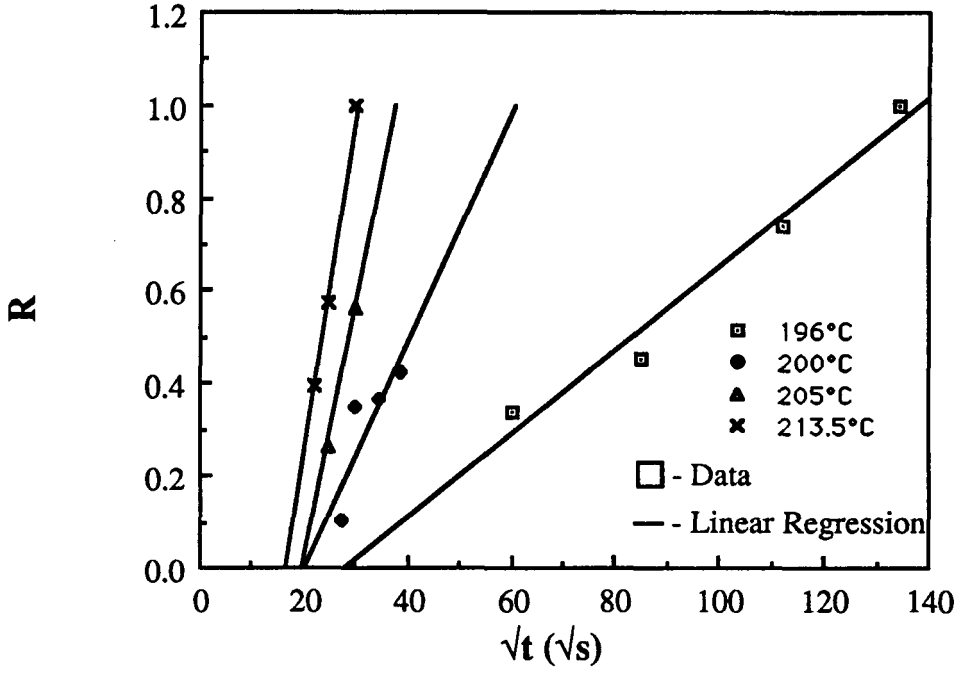

Figure 4.15 Isothermal rehealing data, R versus square root of contact time for Udel® P1700 polysulfone CT specimens. Symbols represent the mean of the data. Solid lines represent linear regression curve fits to the data.

Table 4.3 Time to reach oven temperature, self-diffusion parameters, and correlation coefficients from the least squares fit to the isothermal rehealing data.

Temperature (°C)	Time to T_f (sec)	C(T)	Correlation
196.0	579.7	0.0091	0.98
200.0	581.9	0.0239	0.83
205.0	584.6	0.0543	1.00
213.0	589.0	0.0752	1.00
225.0	594.6		
245.0	603.8		

oven setpoint temperature, the self-diffusion parameter, and the correlation coefficient from the least squares fit to the isothermal data.

Determination of C(T) at temperatures above 213°C was precluded by the fact that the data was not isothermal.

4.5.1 Arrhenius Temperature Dependence

Jud et al [10]., Wool and O'Connor [6], and Prager and Tirrell [9] observed that the experimentally determined macroscopic diffusion coefficients calculated for different temperatures could be approximated by an Arrhenius law. The form of the Arrhenius equation is given as

$$C(T) = K_0 \exp\left[-\frac{E_a}{RT}\right] \tag{4.9}$$

where E_a is the activation energy, R is the universal gas constant (8.31 J / mol K), T is the absolute temperature (K) and K_0 is a pre-exponential factor.

The parameters E_a and K_0 can be determined by plotting the natural log of the self-diffusion parameter, C(T) versus reciprocal temperature as shown in Figure 4.16. Fitting a linear least squares curve to the data, with a correlation coefficient of 0.93, the constants were determined to be 6.73103×10^{22} for K_0, and 221.96 kJ / mol. for E_a.

C-2

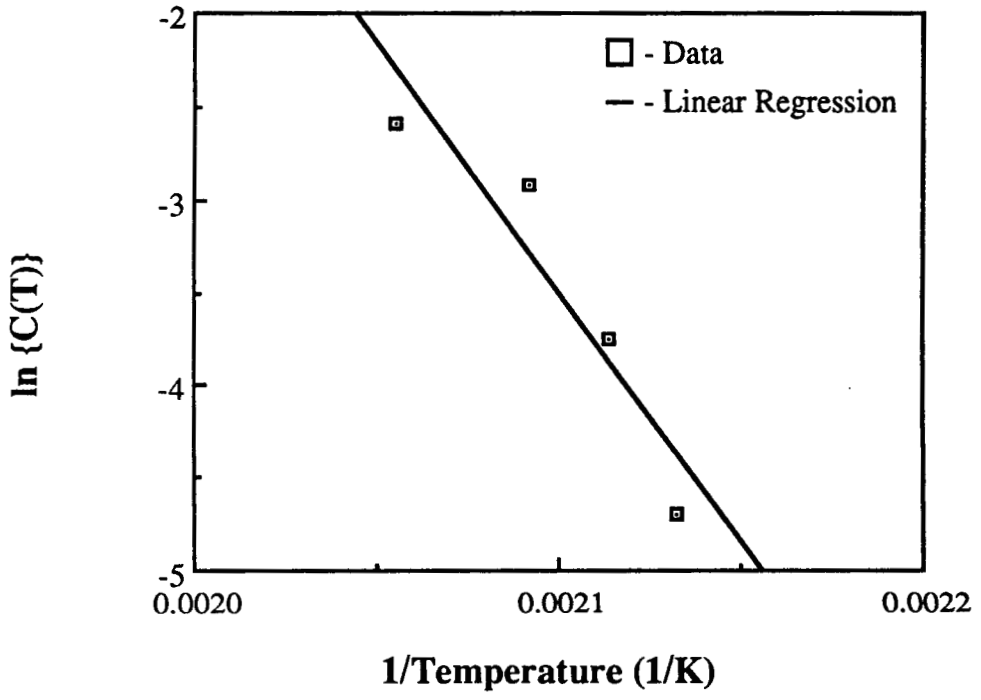

Figure 4.16 Natural log of C(T) versus reciprocal temperature. Symbols represent data. Sold line represents a linear regression curve fit to the data.

The calculated value of E_a is on the same order of magnitude that Jud et al. determined for the self-diffusion activation energy of PMMA, 274 kJ mol^{-1} [10]. Dara and Loos [1] reported a value of 36.7 kJ mol^{-1} for the activation energy of polysulfone. The differences between their results and the result of this study is probably due to different testing methods. Other estimates of the activation energy for polysulfone are not available; however, the activation energy for the zero shear rate viscosity (which is also dependent on the available free volume in the polymer) of polysulfone was measured to be 96.3 kJ mol^{-1} [26].

4.5.2 Williams, Landel and Ferry (WLF) Temperature Dependence

Wool and O'Connor [6] stated that the self-diffusion coefficient should follow a WLF temperature dependence, providing that the mode of failure remains the same between samples rehealed at different temperatures. Ferry [23] states that the WLF relationship is accurate at temperatures between the glass transition temperature, T_g, and fifty degrees above the glass transition temperature, T_g+ 50°C, due to the fact that free volume changes control the mechanical properties of polymers in this range. At higher temperatures, an Arrhenius relationship is more accurate. The testing range used in this study falls within the T_g to T_g+ 50°C range and so the WLF temperature dependence is expected to be most accurate.

The premise behind the WLF theory is that a certain state of a polymer can be achieved by many different approaches. For instance, at a high temperature only a short amount of

time is needed for complete healing of the crack but at a lower temperature more time is needed to heal the crack. The theory relates all movement of the molecules directly to the free volume available to each molecule. As the free volume increases so does the molecular motion and subsequently the self-diffusion. One relationship has been shown to be applicable to a wide variety of polymers and it relates some property, which is temperature dependent, to the same property measured at a reference temperature. The relationship can be written as follows [23]

$$\ln a_T = \frac{-C_1 (T - T_r)}{C_2 + T - T_r} \tag{4.10}$$

where a_T is the shift factor, C_1 and C_2 are constants, T is temperature, and T_r is the reference temperature. a_T is defined as

$$a_T = \frac{C_{S,0}\, T}{C_S\, T_r} \tag{4.11}$$

where $C_{S,0}$ is the property being measured at the reference temperature and C_S is the property at temperature T.

In the present investigation the reference temperature, T_r, is taken at 196°C and C_s represents the self-diffusion parameter, C(T), at the rehealing temperature, T, taken from Table 4.3.

The constants C_1 and C_2 were determined by plotting $1/\ln(a_T)$ against $1/(T-T_r)$. A least

squares linear curve fit to the data gives values of 3.6324 and 11.5053 for C_1 and C_2, respectively (Figure 4.17). The WLF equation provides an excellent fit to the data as shown by the comparison in Figure 4.18.

4.6 Self-Diffusion Coefficient

Using an approach similar to Jud et al., the self-diffusion coefficient was estimated from the following relationship [10]

$$D = \frac{G_0}{135}\left[\frac{\rho RT}{G_0}\right]^2\left[\frac{R_g^2}{M}\right]\frac{M_c}{M^2\eta_0(M_c)} \qquad (4.12)$$

where the definitions and values of the quantities in equation (4.12) are given in Table 4.4. The estimated self-diffusion coefficient for polysulfone P1700 is 1.03 X 10^{-20} m^2 sec^{-1} at 196°C. The self-diffusion coefficient is proportional to the self-diffusion parameter, C(T) and should follow the same temperature dependence. Table 4.5 shows the estimated self-diffusion coefficient at different temperatures calculated using both the Arrhenius and the WLF temperature dependence. In performing the calculations it was assumed that the proportionality constant between the self-diffusion coefficient and the self-diffusion parameter, C(T) did not vary with temperature.

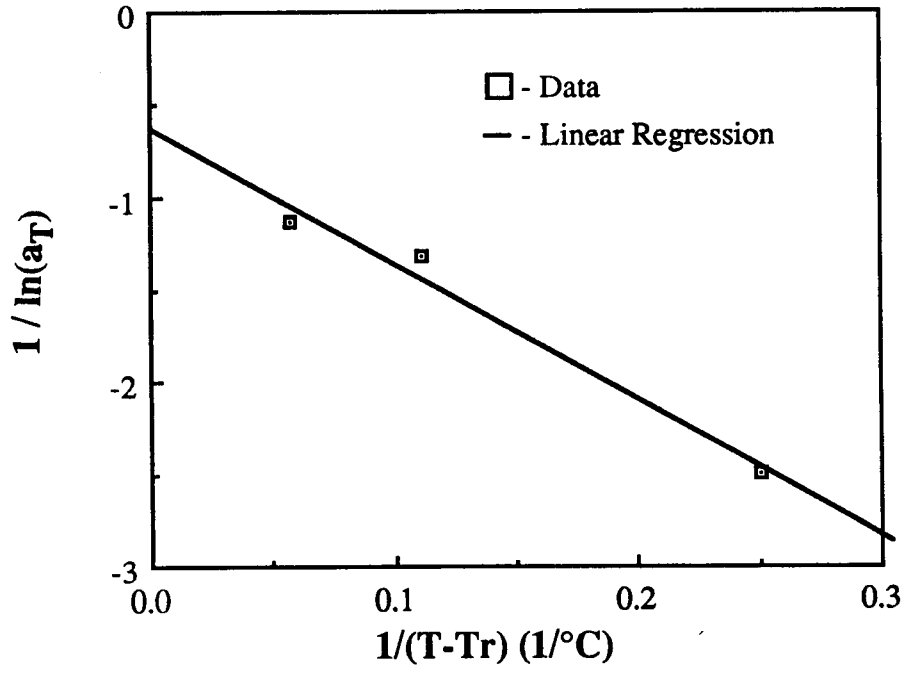

Figure 4.17 Determination of WLF constants for the temperature dependency of autohesion. Symbols represent data. Solid line represents a linear regression curve fit to the data.

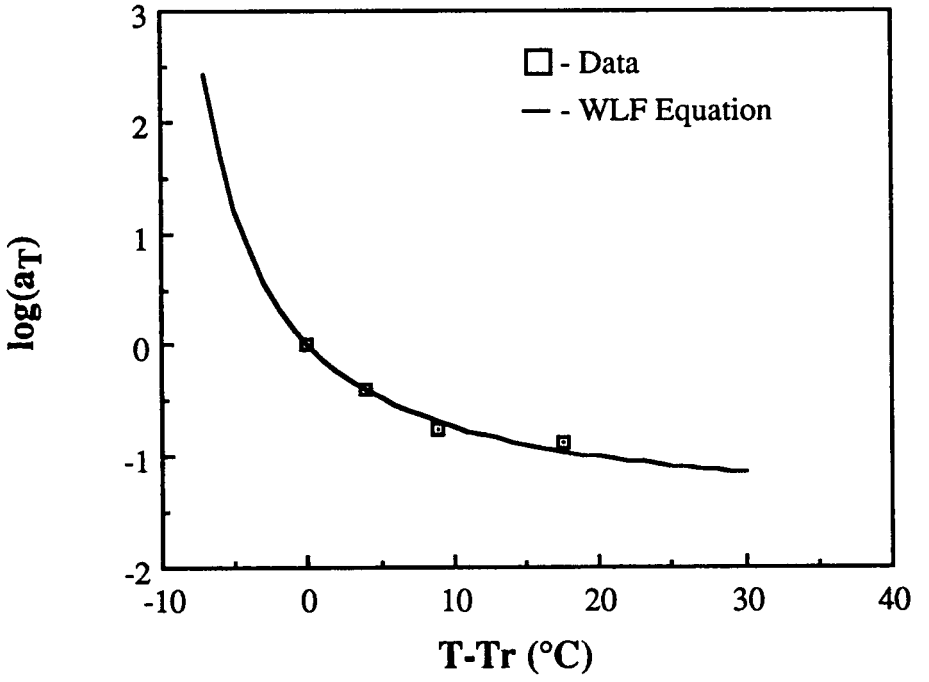

Figure 4.18 Comparison between the WLF equation (solid line) using the constants calculated in Fig. 4.17 and the data (symbols).

Table 4.4 Definition and values of quantities used to estimate the self-diffusion coefficient of polysulfone at 196°C.

Symbol	Quantity	Estimated Value	Reference
G_0	Plateau modulus	10^6 N/m^2	[18]
ρ	Density	1.24 Mg/m^3	[24]
R	Universal gas constant	8.31 J (mol-°K)$^{-1}$	[23]
M	Molecular weight	20,000	[22]
M_c	Critical M for entanglement	3200	[19]
R_g^2/M	Mean square end-to-end distance/M	6.432 X 10^{-17} m^2 mol g^{-1}	[20]
$\eta_0(M_c)$	Zero shear viscosity for M_c	5 X 10^5 Poise	[19]

Table 4.5 Estimated diffusion coefficients (D_s) of polysulfone P1700 using both an Arrhenius and a WLF temperature dependence.

Temperature (°C)	D_s (Arrhenius, m^2 sec^{-1})	D_s (WLF, m^2 sec^{-1})
196	1.03×10^{-20}	1.03×10^{-20}
200	1.67×10^{-20}	2.68×10^{-20}
205	3.01×10^{-20}	5.31×10^{-20}
213	7.99×10^{-20}	1.00×10^{-19}
225	2.84×10^{-19}	1.59×10^{-19}
245	2.25×10^{-18}	2.44×10^{-19}

4.7 Non-Isothermal Rehealing

A non-isothermal rehealing model was developed by combining the isothermal healing model of Wool and O'Connor (equation 4.8) with the NIR heat transfer model (equation 4.6). The model was developed using both an Arrhenius and a WLF temperature dependence for the self-diffusion parameter, C(T).

The first approach followed was to differentiate the isothermal healing model in equation (4.8) with respect to time to obtain the rehealing rate, dR/dt. Using an Arrhenius temperature dependence for the self-diffusion parameter and the NIR heat transfer solution, the following expression for the rehealing rate was obtained

$$\frac{dR}{dt} = K_0 e^{-m/T}\left[\frac{1}{2}t^{-1/2} - \frac{m t^{1/2}(T_i - T_f)e^{-t/\phi}}{\phi T^2}\right] \qquad (4.13)$$

Equation (4.11) proved difficult to solve numerically due to a mathematical singularity at time t=0 and did not fit the data.

A numerical scheme (stepwise) was developed in which the rehealing equation was solved incrementally for small time steps. A flowchart of the solution process is shown in Figure 4.19. At the beginning of rehealing the specimen is at ambient temperature and the initial rehealing function is zero. Time was incremented by a small time step, Δt, and

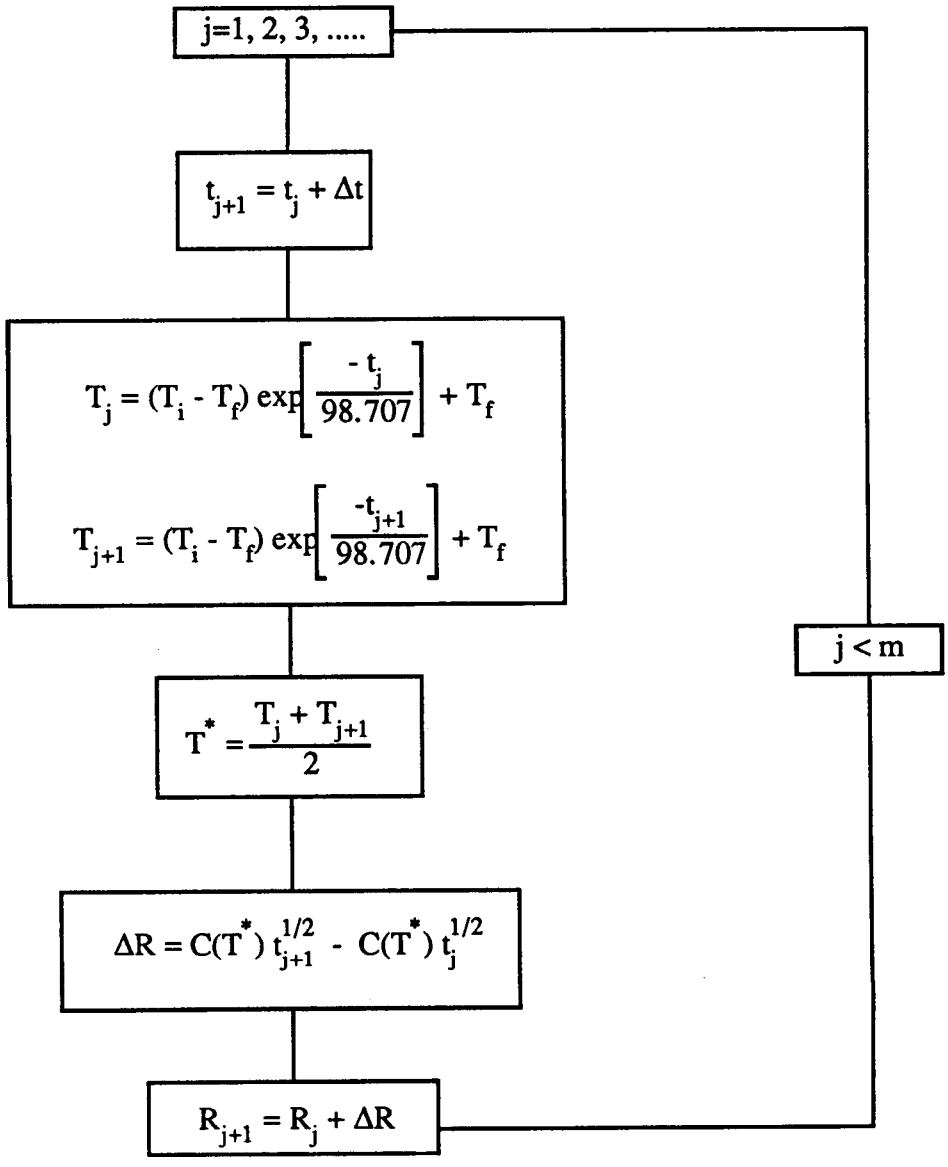

Figure 4.19 Flowchart of the stepwise solution process. The self-diffusion parameter, C(T) is calculated using either the Arrhenius or WLF expressions.

the new temperature of the sample was calculated using the NIR heat transfer solution. The former and new temperatures were averaged over the time step and and the self-diffusion parameter was calculated using this temperature. The incremental rehealing, ΔR, corresponding to Δt at the averaged temperature was calculated and added to the previous R. Then time was incremented and the calculations continue until the time reaches a set flag.

Figures 4.20 through 4.25 show a comparison between the results of the non-isothermal rehealing model using an Arrhenius temperature dependence and the measured CT data. The model accurately predicts the time at which healing first begins for all temperatures but is not accurate at low temperatures close to the T_g (Figure 4.20). At the higher temperatures the model fits the data reasonably well.

Figures 4.26 through 4.31 show a comparison between the results of the non-isothermal rehealing model using a WLF temperature dependence and the measured CT data. Like the solution with an Arrhenius temperature dependence, the WLF model accurately predicts the onset of healing. Furthermore, this model accurately predicts the degree of rehealing at long healing times and for all the temperatures tested. The amount of non-isothermal rehealing can be ascertained from the plots. In Figure 4.26 the curve is linear, with a slope corresponding to the self-diffusion parameter, C(T) at 196°C (see Figure 4.15 and Table 4.3). These results indicate that most of the healing occurred isothermally at the oven temperature. On the other hand, the curve in Figure 4.31 does not approach a straight line, indicating that most of the healing was non-isothermal at temperatures below the oven temperature. Varying degrees of this phenomenon can be seen as the oven temperature increases.

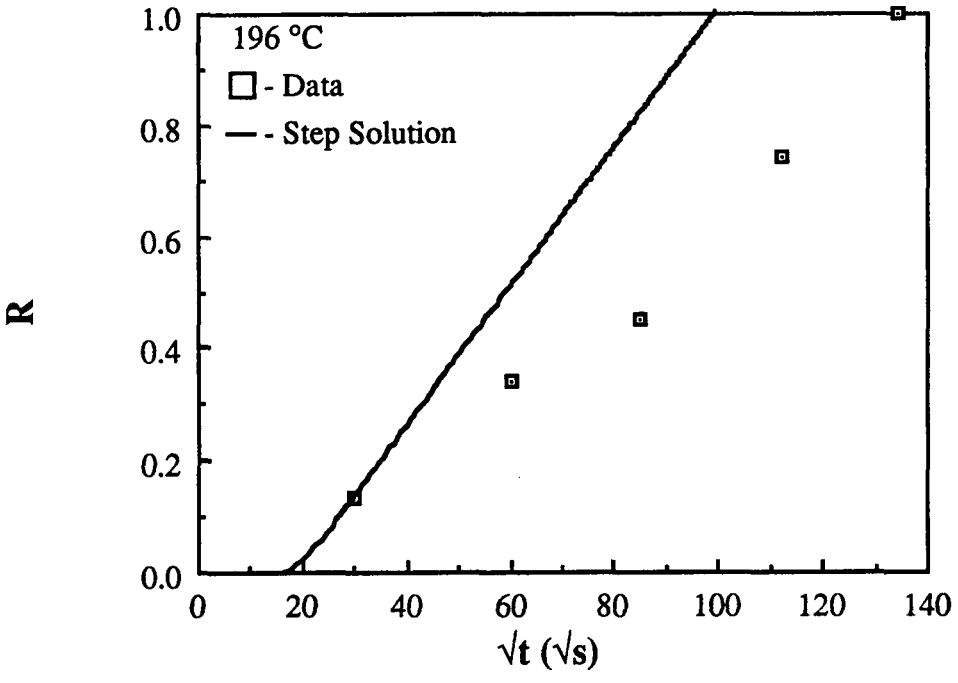

Figure 4.20 Rehealing function versus square root of contact time for Udel® P1700 polysulfone CT specimens bonded at 196°C. Comparison between data (symbols) and the non-isothermal rehealing model using an Arrhenius temperature dependence (solid line).

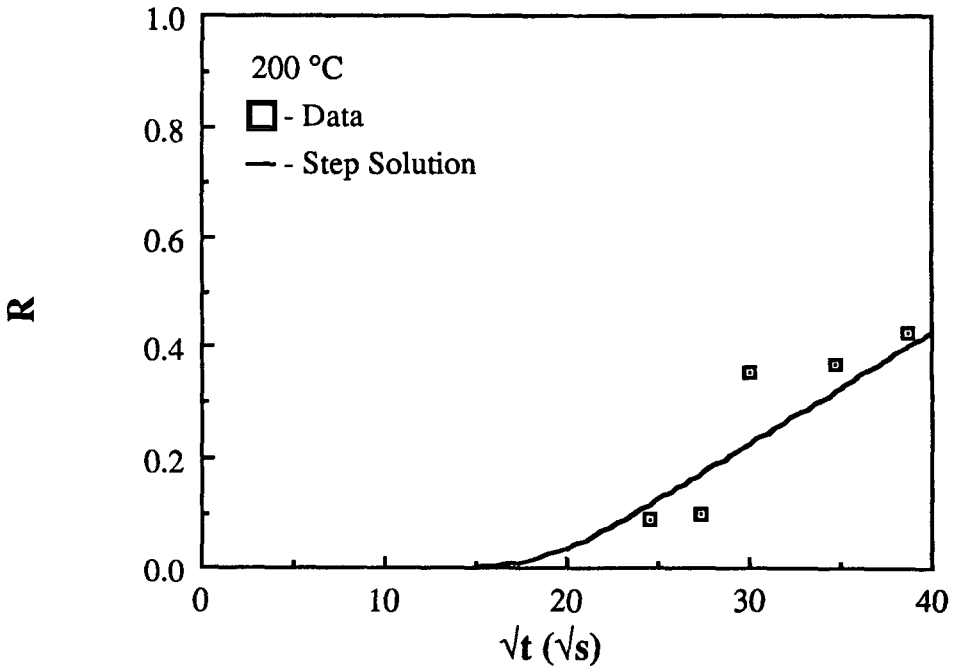

Figure 4.21 Rehealing function versus square root of contact time for Udel® P1700 polysulfone CT specimens bonded at 200°C. Comparison between data (symbols) and the non-isothermal rehealing model using an Arrhenius temperature dependence (solid line).

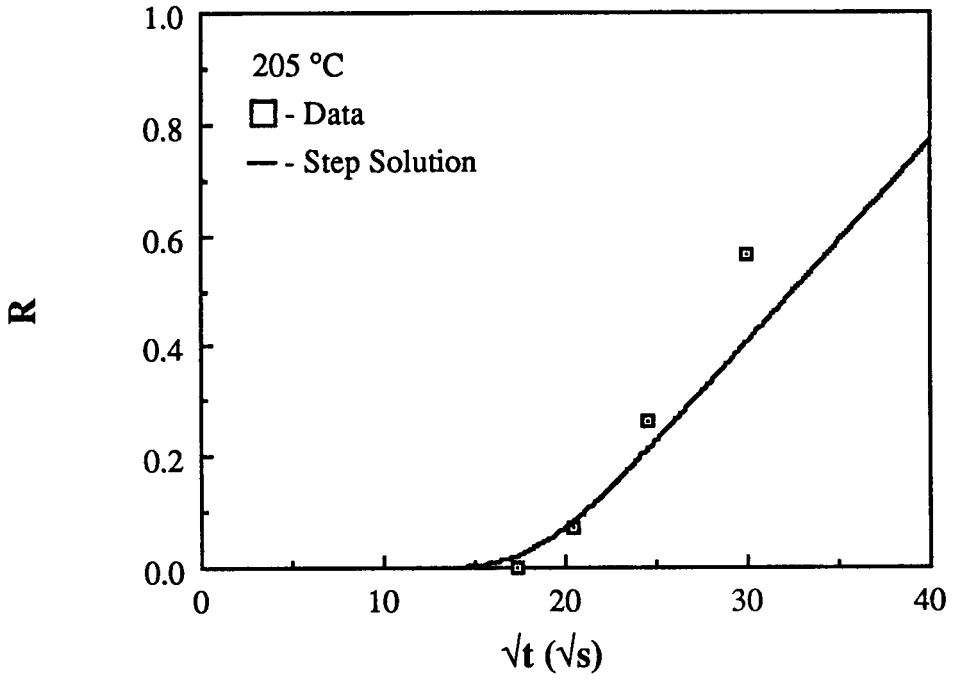

Figure 4.22 Rehealing function versus square root of contact time for Udel® P1700 polysulfone CT specimens bonded at 205°C. Comparison between data (symbols) and the non-isothermal rehealing model using an Arrhenius temperature dependence (solid line).

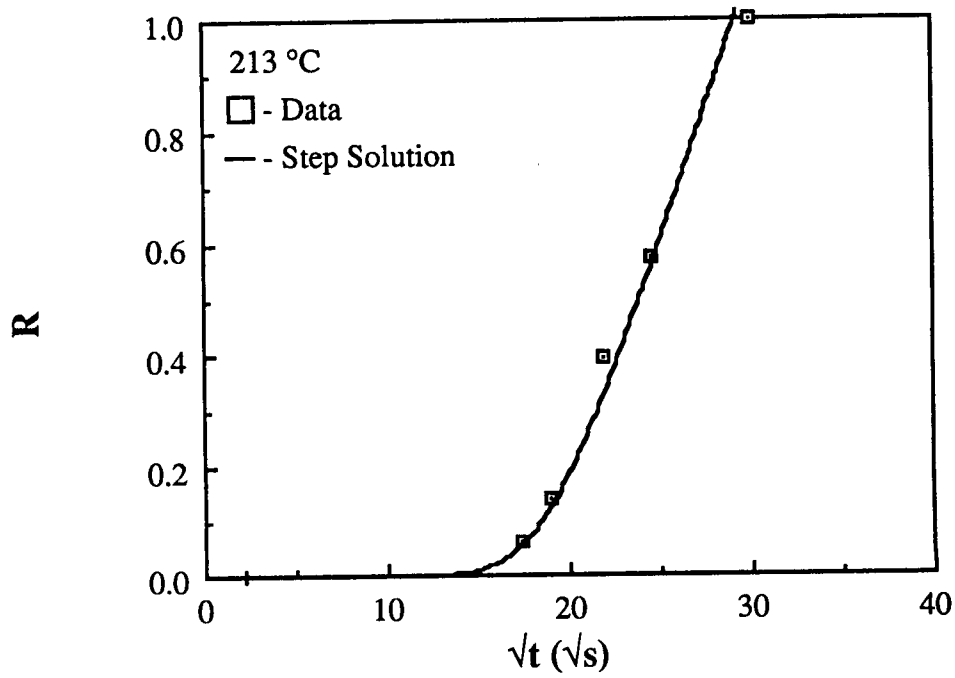

Figure 4.23 Rehealing function versus square root of contact time for Udel® P1700 polysulfone CT specimens bonded at 213°C. Comparison between data (symbols) and the non-isothermal rehealing model using an Arrhenius temperature dependence (solid line).

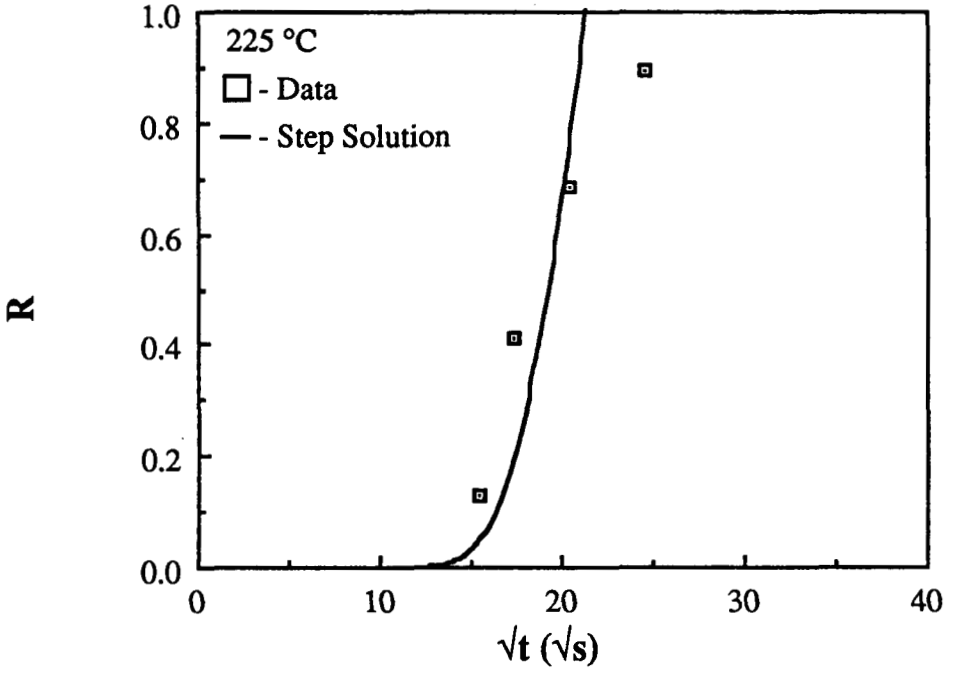

Figure 4.24 Rehealing function versus square root of contact time for Udel® P1700 polysulfone CT specimens bonded at 225°C. Comparison between data (symbols) and the non-isothermal rehealing model using an Arrhenius temperature dependence (solid line).

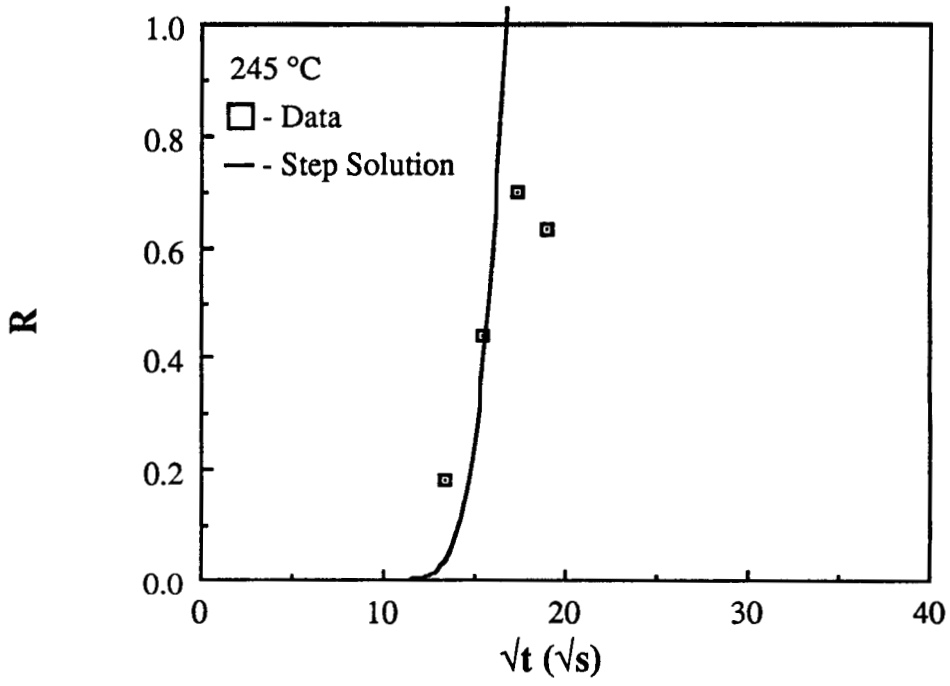

Figure 4.25 Rehealing function versus square root of contact time for Udel® P1700 polysulfone CT specimens bonded at 245°C. Comparison between data (symbols) and the non-isothermal rehealing model using an Arrhenius temperature dependence (solid line).

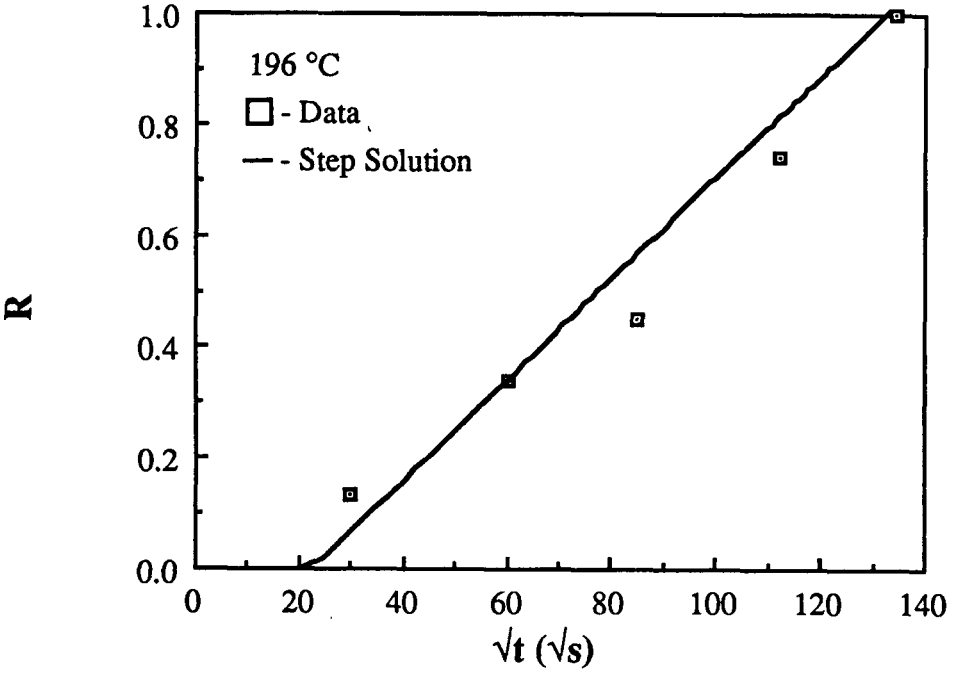

Figure 4.26 Rehealing function versus square root of contact time for Udel® P1700 polysulfone CT specimens bonded at 196°C. Comparison between data (symbols) and the non-isothermal rehealing model using a WLF temperature dependence (solid line).

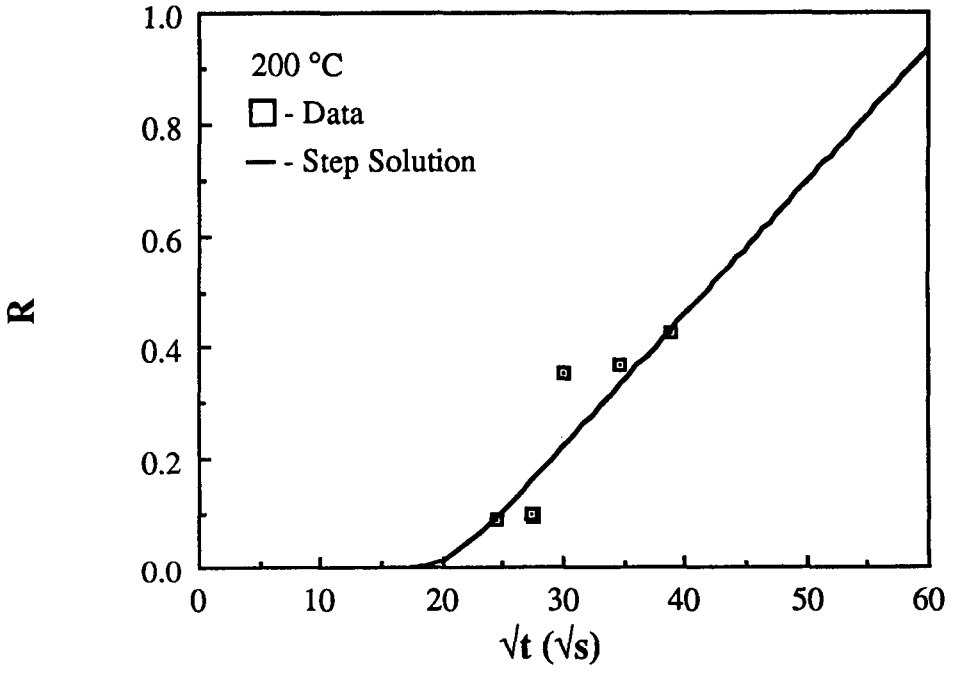

Figure 4.27 Rehealing function versus square root of contact time for Udel® P1700 polysulfone CT specimens bonded at 200°C. Comparison between data (symbols) and the non-isothermal rehealing model using a WLF temperature dependence (solid line).

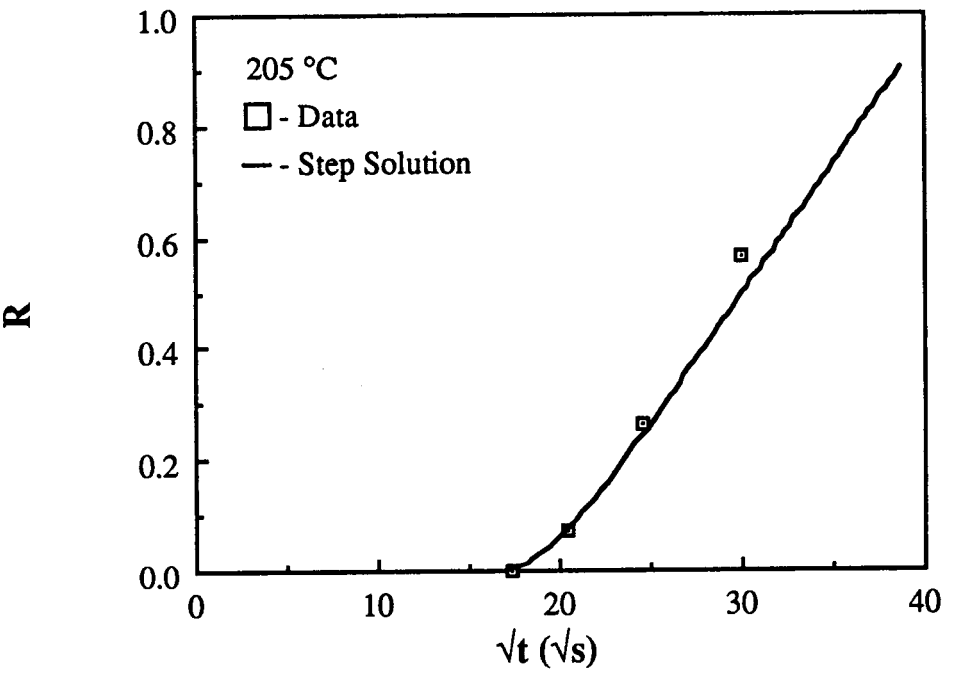

Figure 4.28 Rehealing function versus square root of contact time for Udel® P1700 polysulfone CT specimens bonded at 205°C. Comparison between data (symbols) and the non-isothermal rehealing model using a WLF temperature dependence (solid line).

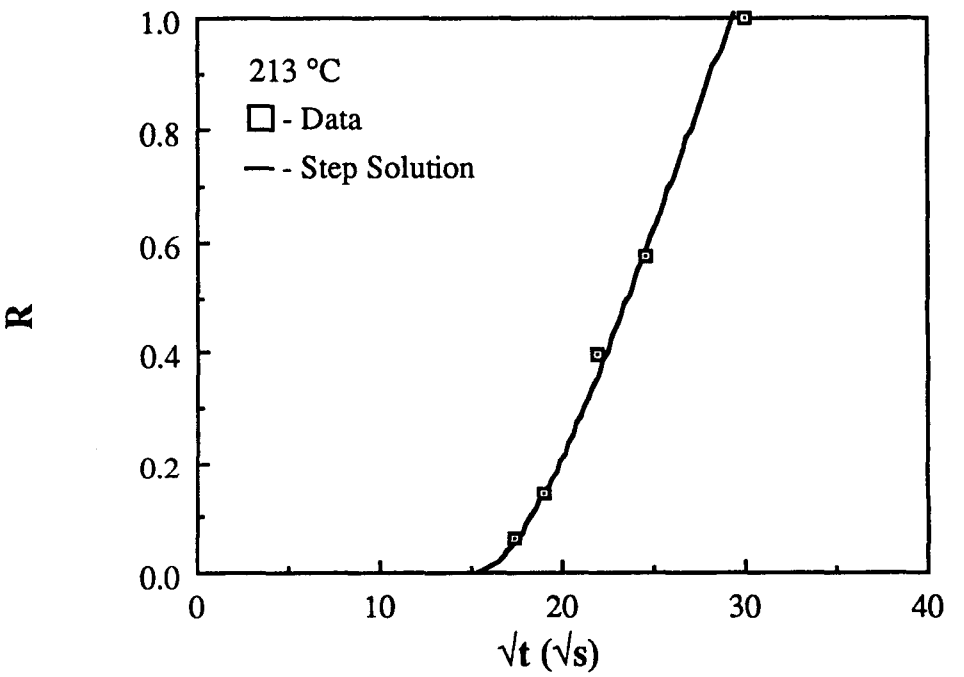

Figure 4.29 Rehealing function versus square root of contact time for Udel® P1700 polysulfone CT specimens bonded at 213°C. Comparison between data (symbols) and the non-isothermal rehealing model using a WLF temperature dependence (solid line).

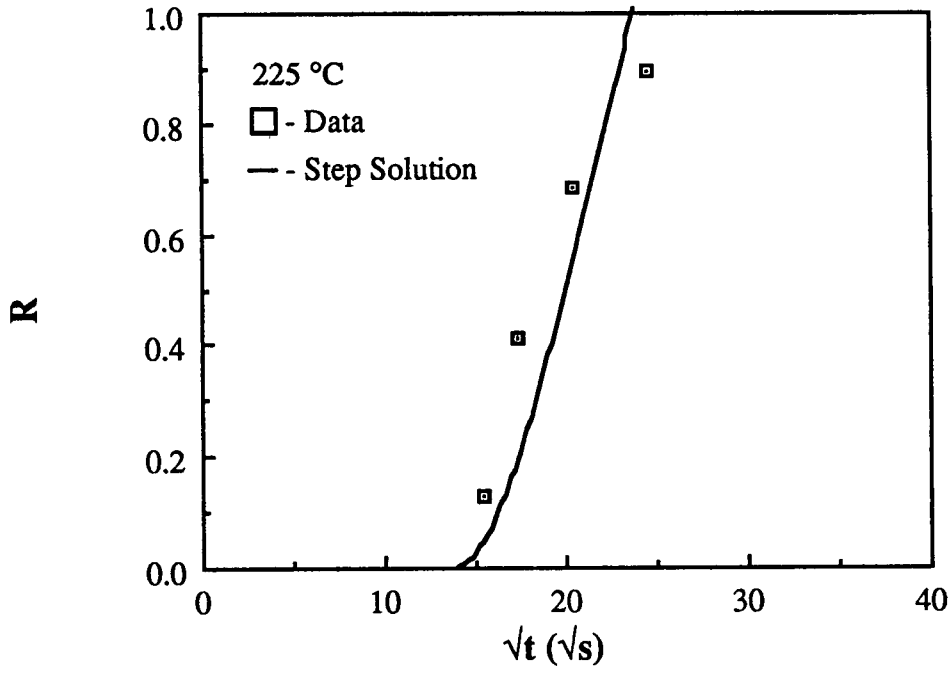

Figure 4.30 Rehealing function versus square root of contact time for Udel® P1700 polysulfone CT specimens bonded at 225°C. Comparison between data (symbols) and the non-isothermal rehealing model using a WLF temperature dependence (solid line).

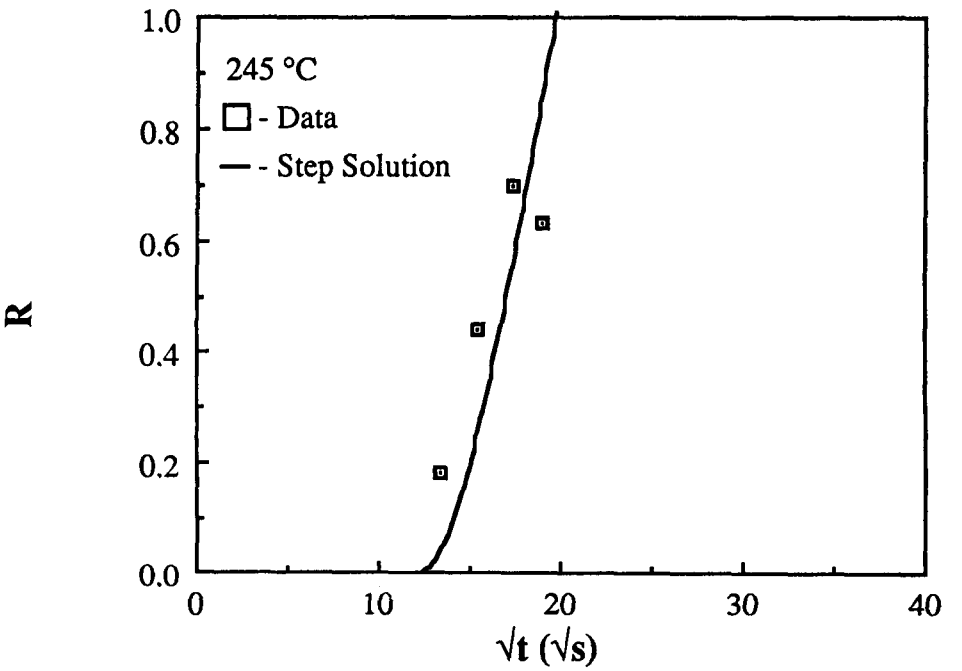

Figure 4.31 Rehealing function versus square root of contact time for Udel® P1700 polysulfone CT specimens bonded at 245°C. Comparison between data (symbols) and the non-isothermal rehealing model using a WLF temperature dependence (solid line).

4.8 CT Fractography

Fractography was performed, in a scanning electron microscope (SEM), on the failed CT specimens. Four different specimens were studied. These included a virgin (i.e. not rehealed) specimen and three specimens that had been rehealed and refractured. The refractured specimens had rehealing function values of 0.37, 0.81, and 1.0. Figure 4.32 shows the failure surface of the virgin sample at magnifications of 48.6X and 163X. Large amounts of deformation are apparent with roughly parallel crazes. Figure 4.33 shows the failure surface of a CT specimen with a rehealing function of 0.37. Much less deformation is apparent but the parallel crazes are discernable. Figures 4.34 and 4.35 show the failure surfaces of samples with rehealing values of 0.81 and 1.0, respectively. The amount of deformation in the failure surface increases with increasing degree of rehealing. The failure surface in Figure 4.35 has a similar appearance to the failure surface in the virgin specimen. This indicates that the same failure mechanisms occur in the rehealed specimens as in the virgin specimens. Thus, it can be concluded that the fracture toughness and failure mechanisms of a completely rehealed polysulfone specimen are the same as the virgin material.

4.9 Double Cantilever Beam Composite Test

A double cantilever beam (DCB) interlaminar toughness test was used to examine interfacial strength development in fiber-reinforced thermoplastic composites. The test

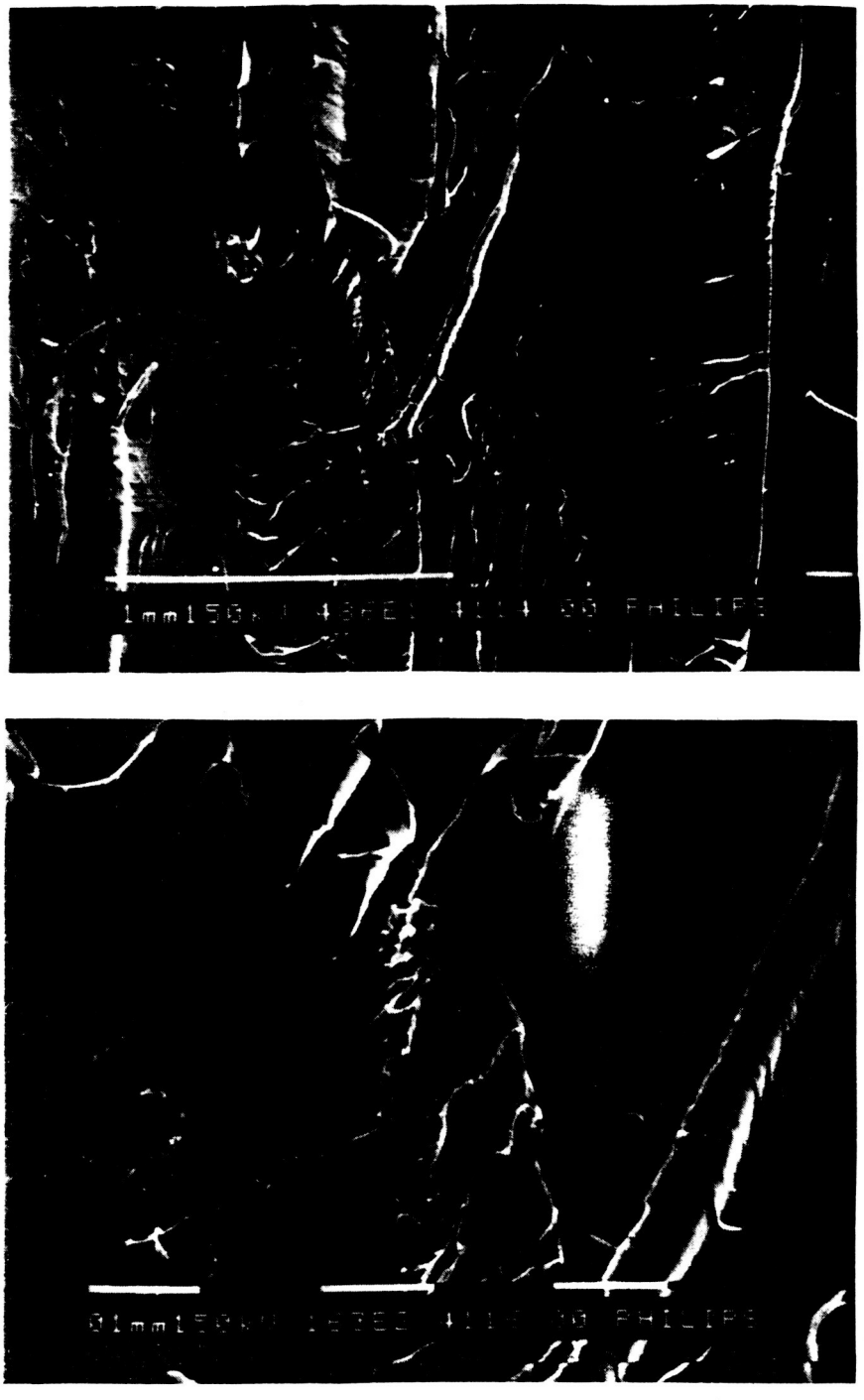

Figure 4.32 Scanning electron micrographs of virgin CT specimen. The top figure is at 48.6X, the bottom figure at 163X. Crack growth is from the top of the figure to the bottom.

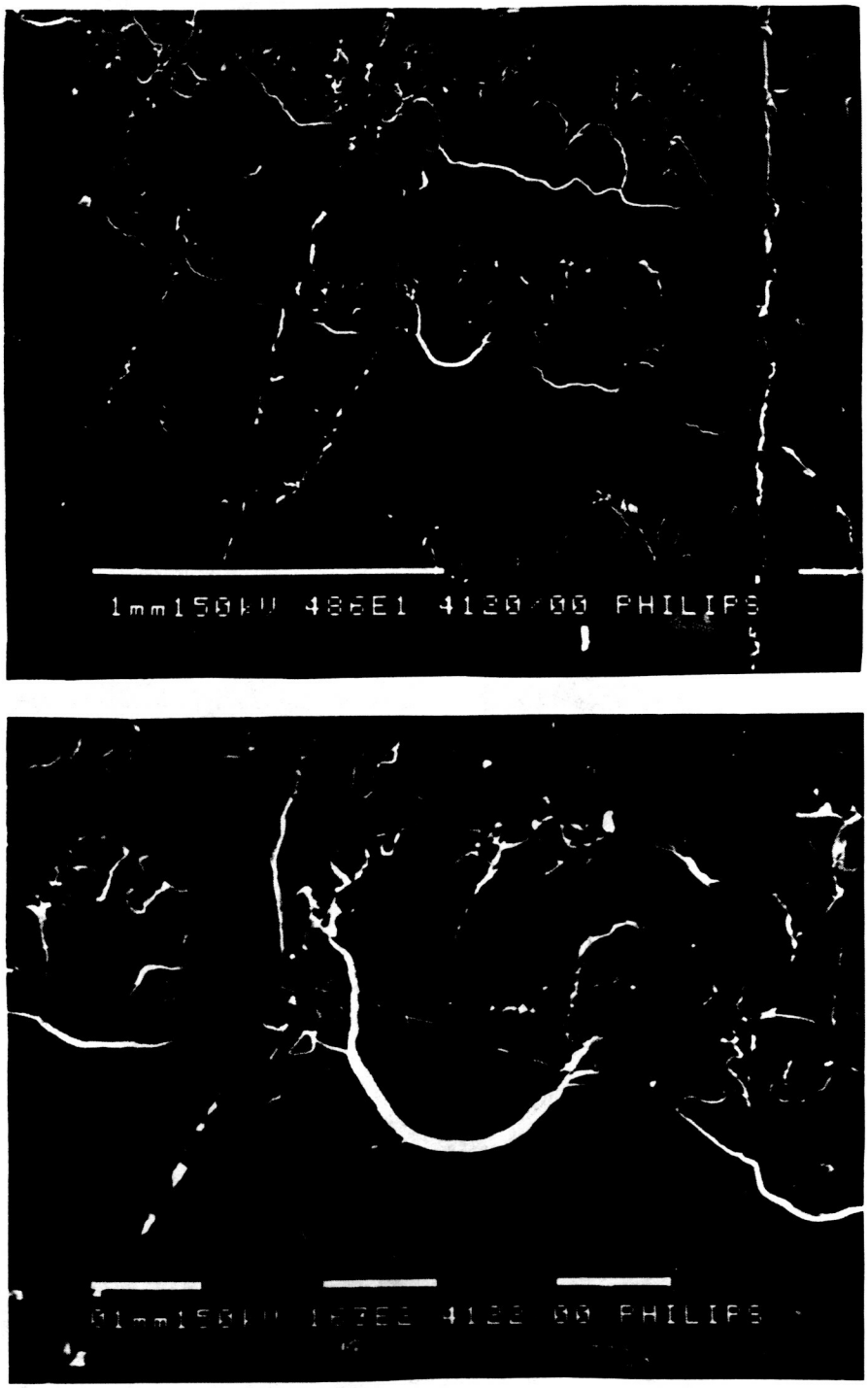

Figure 4.33 Scanning electron micrographs of CT specimen with R of 0.37. The top figure is at 48.6X, the bottom figure at 163X. Crack growth is from the top of the figure to the bottom.

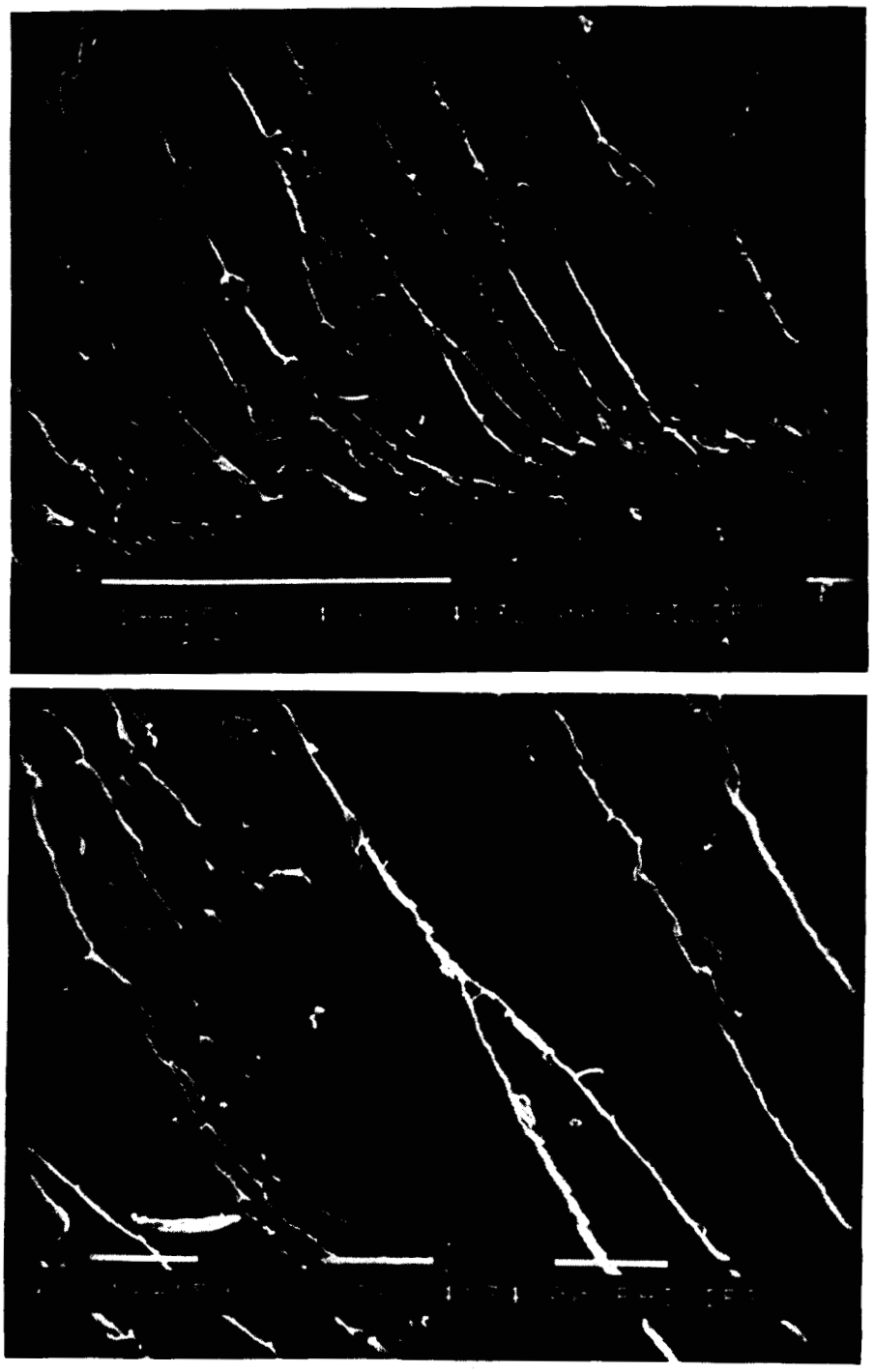

Figure 4.34 Scanning electron micrographs of CT specimen with R of 0.81. The top figure is at 48.6X, the bottom figure at 163X. Crack growth is from the top of the figure to the bottom.

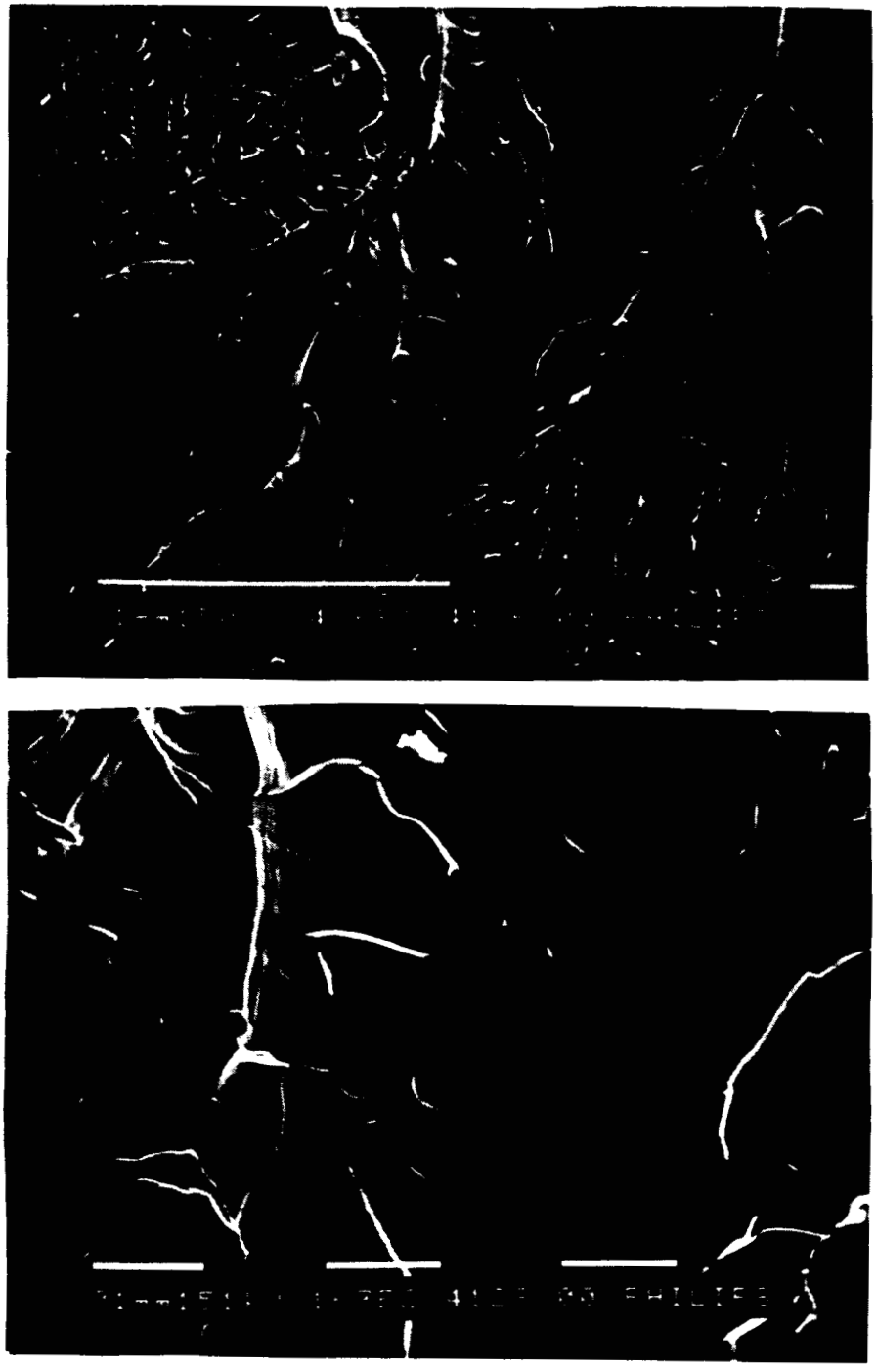

Figure 4.35 Scanning electron micrographs of CT specimen with R of 1.0. The top figure is at 48.6X, the bottom figure at 163X. Crack growth is from the top of the figure to the bottom.

measured the critical strain energy release rate of unidirectional graphite-polysulfone composite rehealed at different temperatures and contact times. Like the CT test, the crack was allowed to propagate only far enough to obtain good data; but the specimen remained in one piece. This ensured that maximum contact was obtained upon rehealing.

The first set of tests measured the critical strain energy release rate of the undamaged composite. The results are plotted in Figure 4.36. The critical strain energy release rate increased with increasing crack length. This was due to the fibers in the unidirectional laminae "bridging" the crack and bearing some of the load that would normally go into the fracture process. As the crack propagated, these fibers pulled out from the rest of the composite absorbing some energy. The mean critical energy release rate for the undamaged specimens was 551.3 n/m (3.148 lb/in.). In reporting values of the critical strain energy release rate for rehealed specimens, the mean of all tests was used since the effect of bridging should be similar for either undamaged or rehealed DCB specimens.

Following the same non-dimensional scheme used for the CT specimens, the rehealing function is defined as

$$R = \frac{G_{1C}}{G_{1C_\infty}} \tag{4.2}$$

The rehealing function, R versus the square root of time is plotted in Figures 4.37 through 4.39 for rehealing temperatures of 213, 225 and 245°C. The symbols represent the mean of the data and the error bars represent the upper and lower bounds on the data.

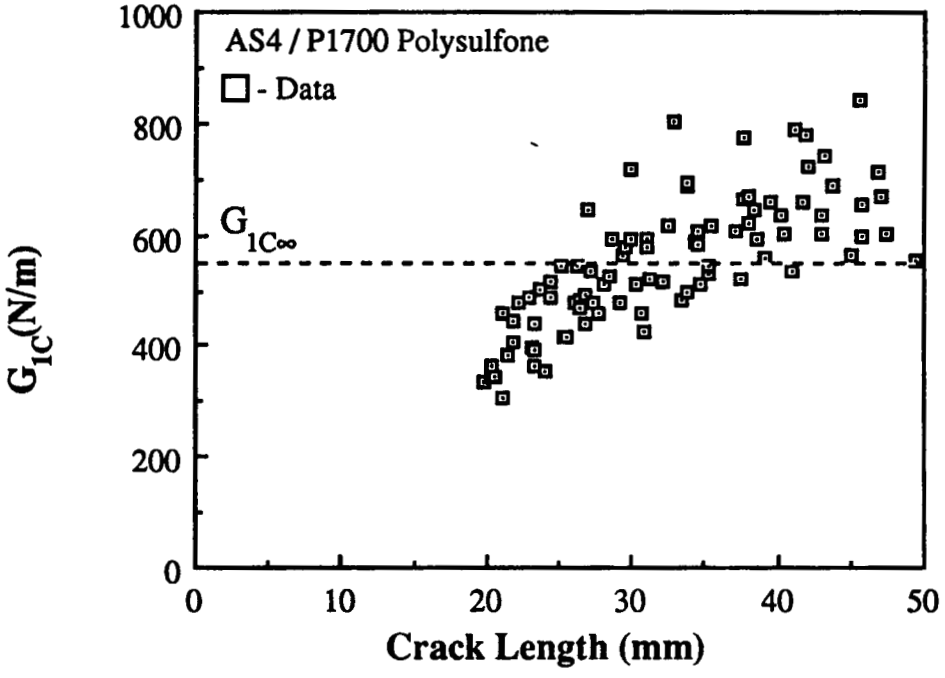

Figure 4.36 Critical strain energy release rate versus crack length for AS4/Polysulfone DCB specimens. Symbols represent data. Dashed line represents the mean of the data ($G_{1C\infty}$).

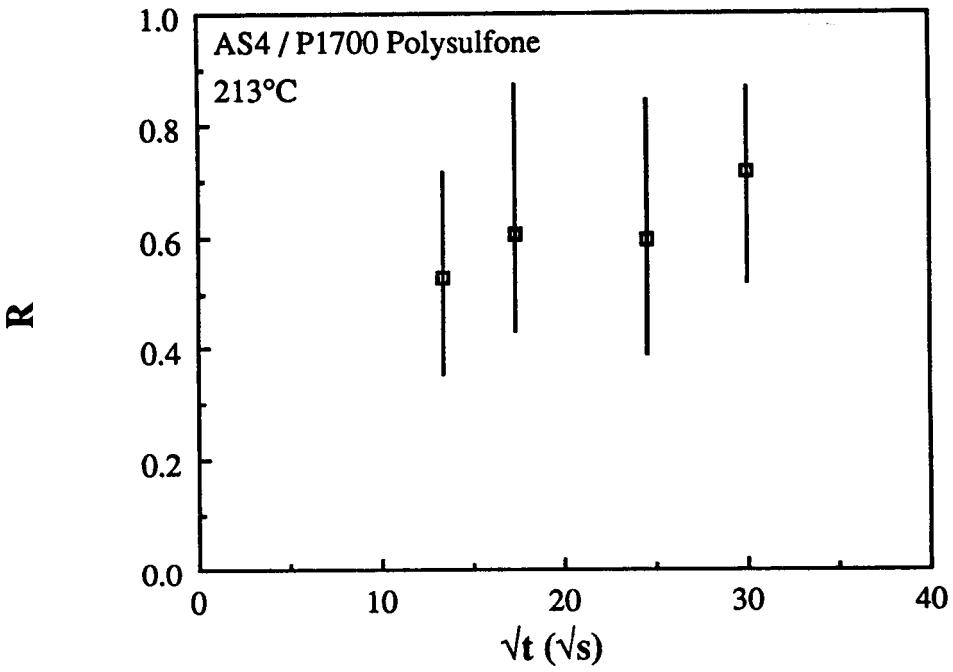

Figure 4.37 Rehealing function, R versus square root of time for AS4 / Polysulfone DCB specimens healed at 213°C. Symbols represent data. Error bars represent the lower and upper bounds on the data.

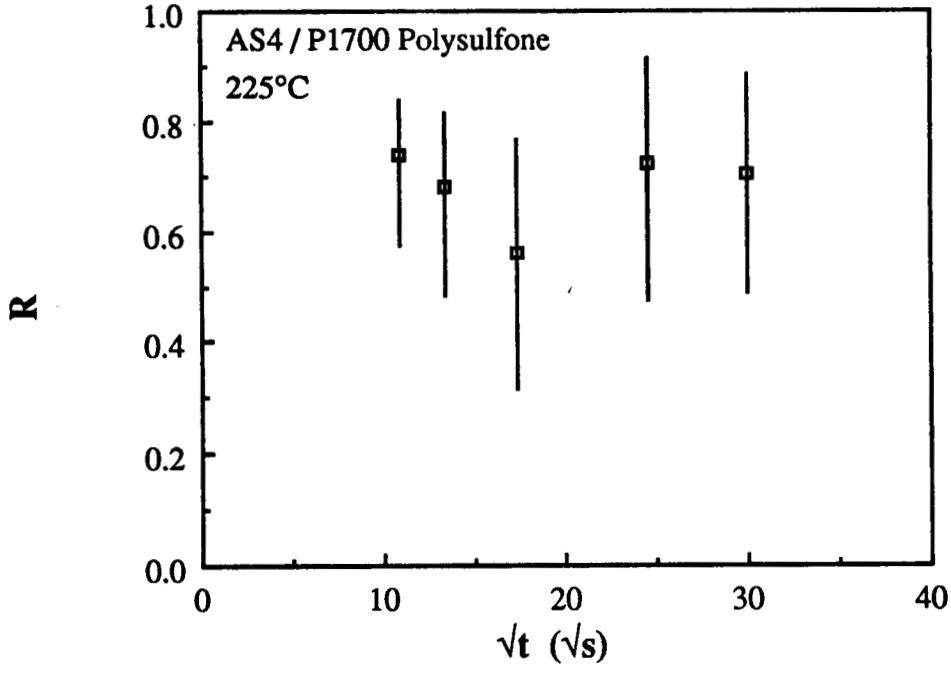

Figure 4.38 Rehealing function, R versus square root of time for AS4 / Polysulfone DCB specimens healed at 225°C. Symbols represent data. Error bars represent the lower and upper bounds on the data.

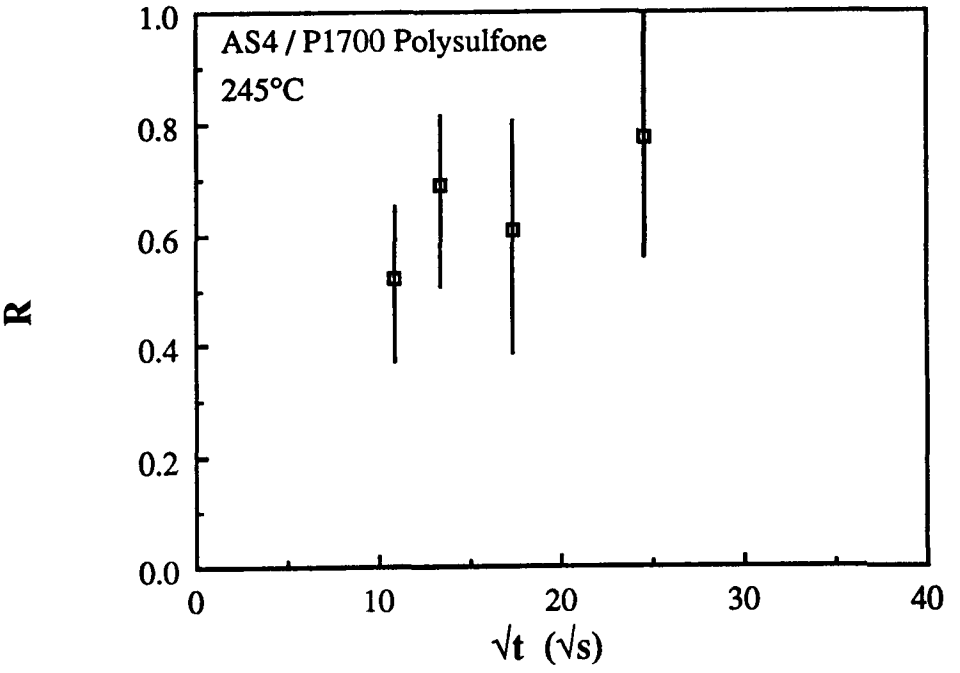

Figure 4.39 Rehealing function, R versus square root of time for AS4 / Polysulfone DCB specimens healed at 245°C. Symbols represent data. Error bars represent the lower and upper bounds on the data.

The composite data do not show the same strong time and temperature dependence that was observed in the neat resin tests. The data obtained at 213°C and 245°C (Figures 4.37 and 4.39) do show a weak increase in the critical strain energy release rate with increasing contact time; however, the data at 225°C do not show an increase in the critical strain energy release rate with increasing contact time (Figure 4.38). This indicates that the theories outlined in Chapter 2, assuming instantaneous wetting, do not apply. Furthermore, only about eighty percent (80%) of the original fracture energy is recovered upon rehealing.

The time required to achieve complete interfacial healing by autohesion was calculated using the isothermal rehealing model in equation (4.8) with the self-diffusion parameter, C(T), determined in Section 4.5. The model predicts that the interface will be completely rehealed in 127 seconds at 213°C, 51 seconds at 225°C, and 22 seconds at 245°C. These calculations of course neglect wetting effects but do show that sufficient time has elapsed for complete healing of the interface by self-diffusion. Thus, it can be concluded that wetting, intimate contact, and resin flow cause a different time dependency than the autohesive phenomenon alone [6].

The lower toughness upon rehealing can be explained by different fracture mechanisms occurring in the undamaged specimens than in the rehealed ones. During the first crack growth, a number of mechanisms contribute to the measured critical strain energy release rate. Among these are resin deformation, interfacial failure, fiber peeling, and fiber breakage [27]. As the crack propagates, microcracks are formed on planes adjacent to the main crack plane which contribute to the amount of energy absorbed during the test.

Also the main crack may not follow a straight path but jump between different crack planes.

Following rehealing of the specimen, the recrack propagation will follow the path of least resistance that was established previously. The recrack may not cause microcracking or breaking of the fibers that were broken in the first test and the lack of these energy absorbing phenomenon cause the discrepancies between the first and subsequent tests of the same specimen.

4.10 DCB Composite Fractography

Scanning electron microscopy (SEM) was performed on the DCB specimens to determine if there were differences in the failure mechanisms between undamaged and rehealed specimens.

Three DCB samples were examined in the SEM. One was a virgin specimen and the other two were fractured and rehealed three times. Both rehealed specimens had rehealing function values that varied between 0.5 and 0.8. Two locations, corresponding to the beginning and the end of the crack, were examined on each specimen. Figures 4.40 and 4.41 show the failure surfaces of the virgin specimens. The specimens show only small amounts of polymer deformation, indicating low toughness. A poor fiber matrix bond is indicated by bare fibers and long polymer tendrils. The polymer tendrils were stripped off the fiber during the test. Stray fibers indicate fiber breakage and pull-out.

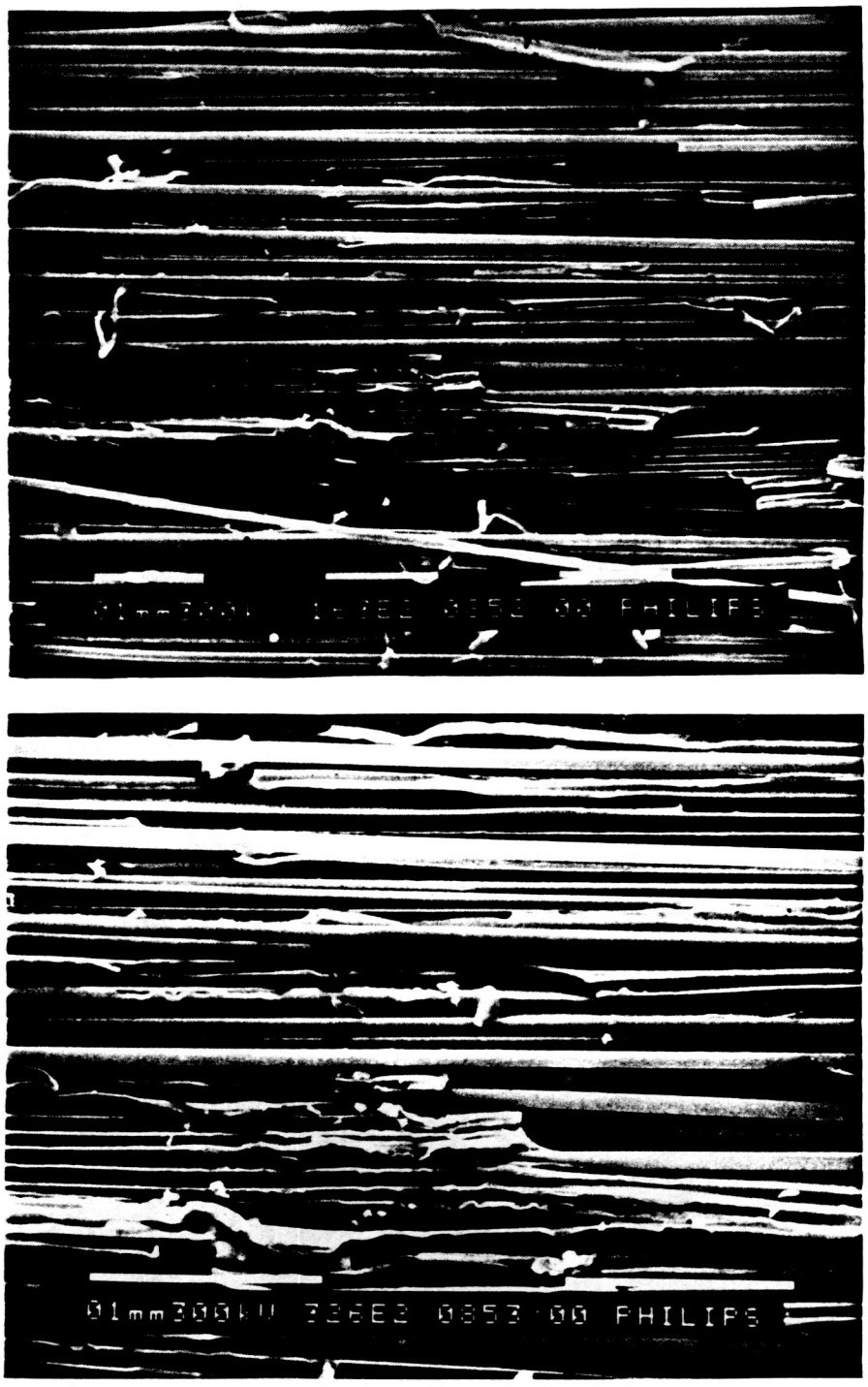

Figure 4.40 Scanning electron micrographs of virgin DCB specimen at beginning of crack. The top figure is at 163X, the bottom figure at 326X.

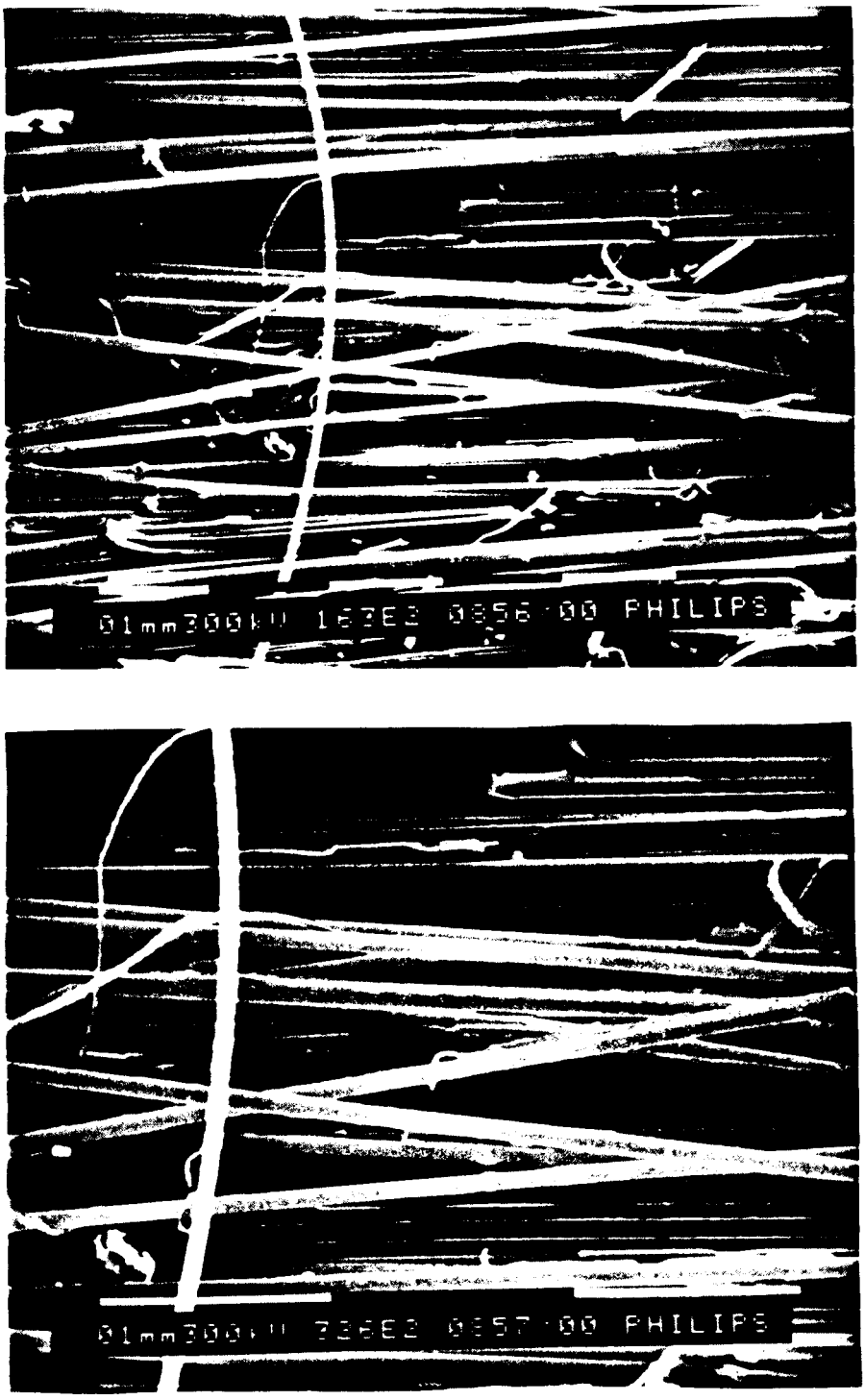

Figure 4.41 Scanning electron micrographs of virgin DCB specimen at end of crack. The top figure is at 163X, the bottom figure at 326X.

The rehealed specimens, shown in Figures 4.42 - 4.45, show a greater amount of resin at the fracture plane than the virgin specimens. This indicates that during rehealing some polymer flow was taking place. The different appearance of the rehealed failure surfaces in the DCB specimens indicates that different failure mechanisms contributed to the rehealed critical strain energy release rate. Some of the possible differences were mentioned above (see the end of Section 4.9). The flow of resin indicates that the surfaces were not in intimate contact immediately and even though the fiber tows were touching, the individual fibers were not necessarily in intimate contact. A possible cause of the lack of intimate contact was due to the stray, broken fibers created during the first crack growth. These fibers did not lie parallel to the other fibers and upon healing interfered with the intimate contact between the crack surfaces.

Differences in both the fracture toughness and the fracture mechanism between virgin and healed DCB specimens indicates that if thermoplastic matrix composites are to be repaired, the repaired part will not have the same toughness as the undamaged material regardless of how long heat and pressure are applied.

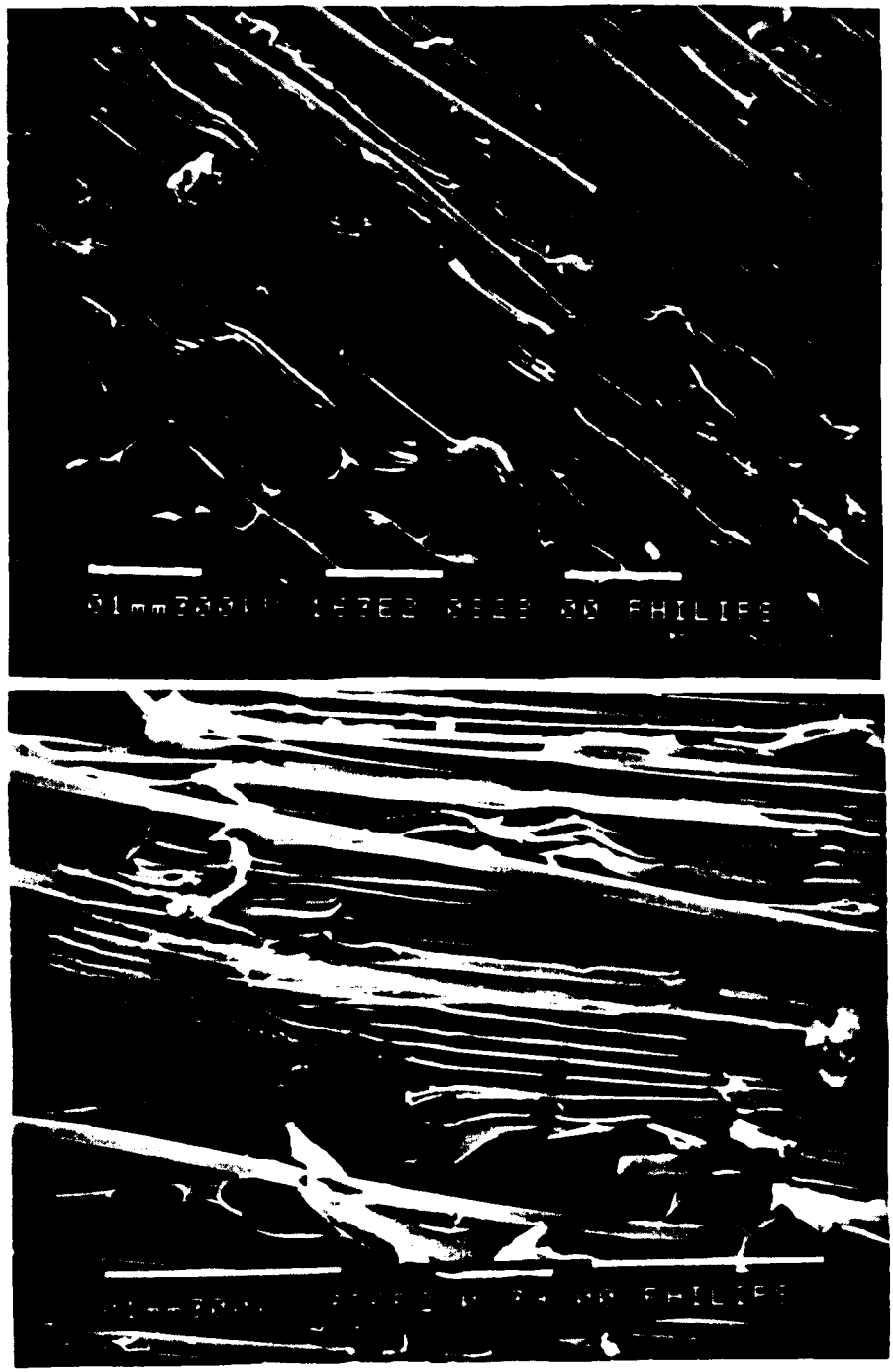

Figure 4.42 Scanning electron micrographs of rehealed DCB specimen at beginning of crack. The top figure is at 163X, the bottom figure at 326X. The value of the rehealing function was 0.5.

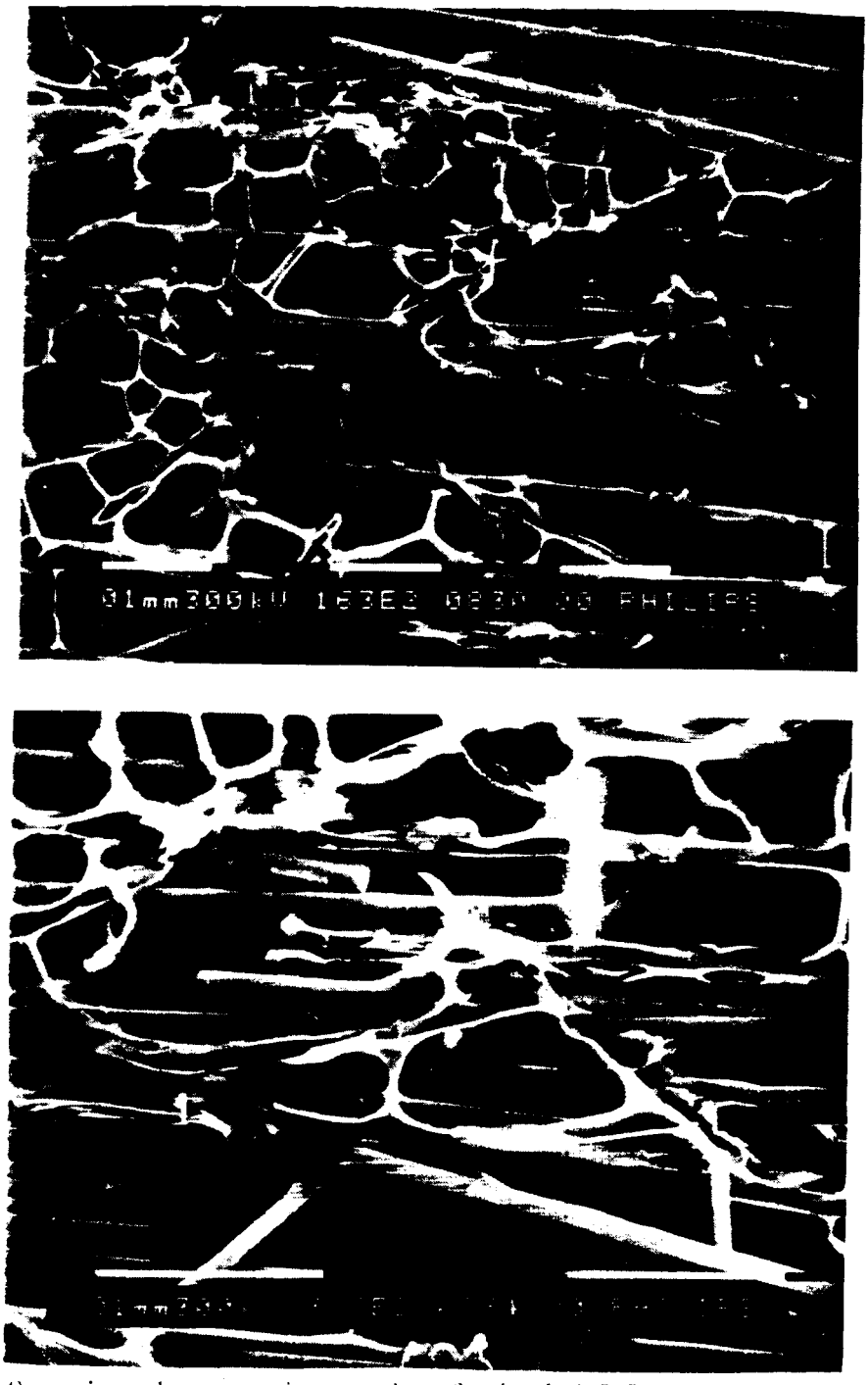

Figure 4.43 Scanning electron micrographs of rehealed DCB specimen at end of crack. The top figure is at 163X, the bottom figure at 326X. The value of the rehealing function was 0.5.

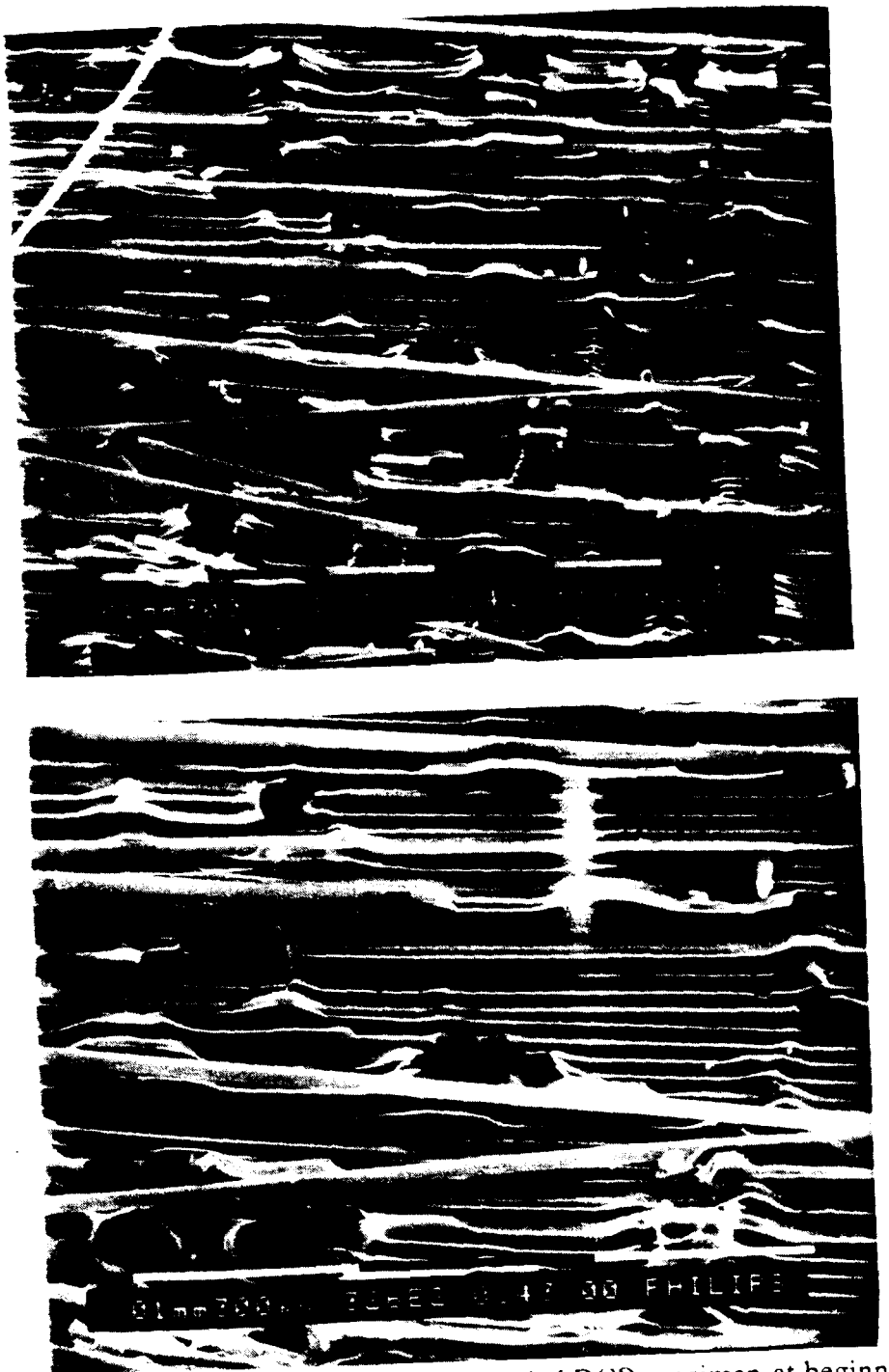

Figure 4.44 Scanning electron micrographs of rehealed DCB specimen at beginning of crack. The top figure is at 163X, the bottom figure at 326X. The value of the rehealing function was 0.8.

Figure 4.45 Scanning electron micrographs of rehealed DCB specimen at end of crack. The top figure is at 163X, the bottom figure at 326X. The value of the rehealing function was 0.8.

5.0 Conclusions

Three mechanical tests were investigated for characterizing autohesive strength in amorphous thermoplastic resins and fiber-reinforced amorphous thermoplastic composites. These included an interfacial tension test, a compact tension fracture toughness test and a double cantilever beam interlaminar toughness test.

Although the healing parameters temperature, pressure, and contact time could be easily controlled, the interfacial test results were very poor. The specimens were difficult to prepare and there were excessive variations in the measured interfacial strength. It was determined that the present interfacial tension test was unacceptable for measuring autohesive strength development in neat resin samples.

The results obtained using the compact tension test were good. The mechanical measurements were repeatable with an acceptable amount of data scatter. However, due to healing in a forced air oven, the specimens were not rehealed isothermally. Therefore, theories developed for isothermal healing cannot be directly applied to the data.

A non-isothermal rehealing model was developed by incorporating a negligible internal resistance heat transfer model into the isothermal rehealing model, and an Arrhenius and WLF type temperature dependent model. The non-isothermal model was applied to the results obtained from the compact tension test and was found to give good results. Using scanning electron microscopy, the failure mechanisms in the healed CT specimens were determined to be the same as in the virgin specimens. It was determined that the CT test

is suitable for self-diffusion parameter measurements.

The self-diffusion coefficient of polysulfone P1700 was estimated at each of the test temperatures using the data obtained in the CT tests. The activation energy of the self-diffusion process was calculated and compared well to the zero shear viscosity activation energy; however, it did not compare well to another studies self diffusion activation energy for polysulfone.

Autohesive strength in fiber-reinforced thermoplastic composites was measured using a double cantilever beam interlaminar toughness test. The data do not show a strong time or temperature dependence as observed in the neat resin tests. Furthermore, only about eighty percent of the undamaged fracture energy can be recovered. This is accounted for by different fracture mechanisms in the virgin than the rehealed DCB specimens. SEM examination of the failure surface revealed that the healed DCB specimens have more resin at the refracture plane than the virgin specimens. Resin flow and the lack of strong time and temperature dependence in the DCB data indicates that intimate contact was not established immediately. It was determined that the DCB test is poor at measuring the autohesive strength development in fiber-reinforced prepreg; however, the test does indicate that repair of fiber-reinforced amorphous thermoplastic composites is possible although the original toughness cannot be attained.

The following recommendations are made for further study:

Analyze the interfacial test results using a fracture mechanics approach.

Develop a composite test that heals new prepreg only, to eliminate the differences in failure mechanisms between new and rehealed samples.

Determine pressure effects on the composite autohesion.

Extend the model to incorporate new advanced tough thermoplastics and thermoplastic matrix composites

6.0 References

1. Dara, P. H. and Loos, A.C., "Thermoplastic Matrix Composite Processing Model," Report No. CCMS-85-10 and VPI-E-85, Center for Composite Materials and Structures, Virginia Polytechnic Institute and State University, Blacksburg, Va. 1985.

2. Voyutskii, S.S., *Autohesion and Adhesion of High Polymers*, Volume 4, Polymer Reviews, Interscience Publishers, New York, 1963.

3. De Gennes, P. G., "Entangled Polymers," *Physics Today*, pp. 33-39, June, 1983.

4. Wool, R.P., "Relations for Healing, Fracture, Self-Diffusion and Fatigue of RandomCoil Polymers," *ACS Polymer Preprints*, **23** (2), 62, 1982.

5. Wool, R.P., "Craze Healing in Polymer Glasses," *Polymer Engineering and Science*,**21**, 970, 1981.

6. Wool, R.P. and O'Connor, K. M., "A Theory of Crack Healing in Polymers," *Journal of Applied Physics*, **52**, 5953, 1981.

7. Wool, R.P. and O'Connor, K. M., "Time Dependence of Crack Healing," *Journal of Polymer Science: Polymer Letters Edition*, **20**, 7, 1982.

8. Wool, R.P., "Molecular Aspects of Tack," *Rubber Chemistry and Technology*, **57**, 307, 1983.

9. Prager, S. and Tirrell, M., "The Healing Process at Polymer-Polymer Interfaces," *Journal of Chemical Physics*, **75**, 5194, 1981.

10. Jud, K., Kausch, J. and Williams, J. G., "Fracture Mechanics Studies of Crack Healing and Welding of Polymers," *Journal of Materials Science*, **16**, 204, 1981.

11. Skewis, J. D., "Self-Diffusion Coefficients and Tack of Some Rubbery Polymers," *Rubber Chemistry and Technology*, **39**, 217, 1966.

12. Bothe, Lothar and Rehage, Guenther, "Autohesion of Elastomers," *Rubber Chemistry and Technology*, **55**, 1308, 1981.

13. Bauer, "Investigation into the Mechanism of Tack of Rubbers," *Journal of Polymer Science: Part A-2*, **10**, 541, 1972.

14. Rhee, C. K. and Andries, J. C., "Factors which Influence Autohesion of Elastomers," *Rubber Chemistry and Technology*, **54**, 101, 1980.

15. Hamed, G. R., "Tack and Green Strength of NR, SBR and NR/SBR Blends," *Rubber Chemistry and Technology*, **54**, 403 , 1980.

16. Boenig, H. V., Willer, C. B. and Shottafer, J. E., "Tack in Urethan Elastomers," *Rubber Chemistry and Technology*, **39**, 974, 1966.

17. Hinkley, J.A., "Small Compact Tension Specimens for Polymer Toughness Screening," *Journal of Applied Polymer Science*, **32**, 5653, 1986.

18. Mills, N. J., "The Role of Entanglement Networks in the Fracture of Polysulfone," *Rheologica Acta,* **13**, 185, 1974.

19. Shaw, M. T. and Miller, J. C., "The Rheology of Polysulfone," *Polymer Engineering and Science*, **18**, 372, 1978.

20. Ham, Joe S., "Effects of Chain Stiffness in a Polysulfone," *Polymer Preprints*, **23**, 13, 1982.

21. Collins, J.A., *Failure of Materials in Mechanical Design*, Wiley, New York, 1981, P. 58.

22. Gales, R.D.R. and Mills, N.J., "The Plane Strain Fracture of Polysulfone," *Engineering Fracture Mechanics*, **6**, 93-104 , 1974.

23. Chapman, Alan J., *Heat Transfer*, Macmillan, New York, 1984, P. 124.

24. Union Carbide, *Udel polysulfone Technical Information*, Union Carbide Corporation, 270 Park Avenue, New York, New York, 10017.

25. Harper, Charles A., *Handbook of Plastics and Elastomers*, McGraw-Hill, New York, 1976, P. 2-50.

26. Ferry, John D., *Viscoelatic Properties of Polymers*, Wiley, New York, 1980, P. 280.

27. Hinkley, Jeffrey A., Private communication

BIBLIOGRAPHIC DATA SHEET	1. Report No. CCMS-87-15, VPI-E-87-20	2.	3. Recipient's Accession No.
4. Title and Subtitle INTERFACIAL STRENGTH DEVELOPMENT IN THERMOPLASTIC RESINS AND FIBER-REINFORCED THERMOPLASTIC COMPOSITES			5. Report Date Sep 1987 6.
7. Author(s) J. C. Howes and A. C. Loos			8. Performing Organization Rept. No. VPI-E-87-20
9. Performing Organization Name and Address Virginia Polytechnic Institute & State University Dept of Engineering Science & Mechanics Norris Hall Blacksburg, Virginia 24061			10. Project/Task/Work Unit No. 11. Contract/Grant No. NAG-1-343
12. Sponsoring Organization Name and Address Polymeric and Applied Materials Branches National Aeronautics and Space Administration Langley Research Center Hampton, Virginia 23665			13. Type of Report & Period Covered 14.

15. Supplementary Notes

16. Abstracts

An experimental program to develop test methods which can be used to characterize interfacial (autohesive) strength development in polysulfone thermoplastic resin and graphite-polysulfone prepreg during processing is reported. Two test methods were used to examine interfacial strength development in neat resin samples. These included an interfacial tension test and a compact tension (CT) fracture toughness test. The interfacial tensile test proved to be very difficult to perform with a considerable amount of data scatter. Thus, the interfacial test was discarded in favor of the fracture toughness test. Interfacial strength development was observed by measuring the refracture toughness of precracked compact tension specimens that were rehealed at a given temperature and contact time. The measured refracture toughness was correlated with temperature and contact time. Interfacial strength development in graphite-polysulfone unidirectional composites was measured using a double cantilever beam (DCB) interlaminar fracture toughness test. The critical strain energy release rate of refractures composite specimens was measured as a function of healing temperature and contact time.

17. Key Words and Document Analysis. 17a. Descriptors

autohesion, self-diffusion, polysulfone, thermoplastic, thermoplastic composites, process modeling, composite processing

17b. Identifiers/Open-Ended Terms

17c. COSATI Field/Group

18. Availability Statement	19. Security Class (This Report)	21. No. of Pages
unlimited	UNCLASSIFIED	146
	20. Security Class (This Page) UNCLASSIFIED	22. Price

VIRGINIA TECH CENTER FOR COMPOSITE MATERIALS AND STRUCTURES

The Center for Composite Materials and Structures is a coordinating organization for research and educational activity at Virginia Tech. The Center was formed in 1982 to encourage and promote continued advances in composite materials and composite structures. Those advances will be made from the base of individual accomplishments of the forty members who represent ten different departments in two colleges.

The Center functions through an Administrative Board which is elected yearly and a Director who is elected for a three-year term. The general purposes of the Center include:

- collection and dissemination of information about composites activities at Virginia Tech,
- contact point for other organizations and individuals,
- mechanism for collective educational and research pursuits,
- forum and agency for internal interactions at Virginia Tech.

The Center for Composite Materials and Structures is supported by a vigorous program of activity at Virginia Tech that has developed since 1963. Research expenditures for investigation of composite materials and structures total well over seven million dollars with yearly expenditures presently approximating two million dollars.

Research is conducted in a wide variety of areas including design and analysis of composite materials and composite structures, chemistry of materials and surfaces, characterization of material properties, development of new material systems, and relations between damage and response of composites. Extensive laboratories are available for mechanical testing, nondestructive testing and evaluation, stress analysis, polymer synthesis and characterization, material surface characterization, component fabrication, and other specialties.

Educational activities include eight formal courses offered at the undergraduate and graduate levels dealing with the physics, chemistry, mechanics, and design of composite materials and structures. As of 1984, some 43 Doctoral and 53 Master's students have completed graduate programs and several hundred Bachelor-level students have been trained in various aspects of composite materials and structures. A significant number of graduates are now active in industry and government.

Various Center faculty are internationally recognized for their leadership in composite materials and composite structures through books, lectures, workshops, professional society activities, and research papers.

MEMBERS OF THE CENTER

Aerospace and Ocean Engineering
- Raphael T. Haftka
- Eric R. Johnson
- Rakesh K. Kapania

Chemical Engineering
- Donald G. Baird

Chemistry
- James E. McGrath
- Thomas C. Ward
- James P. Wightman

Civil Engineering
- R. M. Barker

Electrical Engineering
- Ioannis M. Besieris
- Richard O. Claus

Engineering Science and Mechanics
- Hal F. Brinson
- Robert Czarnek
- David Dillard
- Norman E. Dowling
- John C. Duke, Jr.
- Daniel Frederick
- O. Hayden Griffin, Jr.
- Zafer Gurdal
- Robert A. Heller
- Edmund G. Henneke, II
- Carl T. Herakovich
- Robert M. Jones
- Liviu Librescu
- Alfred C. Loos
- Don H. Morris
- John Morton
- Ali H. Nayfeh
- Marek Pindera
- Daniel Post
- J. N. Reddy
- Kenneth L. Reifsnider
- C. W. Smith
- Wayne W. Stinchcomb
- Surot Thangjitham

Industrial Engineering and Operations Research
- Joel A. Nachlas

Materials Engineering
- D. P. H. Hasselman
- Robert E. Swanson

Mathematics
- Werner E. Kohler

Mechanical Engineering
- Charles E. Knight

Inquiries should be directed to:

Center for Composite Materials and Structures
College of Engineering
Virginia Tech
Blacksburg, VA 24061
Phone: (703) 961-4969

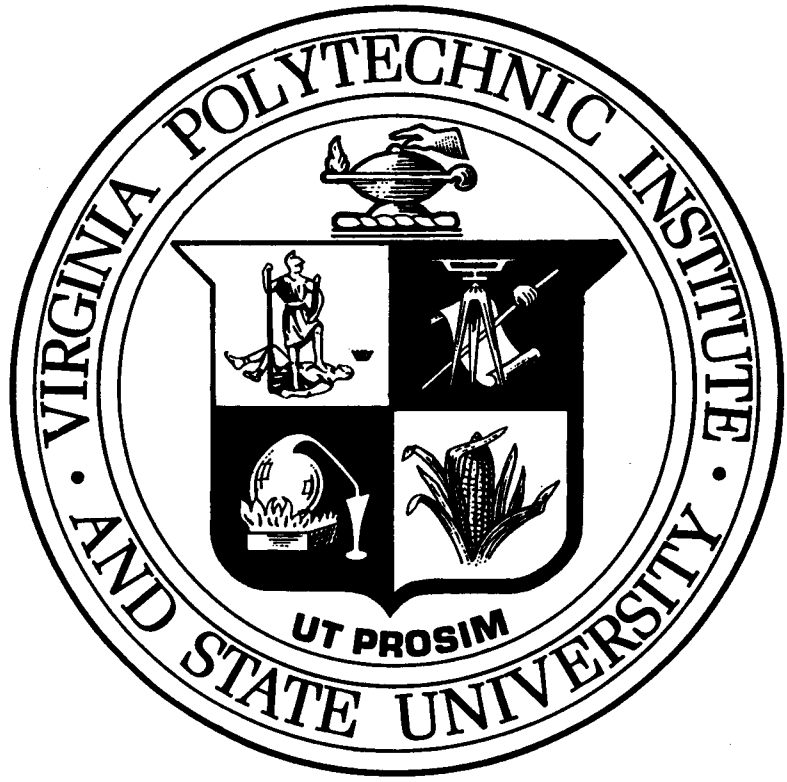
VIRGINIA POLYTECHNIC INSTITUTE
AND STATE UNIVERSITY
UT PROSIM